Influence of structurally bound water on the subcritical crack growth in silicate glasses

Doctoral Thesis (Dissertation)

to be awarded the degree

Doctor of Engineering (Dr.-Ing.)

submitted by

M.Sc.

Philipe Kiefer

from Koblenz

approved by the Faculty of Natural and Materials Science,
Clausthal University of Technology

Date of oral examination
25.03.2021

Dean
Prof. Dr.-Ing. Karl-Heinz Spitzer

Chairperson of the Board of Examiners
Prof. Dr.-Ing. Dieter Meiners

Supervising Tutor
Prof. Dr.-Ing. Joachim Deubener

Reviewer
apl. Prof. Dr. rer. nat. Harald Behrens
Prof. Dr. rer. nat. Gerhard Heide

Zusammenfassung

Das Ziel der vorliegenden Arbeit ist es den Einfluss von strukturell gebundenem Wasser auf das unterkritische Risswachstum in silikatischen Gläsern zu untersuchen. Der Prozess des unterkritischen Risswachstums beschreibt das langsame Voranschreiten eines Risses in einem Material bei Anliegen einer unterkritischen, d.h. nicht zum unmittelbaren Versagen des Materials führenden, Spannung. Im Fall von silikatischen Gläsern ist bekannt, dass die Anwesenheit von Wasser zu einer Hydrolyse des Si-O-Netzwerkes, insbesondere an der Rissspitze, führt und somit einen Anstieg der Rissausbreitungsgeschwindigkeit zur Folge hat.

Um die Bedingungen an der Rissspitze nachzustellen, wurden in der vorliegenden Arbeit Gläser mit strukturellen Wassergehalten c_W >20 mol% synthetisiert und mittels einer Kombination verschiedener Analysemethoden untersucht. Thermoanalytische Messungen zeigen, dass der Einbau von Wasser in Natrium-Borosilikatgläsern die Glasübergangstemperatur T_g um bis zu 45% absenkt. Darüber hinaus wurde mittels dynamisch-mechanischer Thermoanalyse nachgewiesen, dass die durch Wassermoleküle verursachte β-Relaxation bereits bei einer Temperatur von 57 °C feststellbar ist. Letzteres legt nahe, dass diese Form der mechanischen Relaxation in wasserreichen Regionen des Glases, wie sie an der Rissspitze vorzufinden sind, bereits bei Raumtemperatur einen Beitrag zum unterkritischen Risswachstum in silikatischen Gläsern leisten könnte.

Messungen der elastischen Eigenschaften von Kalk-Natron-Silikatgläsern zeigten weiterhin, dass die Querkontraktionszahl positiv mit dem Wassergehalt korreliert. Gleichzeitig nehmen die Dichte, die Vickershärte sowie die elastischen Konstanten der untersuchten Gläser mit zunehmendem Wassergehalt ab. Härtemessungen in Toluol, Stickstoff sowie Luft deuten darauf hin, dass ein zeitabhängiger Erweichungseffekt sowohl bei Messung von nominell wasserfreien Gläsern in feuchter Luft als auch bei Messung von wasserhaltigen Gläsern in trockener Atmosphäre nachweisbar ist.

Um den Einfluss des strukturell gebundenen Wassers auf das Risswachstum der untersuchten Gläser beschreiben zu können, wurde weiterhin

der stochastische Charakter von Radialrissen, welche durch eine Vickerspyramide induziert wurden, analysiert. Durch Anwendung statistischer Verfahren wurde gezeigt, dass eine Vergleichbarkeit von Daten der Eindruckbruchmechanik mit Daten von herkömmlichen Messverfahren nur dann gegeben ist, wenn eine statistisch signifikante Anzahl von Rissdaten vorhanden ist. Mit den Ergebnissen der Analyse wurde eine statistisch basierte Transferfunktion entwickelt, die einen Vergleich von Daten der Eindruckbruchmechanik mit denen von herkömmlichen Methoden erlaubt. Mittels des statistisch basierten Ansatzes wurde anschließend der Einfluss des strukturell gebundenen Wassers auf das Risswachstum in Kalk-Natron-Silikatgläsern untersucht. Es konnte gezeigt werden, dass die Anwesenheit von Luftfeuchte einen stärkeren Einfluss auf das unterkritische Risswachstum hat als strukturell gebundenes Wasser. Messungen in wasserarmer Stickstoffatmosphäre konnten jedoch auch zeigen, dass ein zunehmender struktureller Wassergehalt eine Abnahme des Risswachstumsexponenten zur Folge hat, was darauf hindeutet, dass Wasser unabhängig von seiner Herkunft (d.h. Luftfeuchte vs. Glasstruktur) das Risswachstum an der Rissspitze fördert.

Abstract

The aim of the present thesis is to investigate the influence of structurally bound water on the subcritical crack growth in silicate glasses. The process of subcritical crack growth describes the slow propagation of a crack in a material in presence of a subcritical, i.e. not to immediate failure leading, stress. In the case of silicate glasses, it is known that the presence of water leads to hydrolysis of the Si-O network, especially at the crack tip, and thus to an increase in the crack propagation rate.
In order to mimic the conditions at the crack tip, glasses with structural water contents $c_W > 20$ mol% were synthesized and analyzed using a combination of different analysis methods. Thermoanalytical measurements show that the incorporation of water into sodium borosilicate glasses lowers the glass transition temperature T_g by up to 45%. In addition, it was demonstrated by means of dynamic mechanical analysis that the β-relaxation caused by water molecules can already be observed at a temperature of 57 °C. The latter suggests that this form of mechanical relaxation in water-rich regions of the glass, such as those found at the crack tip, could contribute to subcritical crack growth in silicate glasses at room temperature.
Measurements of the elastic properties of soda-lime glasses also showed that the Poisson's number correlates positively with the water content. Simultaneously, the density, the Vickers hardness and the elastic constants of the glasses decrease with increasing water content. Hardness measurements in toluene, nitrogen and air indicate that a time-dependent softening effect can be observed when measuring both nominally water-free glasses in humid air and measuring hydrous glasses in a dry atmosphere.
In order to be able to describe the influence of the structurally bound water on the crack growth of the investigated glasses, the stochastic nature of radial cracks, which were induced by a Vickers indenter, was analyzed. The application of statistical methods showed that data from indentation fracture toughness can be compared with data from conventional fracture toughness methods only, if there is a statistically significant number of crack data available. With the results of the analyses, a statistically based

transfer function was developed, which allows a direct comparison of data from indentation fracture toughness with that of conventional fracture toughness methods.
Subsequently, the influence of structurally bound water on the crack growth was investigated using the statistically based approach. It was shown that the presence of humidity has a stronger influence on the subcritical crack growth than structurally bound water. However, measurements in a dry nitrogen atmosphere also showed that an increasing water content leads to a decrease in the crack growth exponent, which indicates that water promotes crack growth at the crack tip regardless of its origin (i.e. air humidity vs. glass structure).

"Zur Methode wird nur der getrieben, dem die Empirie lästig wird"

- Johann Wolfgang von Goethe (1749-1832)

Danksagung

Die Erstellung der vorliegenden Arbeit wäre in dieser Form ohne die Unterstützung zahlreicher Personen nicht realisierbar gewesen. Für die vielfältig erfahrene Hilfe möchte ich mich an dieser Stelle sehr herzlich bedanken.
Mein Dank gilt zunächst meinem Doktorvater Prof. Dr.-Ing. Joachim Deubener, welcher mir diese Arbeit ermöglicht hat und durch zahlreiche Diskussionen und Gespräche sowie die stete Unterstützung maßgeblich zum Gelingen ebendieser beigetragen hat.
Herrn Prof. Dr. Harald Behrens und Herrn Prof. Dr. Gerhard Heide möchte ich für die Übernahme der Korreferate danken.
Darüber hinaus möchte ich Herrn Prof. Dr. Harald Behrens sowie Herrn Dr. Ralf Müller für die hilfreichen Diskussionen während der Projekttreffen sowie im Rahmen verschiedener Tagungen danken.
Außerdem gilt mein Dank Tina Waurischk (Bundesanstalt für Materialforschung und -prüfung, BAM), Robert Balzer (Leibniz Universität Hannover) sowie Stefan Reinsch für die hervorragende Kooperation im Rahmen des Schwerpunktprogramms SPP1594.
Ein weiterer Dank gilt auch meinen ehemaligen Kollegen am Institut für Nichtmetallische Werkstoffe der TU Clausthal. Im Speziellen danke ich Herrn Dr.-Ing. Hansjörg Bornhöft für die gute Zusammenarbeit sowie die zahlreichen Diskussionen zu diversen wissenschaftlichen und auch nichtwissenschaftlichen Themen. Frau Angelika Ohlendorf, Herrn Ralf Putzig sowie Herrn Reiner Holly möchte ich für die Probenpräparation bzw. die fortwährende Unterstützung bei technischen Fragestellungen danken. Für die überaus gute und zuverlässige Durchführung

der zahlreichen Messungen möchte ich mich darüber hinaus auch herzlichst bei Herrn Martin Maiwald bedanken.
Der Deutschen Forschungsgemeinschaft danke ich für die finanzielle Unterstützung im Rahmen des Schwerpunktprogrammes 1594.
Zu guter Letzt möchte ich mich auch bei meiner Familie, meinen Freunden sowie insbesondere meiner Frau Sandra für die fortwährende geistige und moralische Unterstützung während der Promotionsphase bedanken. Spezieller Dank gilt auch Herrn Matthias Wagner für das Korrekturlesen der Dissertation.

Table of contents

1

General introduction

Modern applications such as architectural glasses, smartphone displays and fiber optics have become an important part of our daily lives over the last decades. However, it is also well known that the application of glasses for modern and conventional applications is limited due to the brittleness of the material when subjected to mechanical stresses [1]. With theoretical strengths of more than 30 GPa, inorganic glasses belong to the strongest man-made materials that can be produced on an industrial scale [1], [2]. Nevertheless, experimentally derived bending strengths of soda-lime float glasses yield values of 45 MPa only, which is far below the theoretical strength of a glass [1]–[3]. Due to these differences, it is necessary, to distinguish between the intrinsic and practical strength of glasses. The deviation of the practical strength from the theoretical strength is governed by the presence of flaws, especially on the materials surface, and the materials tendency to interact with the surrounding atmosphere, i.e. with the humidity [4]–[13]. When glasses are exposed to mechanical stresses, e.g. tensile stresses, cracks are extending from surface flaws through the bulk because stresses accumulate at the tips of the flaws [14]. Figure 1.1 shows that this effect can reduce the materials strength over several orders of magnitude.

Furthermore, figure 1.1 shows that the reduction in strength can be displayed as a function of the flaw depth on the materials surface. Using

an elliptic flaw as descriptive model for a real surface flaw on a glass plate, Inglis [14] developed an approach to describe the stress at the crack tip assuming an ideal linear-elastic behavior. In his study Inglis found out that the stress at the crack tip depends on the crack length and the tip radius, as expressed by the following equation 1.1 [14]:

$$\sigma_{local} = 2\sigma_{app}\sqrt{\frac{c}{r}}, \tag{1.1}$$

with σ_{local} = stress concentration at the crack tip, σ_{app} = applied (tensile) stress, c = crack length/flaw depth and r = crack tip radius. As shown by equation 1.1, the stresses at the crack tip are increased when the crack tip radius is small and the crack length increases, which is the case for a propagating crack in a glass.

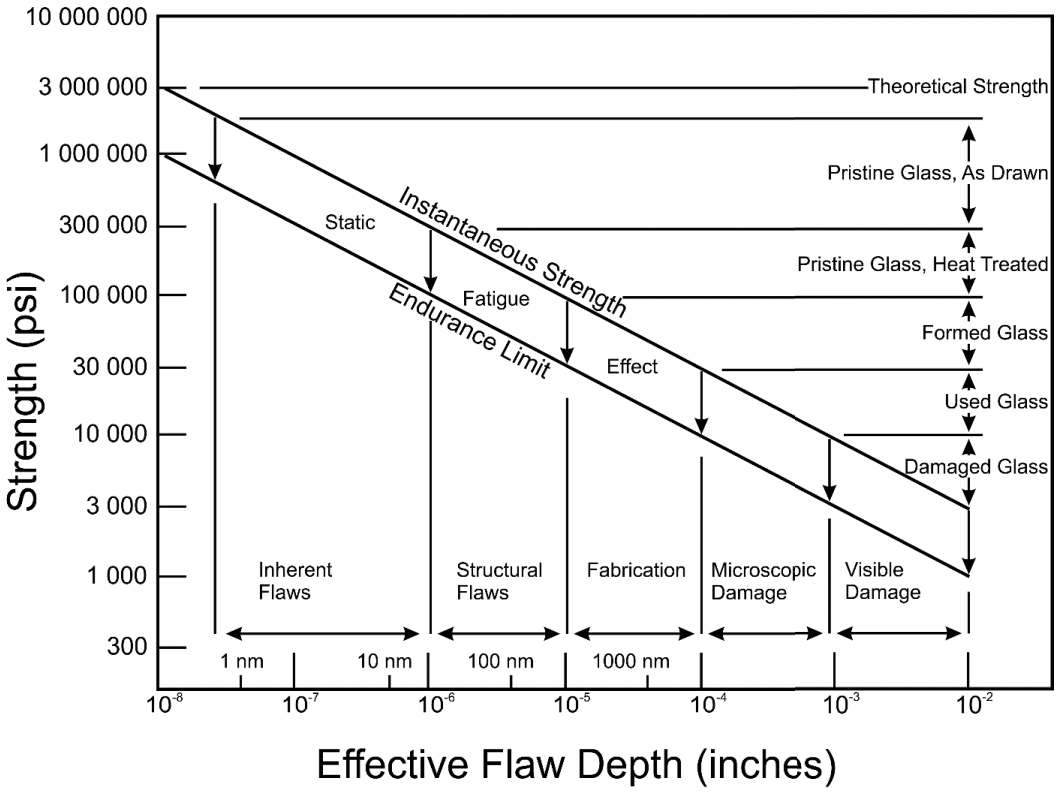

Figure 1.1: Strength of glasses versus flaw depth. The data show that the strength of glasses is decreasing with an increasing flaw depth. The flaw depth is furthermore related to different surface conditions and types of flaws. Image redrawn after [8].

Based on the findings of Inglis, Griffith developed an energy balance of the process of crack propagation in a linear-elastic material [15]. Therefore,

Griffith related the strain energy release, i.e. the energy that is released due to the breakage of strained bonds, and the bond energy, i.e. the energy that is needed to break the bonds in the material [16]. Figure 1.2 exemplary represents such an energy balance for an arbitrary crack. The figure shows that the strain energy decreases with increasing crack length, since the bonds, which are strained by the application of a stress, break. However, with increasing crack length c also the number of bonds that needs to be broken increases. Thus, the bond energy is increasing linearly with an increasing crack length. The summation of both energies reveals a parabolic shaped curve, showing an energetic maximum that is related to a certain crack length. If the crack length is increasing above this energy maximum, the internal energy of the material will decrease with further increasing crack length, ultimately leading to the materials failure. Thus, this crack length is referred to as critical crack length c_{crit}. By differentiating the sum curve of energies for the crack length, the critical crack length c_{crit} can be related to a critical stress σ_{crit}, which is given by equation 1.2 [16]:

$$\sigma_{crit} = \sqrt{\frac{2\gamma_{surf}E}{\pi c_{crit}}}, \tag{1.2}$$

with γ_{surf} = surface energy (surface tension) and E = Young's modulus.

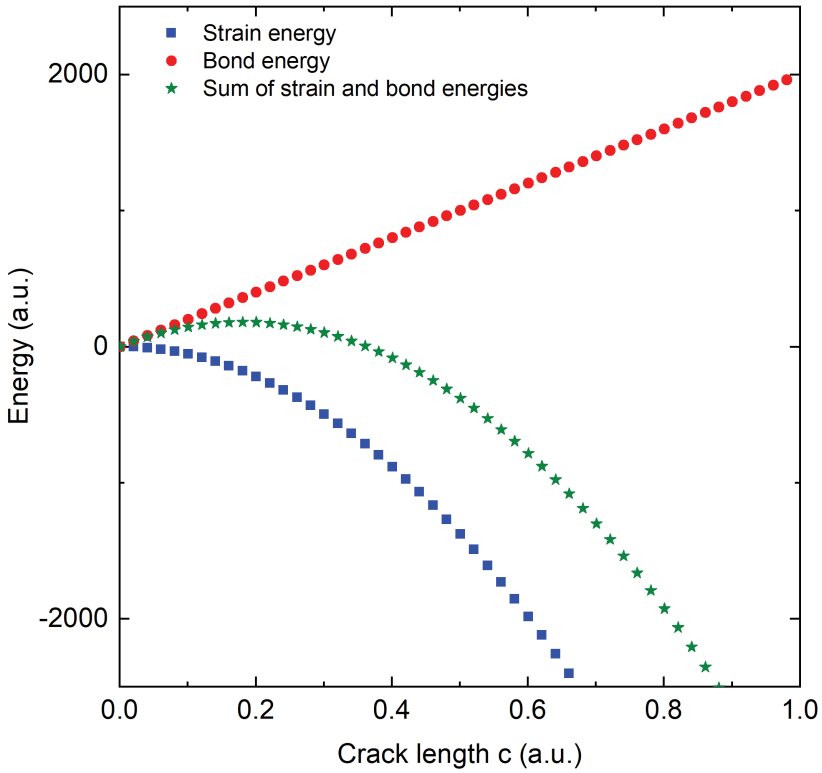

Figure 1.2: Example of Griffith's energy balance. The sum (green asterisk) of the two energies 1) strain energy release (blue squares) and 2) bond energy (red dots) contributing to crack propagation shows a maximum at a particular crack length. This crack length is defined as the critical crack length c_{crit} since the material decreases its internal energy with a further increase in crack length. Figure modified after [17].

Apart from the critical crack growth another crack propagation process acts at stresses $< \sigma_{crit}$, which is referred to as subcritical crack growth (SCCG). SCCG, also known as delayed fracture [13], is often preceding the failure due to critical crack growth and can have an impact on the materials strength as depicted in figure 1.1 (static fatigue effect) [8]. The effect of SCCG was first observed by Milligan in 1929 [18], who noted that scratched glasses, which are in contact with water, show a strength decrease of up to 20%. Further studies of Charles & Hillig then provided a mechanistic description of the SCCG [9]–[11], [19]. However, it was Wiederhorn in 1967 [12] who published a coherent and systematic set of data that describes the influence of water vapor, i.e. humidity, on the

crack growth of glasses. In his study, Wiederhorn measured the crack propagation rates as a function of the applied load for various levels of humidity. Figure 1.3 shows the dependence of the crack propagation rate ν as a function of the stress intensity factor K_I ($K_I = \sigma_{app}(\pi c)^{0.5}$) at various levels of humidity [12]. The diagram shows that ν increases with increasing humidity for a given K_I.

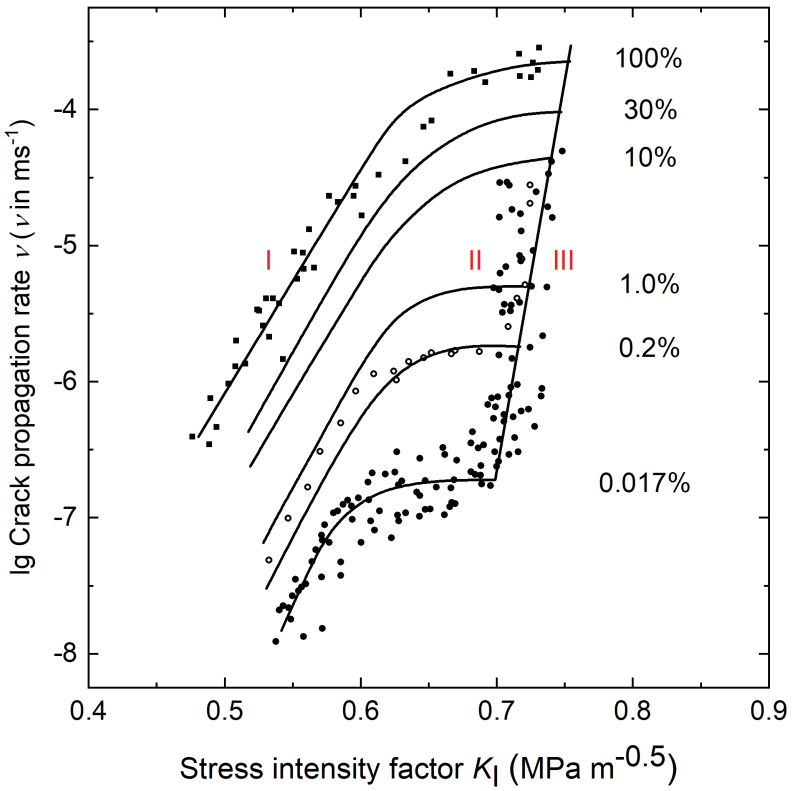

Figure 1.3: Crack propagation rate ν versus stress intensity factor K_I for measurements at different levels of humidity. The diagram shows that ν increases for a given K_I with increasing humidity. Figure after [12].

Furthermore, the diagram shows that the ν-K_I-curves can be subdivided into three different regions or stages (I, II and III). Based on the fatigue theory of Charles & Hillig, Wiederhorn describes that the crack propagation rate in Region I of the ν-K_I-diagram is governed by the hydrolysis rate of the Si-O-bonds at the crack tip, based on the reaction H_2O + ≡Si-O-Si≡→≡2SiOH [9], [12], [19]. With increasing crack propagation rate a change in the rate limiting parameter is observed. Due

to a high consumption of water molecules in later stages of region I, the crack propagation rate in region II is limited by the transport rate of water to the crack tip [12]. This limitation is reflected by the plateaus shown in figure 1.3, indicating that ν is independent of K_I. In region III, however, ν again shows a strong dependence on the applied stress. The unification of all curves of different humidity implies that the crack propagation rate in region III depends on the intrinsic properties of the tested material rather than the test environment [12], [20]. Thus, region III of the ν-K_I diagram is referred to as inert crack growth [12].
Based on these findings, numerous studies were published to increase the understanding of the process of subcritical crack growth. These studies showed that water is adsorbed at the crack tip leading to stress corrosion [21], a reduction in surface energy [22] and bond strength [23], [24]. However, crack propagation is also affected by water molecules that enter the glass structure at the crack tip [25]. This process is additionally accelerated by the presence of tensile stresses [24], [26]. As a consequence, local changes of the mechanical relaxation and elastic moduli are induced in the vicinity of the crack tip, leading to a complex interplay of different mechanisms [27].
Because it is difficult to measure the influence of water on the processes at the crack tip in-situ, the present thesis consists of four chapters aiming to provide macroscopically scaled information by mimicking the processes at the crack tip. In the first two parts (chapters 3 and 4) the influence of structurally bound water on the mechanical properties of hydrous glasses is analyzed. It is supposed that the mechanical relaxation and the elastic constants, including the Poisson's ratio, are subject to changes upon the addition of water into the glass structure. As both the mechanical relaxation and the elastic constants are supposed to have significant influences on the subcritical crack growth of glasses, as was found by various authors [12], [16], [20], [28]–[30], the results presented in the first two parts of this study may contribute to a more accurate understanding of SCCG. As the quantity and sample size of the hydrous glasses that are investigated in this thesis are limited to approximately

$5\times20\times1$ mm^3, standard methods for measuring fracture mechanical parameters are limited either in feasibility or in statistical significance. Because alternative test methods like Indentation Fracture Toughness (IFT) are widely discussed because of their statistical significance and the unknown stress distribution during crack propagation [31], [32], chapter 5 of this study provides a statistically based approach to use IFT methods for the estimation of the fracture mechanical parameter K_I. In chapter 6 of this thesis, the influence of structurally bound water is tested for soda-lime silica glasses with up to 6 wt% water. Based on the results of the data presented by chapter 5, the experiments were conducted using Vickers indentation to induce cracks in the glasses. To provide statistical significance, more than 3200 cracks of the hydrous glasses were analyzed. In order to distinguish between the effects of both, structurally bound water and humidity on the crack growth, the experiments were additionally carried out in two different atmospheres with low and high water vapor pressure (~30 vs. ~942 Pa).

2

Overview of the publications

2.1 Structural relaxation mechanisms in hydrous sodium borosilicate glasses

- Copyright: © 2018. This manuscript version is made available under the CC-BY-NC-ND 4.0 license http://creativecommons.org/licenses/by-nc-nd/4.0/

- Status: published

- Authors and their contribution to the publication
  - P. Kiefer: measurement of sphere penetration viscometry (SPV) data, evaluation of SPV data, production of section 3.2.3
  - H. Behrens, U. Bauer, S. Reinsch, R. Müller, J. Deubener: conception and design of the study, preparation of hydrous glasses, draft of the manuscript, revision of the manuscript

- Year: 2018
- Title: Structural relaxation mechanisms in hydrous sodium borosilicate glasses
- Scientific Journal: Journal of Non-Crystalline Solids
- Volume: 497
- Pages: 30-39
- DOI: 10.1016/j.jnoncrysol.2018.05.025

- Content and relevance within the thesis:

The publication analyses the effects of water on the mechanical and thermal properties of sodium borosilicate glasses ($16Na_2O$-$10B_2O_3$-$74SiO_2$) with up to 22 mol% H_2O.
Differential thermal analyses showed that the glass transition temperature T_g and the isokom temperature T_{12}, measured by viscometry, are in

excellent agreement and confirm that enthalpy and viscous relaxation can be considered as equal. Furthermore, a combination of T_g data with quantitative information about the water speciation revealed that the decrease in T_g upon hydration correlates with the amount of OH groups in the glass rather than with the content of molecular water.
Measurements of the internal friction show that molecular water is highly influencing the mechanical relaxations withing the hydrous glasses, thus confirming the observations made by previous authors [29]. The internal friction measurements revealed that the temperature range of the α-relaxation, i.e. glass transition, strongly decreases from 670 to 450 K upon hydration of the glasses from 0.01 to 5 wt%. Along with the temperature decrease of the α-Relaxation, a β-relaxation mode that is related to molecular water, is detectable within the internal friction spectra at 380 and 330 K, respectively for glasses containing 3 and 5 wt% of water, also confirming the results of previous authors made for other glass compositions [29]. The results of the study provide new insights about the role of water during the network relaxation in hydrous sodium borosilicate glasses, but also confirm the findings of other authors made for glasses with different composition (i.e. soda-lime silicate glasses) [29]. Because it is supposed that water can diffuse into the glass network at the crack tip, the findings made by this study represent an indication about the effect on the local relaxation behavior at the crack tip during (sub-)critical crack growth.

2.2 Density, elastic constants and indentation hardness of hydrous soda-lime-silica glasses

- Copyright: © 2019. This manuscript version is made available under the CC-BY-NC-ND 4.0 license http://creativecommons.org/licenses/by-nc-nd/4.0/

- Status: published
- Authors and their contribution to the publication
  - P. Kiefer: design of the study and experiments, experimental work, programming of software, data evaluation, draft of manuscript
  - R. Balzer, J. Deubener, H. Behrens, T. Waurischk, S. Reinsch, R. Müller: conception and design of the study, preparation of hydrous glasses, discussion of results, revision of the manuscript
- Year: 2019
- Title: Density, elastic constants and indentation hardness of hydrous soda-lime-silica glasses
- Scientific Journal: Journal of Non-Crystalline Solids
- Volume: 521
- Pages: 1-9
- DOI: 10.1016/j.jnoncrysol.2019.119480
- Content and relevance within the thesis:

The publication describes the effects of increasing water contents on the density, elastic constants and indentation hardness of soda-lime-silica glasses. For this purpose, commercially available soda-lime-silica glasses were hydrated up to water contents of 21.5 mol%. The main target of the

study was to investigate the influence of water on the elastic constants of hydrous glasses but also to investigate the influence of water on the Vickers hardness of such glasses, with respect to the origin of water, i.e. structural water or humidity. Ultrasound measurements revealed that the Poisson's ratio correlates positively with increasing water contents. In contrast, it was found that the density and elastic constants of the analyzed glasses decrease upon hydration. Simultaneously, for the glass with 21.5 mol% of water, it was found that the Vickers hardness decreased by approximately 27% when compared to a dry glass of the same chemical composition. Moreover, the results show that the changes in the elastic constants induced by water are non-linear, reflecting the non-linear changes in OH and H_2O concentrations in the glasses upon hydration. The measurements of the Vickers hardness in toluene, nitrogen and air revealed that a time-dependent softening effect is observable in two scenarios, i.e. i) testing a hydrous glass in dry atmospheres and ii) testing dry glasses in a humid atmosphere. The results of the study provide new insights about how water is affecting the elastic constants of glasses. In addition, the observed softening effect suggests that water can relax stressed glasses, independent of its origin.

2.3 Statistical analysis of propagation rates of indentation-induced radial cracks in soda-lime-silicate glass

- Copyright: © 2019. This manuscript version is made available under the CC-BY-NC-ND 4.0 license http://creativecommons.org/licenses/by-nc-nd/4.0/

- Status: published
- Authors and their contribution to the publication
  - P. Kiefer: design of the study and experiments, experimental work, programming of software, data evaluation, draft of manuscript
  - J. Deubener, R. Müller, H. Behrens: conception and design of the study, discussion of results, revision of the manuscript
- Year: 2020
- Title: Statistical analysis of propagation rates of indentation-induced radial cracks in soda-lime-silicate glass
- Scientific Journal: Journal of Non-Crystalline Solids
- Volume: 527
- Pages: 1-8
- DOI: 10.1016/j.noncrysol.2019.119739
- Content and relevance within the thesis:

The publication explores the stochastic nature of crack nucleation by Vickers indentation in a commercial soda-lime-silica glass. Because the sample dimensions of hydrous glasses are limited by the preparation technique, standard methods, i.e. double cantilever beam (DCB), for measuring fracture mechanical parameters like $K_{I(C)}$ are limited either

in feasibility or statistical significance. Additionally, indentation fracture toughness (IFT) methods are under discussion in literature because these methods often apply empirical equations that were developed based on data of numerous materials [31]–[33]. Thus, IFT methods are reported to yield relative uncertainties of K_I of up to ±50% [34]. In order to increase the accuracy and to use IFT methods for the estimation of fracture mechanical parameters of hydrous glasses, the main scope of the study was to investigate the stochastic nature of nucleation and growth of Vickers induced radial cracks and to align these data with data from fracture mechanical standard tests. In-situ observation of crack nucleation and growth revealed that the crack propagation rates are controlled by the interactions of the glass network at the crack tip and the environment, shortly, i.e. <1 s, after the crack is initiated. The analysis of 185 Vickers induced radial cracks showed that both, the residual stress factor χ and the exponent n of the equation $K_I{=}\chi P c^{-n}$ (with P = load and c = crack length) are broadly distributed. An analysis of the distributions of χ and n revealed that the most frequent values of χ and n are 0.052 and 1.47, respectively. The study shows that a correlation of indentation induced crack lengths to the stress intensity $K_{I(C)}$ requires the application of statistically significant data that are calibrated by the reactions of the glass network at the crack tip with the atmosphere. In context of this thesis the study provides a new approach that can be applied to estimate the fracture mechanical parameter K_I by IFT methods.

2.4 Automated analysis of slow crack growth in hydrous soda-lime silicate glasses

- Copyright: © 2020. This manuscript version is made available under the CC-BY 4.0 license http://creativecommons.org/licenses/by/4.0/

- Status: published

- Authors and their contribution to the publication

  – P. Kiefer: design of the study and experiments, experimental work, programming of software, data evaluation, draft of manuscript

  – M. Maiwald: experimental work, data evaluation

  – J. Deubener, R. Balzer, H. Behrens, T. Waurischk, S. Reinsch, R. Müller: conception and design of the study, preparation of hydrous glasses, discussion of results, revision of the manuscript

- Year: 2020

- Title: Automated analysis of slow crack growth in hydrous soda-lime silicate glasses

- Scientific Journal: Frontiers Materials – Ceramics and Glass

- Volume: 7:268

- Pages: 1-11

- DOI: 10.3389/fmats.2020.00268

- Content and relevance within the thesis:

The publication investigates the impact of structural and ambient water on the static fatigue of hydrous glasses. For this purpose the statistical approach that was developed in the publication “Kiefer et al. 2020 - Statistical analysis of propagation rates of indentation-induced

radial cracks in soda-lime-silicate glass" [35], was applied on 3279 Vickers induced radial cracks. It was found that humidity has a higher efficiency than structurally bound water considering the initiation and propagation of cracks. Measurements in dry nitrogen gas showed that the crack growth exponent n decreases upon hydration, while repetitive measurements in air showed that the crack exponent n remains constant but the stress intensity χ is reduced. The observations made in this study suggest that water promotes crack propagation independent of its origin but also that ambient water, i.e. humidity, is the more efficient agent. The results of this study reassemble the observations made in the previous publications of this thesis and provide new insights about the influence of both, structurally bound water and humidity on the crack propagation in soda-lime-silica glasses. Along with the data of Waurischk et al. and McMillan, [36], [37], the results presented in this publication represent some of the first fracture mechanical data for hydrous anorganic, non-metallic glasses. By this, the data enable for a more precise description of the impact of water on crack initiation and propagation, which was the main target of this thesis.

3

Structural relaxation mechanisms in hydrous sodium borosilicate glasses

H. Behrens[a], U. Bauer[a], S. Reinsch[b], P. Kiefer[c], R. Müller[b], J. Deubener[c]

[a]Leibniz Universität Hannover, Institute of Mineralogy, Callinstr. 3, 30167 Hannover, Germany

[b]Bundesanstalt für Materialforschung und -prüfung (BAM), 12489 Berlin, Germany

[c]Clausthal University of Technology, Institute of Non-Metallic Materials, 38678 Clausthal-Zellerfeld, Germany

Abstract

Borosilicate glasses ($16Na_2O$–$10B_2O_3$–$74SiO_2$, NBS) with water contents up to 22 mol% H_2O were prepared to study the effect of water on structural relaxation using DTA, viscometry and internal friction measurements. The results show that the glass transition temperature T_g of DTA and the isokom temperature T_{12}, of viscometry are in excellent agreement, confirming the equivalence of enthalpy and viscous relaxation for NBS glass. Combining T_g data with water speciation data demonstrates that OH groups are mainly responsible for the decrease of T_g with increasing hydration, while molecular water plays only a minor role. Internal friction spectra at 7.125 Hz confirm the decisive influence of water on mechanical relaxation. The temperature range of α-relaxation (glass transition) strongly decreases while two β-relaxation peaks (sub-T_g) progressively appear with increasing water content. A high temperature β-relaxation peak, attributed to the presence of OH groups, shifts from 670 to 450 K as total water content increases from 0.01 to 5 wt%. A low temperature β-relaxation peak, attributed to molecular water, appears at 380 K and 330 K in glasses containing 3 and 5 wt% H_2O, respectively. These findings suggest that relaxation mechanism of different hydrous species at low temperature may contribute to fatigue of stressed glasses.

3.1 Introduction

It is well known that water plays an important role in the structure and properties of silicate melts and glasses. This is particularly the case for natural glasses, in which several weight percent of water can be dissolved due to elevated pressures [38], [39]. The investigation of water in industrial relevant glasses is also a crucial issue, since water has drastic influence on mechanical relaxation phenomena. Viscosity can be strongly reduced upon hydration [40], e.g., ≈3 wt% water decreases the glass transition temperature T_g by more than 30% for numerous glasses. Stress relaxation is also enhanced, a phenomenon used for instance to strengthen glass

fibers by exposing them to water vapor under stress [30], [41] Furthermore, low temperature processes in glasses such as internal friction [42], [43], aging [44], crack growth and fatigue [12], [25], [45] may be affected even by small amounts of water. For instance, ambient moisture can enhance subcritical growth rate in soda-lime-silicate glass by up to 4 orders of magnitude [20]. Such sub-T_g processes can be of relevance also in nature, e.g. in the fragmentation of ascending magmas during volcanic eruptions. Wiederhorn [20] showed that subcritical crack growth (SCCG) is strongly affected by the mechanical properties of the crack tip near the cohesive region. Water can be easily adsorbed at the crack tip, leading to stress corrosion [21], reduction in surface energy [22], and bond strength [23]. However, crack propagation can also be affected by entry of water into the glass structure at the crack tip [25], accelerated by tensile stress at the crack tip [26]. As a consequence, mechanical relaxation and elastic moduli change locally very strongly [27]. Since these local phenomena are difficult to measure in situ, we used studies on hydrous glasses to mimic such relaxation phenomena.

Network relaxation in the range of the glass transition is well investigated for a wide range of hydrous and anhydrous silicate and aluminosilicate glasses [39], [46], [47]. Considerably less information is available about relaxation processes in hydrous boron-bearing glasses. It is known that water in glasses is present as two main species in glasses: as molecular water (H_2O_{mol}) and as dissociated water forming OH groups [48]–[51]. In silicate and aluminosilicate glasses the strongest decrease of the glass transition temperature T_g upon incorporation of water occurs in the range of low water contents ($\leq$2 wt% H_2O), where OH groups are the predominant water species. At water contents above ~3 wt% the content of hydroxyl groups apparently level off, and the amount of molecular water rises strongly. This trend is a consequence of the decrease in fictive temperature of the glass with increasing water content, i.e. water speciation is frozen in at lower temperatures.

Only a few studies on the speciation of water in borosilicate and boroaluminosilicate glasses with high water contents (up to 10 wt% H_2O)

are available [48], [49], [52], [53]. These studies revealed that OH groups are increasingly stabilized with increasing boron content. While molecular water is the dominant water species at water contents >7 wt% H_2O in borosilicate and boroaluminosilicate glasses, only ~1 wt% molecular H_2O was found in soda-lime borate glasses with 7.5 wt% H_2O [50].

In the three-component model of Tomozawa [51] the influence of water species and dry glass component was considered to model the decrease of the glass transition temperature with increasing water content. Deubener et al. [40] applied this concept to a variety of silicate and aluminosilicate glasses and showed that the effect of OH groups on T_g is by far stronger compared to that of molecular water in these compositions. The limitation of this concept so far has been that the applied water speciation data measured on the glasses do not represent T_g since the cooling rate of the glasses differs from the standard cooling rate [54].

There is only rare knowledge about the influence of total water and water species on sub-T_g relaxation in oxide glasses [29]. Internal friction measurements indicate up to three relaxation modes in glasses. These modes are often denoted as α-, β-, and γ- relaxation in the order of decreasing temperature [55]–[57]. The dominating α-relaxation mode is mainly responsible for viscous flow, stress relaxation and internal friction at elevated temperatures [55]. Typically, only the low-temperature flank of this broad peak can be measured, and the maximum is supposed to be close to T_g. With increasing water content, the α-relaxation peak and T_g shift to lower temperatures [42], [55], [58].

In some glasses an additional relaxation mechanism, labelled as β-relaxation, has been observed as a shoulder on the low temperature flank of the α-relaxation peak and has been assigned to movements of non-bridging oxygens (NBOs) [43], [57], cooperative movements of equal or dissimilar mobile species such as alkali or alkaline-earth ions [55], [59]–[64] or movements within a cluster of alkaline-earth cations [57]. In water-poor ($\leq$ 0.3 wt% H_2O) phosphate, borate and silicate glasses β-relaxation was correlated with cooperative motions of alkali ions and neighboring protons [65]–[69]. β-relaxation phenomena in glasses with high water

contents, when a significant amount of molecular water is present, are rarely investigated. In the study of Reinsch et al. [29] two distinct β-relaxation peaks in mechanical loss spectra were attributed to dynamics of OH groups and molecular water in hydrated silicate glasses ($\leq$1.9 wt% H_2O). The relaxation mode of H_2O_{mol} was found to be faster compared to OH groups and is probably caused by jumps of H_2O molecules between adjacent cavities in the network. It is worth noting that rotation of H_2O molecules around their bisector axis, another low temperature process in hydrous glasses identified by NMR spectroscopy and quasielastic neutron scattering, is too fast to contribute to the β-relaxation peak [70], [71]. In contrast to α-relaxation, which governs global network relaxation, β-relaxation may be considered as a more regional process embedded within the much more rigid global network.

The γ- relaxation mode, observed at temperatures < 373 K [72], is attributed to the motion of alkalis, since the range of activation energies ($E_\gamma \approx 63 - 105$ kJ mol^{-1}) [73] resembles those of alkali diffusion (63 - 84 kJ mol^{-1}) [43]. In contrast to α- and β-relaxation, γ-relaxation is more a local phenomenon.

Our study is aimed to improve the understanding of the influence of water content and speciation on mechanical relaxation in borosilicate glasses using differential thermal analysis (DTA), sphere penetration viscometry (SPV), and dynamic mechanical analysis (DMA) to study relaxation mechanisms. The composition of the investigated borosilicate glass (16 mol% Na_2O, 10 mol% B_2O_3 and 74 mol% SiO_2) was chosen as representative for a technical glass since the borosilicate crown glass BK7 from Schott AG is very similar in composition. A detailed characterization of the anhydrous and hydrous borosilicate glass structure was published in Bauer et al. [50], including analysis of water speciation, boron speciation as well as Q^n-speciation (SiO_4 tetrahedron with n = number of bridging oxygen).

3.2 Experimental and analytical methods

3.2.1 Sample preparation

For the synthesis of the borosilicate glass a powder mixture of Na_2CO_3, B_2O_3 and SiO_2 was used. A detailed description of the synthesis is given in Bauer et al. [50]. Samples with 0.2 wt% H_2O were synthesized from the base glass in 110 ml alumina crucibles by re-melting and water steam bubbling at 1753 K and 0.5 MPa argon pressure within 3 hours. Subsequently, the temperature was lowered, and the melt was cooled with 3 K/min through the regime of ($T_g \pm 150$ K) to avoid internal stress in the glasses. The procedure was described in the study of Reinsch et al. [29]. Electron probe microanalysis indicate ca. 4 wt% Al_2O_3 in this particular glass. Consistency of experimental data with the other (Al-free) glasses implies that this contamination has minor effect on our study. All samples with water contents ≥ 0.5 wt% were synthesized in an internally heated pressure vessel (IHPV) at 500 MPa and 1423 K for 14 - 20 hours using the same procedure as given in [50]. Cooling rate in the regime of glass transition was ~8 K/s for NBS0-500MPa, NBS0.5 and NBS1, ~6 K/s for NBS3 and ~3.5 K/s for NBS5. The water-rich glass NBS8 was quenched much faster (~200 K/s) to avoid crystallization during cooling.

3.2.2 Differential thermal analysis

The glass transition temperature, T_g, was determined by differential thermal analysis in air using 15 - 20 mg of glass pieces or powdered glass placed in Pt-crucibles (thermobalance TAG 24, Setaram, Caluire, France). The same measurement routine and data evaluation (tangent method) was applied to hydrous borate glasses, and T_g values were found to be in perfect agreement with isokom temperatures (T_{12}) at which the viscosity equals 10^{12} Pa $\cdot$ s [50]. For each sample four heating and cooling cycles with 10 K min^{-1} were applied. The maximum temperature did not exceed T_g by more than 50 K. The first cycle represents the fictive temperature T_f of the glasses, since the cooling history of the samples reflects the

status of quenching after IHPV synthesis. The following three cycles were used for the determination of T_g. Definition of T_f and T_g is based on the onset of the endothermic step in the DTA curve according to Mazurin [74], [75]. The average T_g values for all investigated glasses are included in table 3.1.

In order to detect a possible loss of water of high water-bearing glasses, the thermal gravimetric (TG) signal was simultaneously recorded during DTA measurement. Additionally, a mass spectrometer (MS, Balzers Quadstar 421) was used for analysis of evolved gases, coupled to the DTA by a heated (453 K) quartz glass capillary. Neither a significant mass loss nor a distinct signal for water by mass spectroscopy could be detected. The good reproducibility of T_g determination further supports a negligible water loss during the DTA procedure. The maximum error of temperature for this method is ±5 K.

Table 3.1: Water contents and DTA results of samples used in this study.

	$cH_2O_{(t)}$ [wt%]	T_f 1st run [K]	T_g 2nd run [K]	T_g 3rd run [K]	T_g 4th run [K]	T_g mean [K]	further analysis
NBS0(0.1MPa)*	0.010 ± 0.001	850	845	846	846	847 ± 2	SPV, DMA
NBS1	0.89 ± 0.05	722	721	723	720	721 ± 2	SPV
NBS3	2.82 ± 0.08	613	603	600	604	602 ± 2	
NBS3c	3.14 ± 0.05	575	568	570	573	570 ± 3	NMR, SPV
NBS5	4.64 ± 0.10	529	549	553	552	551 ± 2	
NBS5c	5.00 ± 0.06	536	528	531	530	530 ± 2	NMR, SPV
NBS8c	7.96 ± 0.09	465	467	470	466	465 ± 2	NMR, Raman
NBS0.2b*	0.23 ± 0.05						DMA
NBS0.5b-I	0.56 ± 0.10						DMA
NBS0.5b-II	0.57 ± 0.07						
NBS3b-I	2.99 ± 0.11						DMA, Raman
NBS3b-II	2.82 ± 0.08						
NBS5b-I	4.86 ± 0.11						DMA, Raman
NBS5b-II	4.54 ± 0.08						

Notes. Numbers in the sample name refer to the nominal water content. Letter b characterizes samples synthesized for DMA and letter c indicates samples which were also analyzed by NMR spectroscopy. I or II in the sample name refer to glass pieces from both ends of the sample. $cH_2O_{(t)}$ is the total water content measured with KFT except for samples labeled with*, for which mid-infrared spectroscopy was used for determination (see [52] for more information).

3.2.3 Sphere penetration viscometry (SPV)

Viscosity data were obtained by sphere penetration measurements. Cylindrical samples with diameters of ~6 mm and heights of 1-2 mm were sliced from the synthesized glasses. Coplanar surfaces were obtained by grinding and polishing the sample surfaces.
The vertical dilatometer (VIS 404, Bähr GmbH) is equipped with a pushing rod made of silica glass and a sapphire sphere (radius r = 0.75 mm). The force applied on the pushing rod was adjusted to 3.9 N. The temperature was controlled with an S-type thermocouple (Pt-PtRh) placed in the vicinity (2 - 3 mm) of the sample surface. The thermal gradient along the sample axis was less than ± 1 K mm^{-1}. Considering the accuracy of thermocouples and measurement equipment, the maximum error on the temperature is ± 5 K.
A linear variable displacement transducer continuously recorded the indentation depth of the sapphire sphere into the glass. The shear viscosity was calculated according to [76]:

$$\eta = \frac{3F}{16\sqrt{2rL}\frac{\delta l}{\delta t}}, \tag{3.1}$$

with η = Newton viscosity, F = applied force, t = time, r = radius of the sphere, L = cumulative indentation depth and δl = indentation within a measurement interval δt.
The system was calibrated by the standard glass G1 of the Physikalisch-Technische Bundesanstalt (PTB) [77]. Viscosity data of the standard glass G1 were reproduced with a standard deviation of ± 0.10 in log units. The measurements were performed on a set of dry and hydrous NBS glasses (see table 3.2 for details). The first two runs reported in table 3.2 were conducted on two different samples from the same synthesis charge. In the case of NBS1 runs 3 and 4 are repeated measurements on samples which were previously used in run 1 and 2, respectively.
The temperature program of the anhydrous NBS glass and the glass with 1 wt% H_2O include several temperature steps (dwell times between 30-250 min) within one run (table 3.2), since the low water-bearing samples

are expected to be not sensitive to water loss at the chosen temperatures. The temperature program for samples with higher water contents (NBS3c and NBS5c) was subdivided into three steps ($T_{II} = T_I + 10$ K and $T_{III} = T_I$) with dwell times of 150 to 200 min for viscosities close to 10^{12} Pa·s, while for viscosities in the range of 10^{11} - 10^{10} Pa·s dwell times of 100 min were selected. This program was chosen to avoid on the one hand long exposure of samples to elevated temperatures and thus risk of water loss, and on the other hand to check for any water loss during the viscosity measurement. To reach the first dwell temperature, a heating rate of 20 K min^{-1} was applied. In subsequent steps heating or cooling rates of 5 K min^{-1} were used.

3.2.4 Dynamic mechanical analysis

Internal friction measurements were made by dynamic mechanical analysis (DMA). A sinusoidal force is applied on the sample, and the force, the displacement of the sample and the phase shift, δ, between force and displacement curves are measured. Tan δ is often referred to as the mechanical loss.

The used DMA analyzer (Gabo Eplexor 150 N, Ahlden, Germany) was operated in asymmetric three-point bending mode performing temperature-frequency sweeps at 4 N static force and 2 N dynamic force. Dynamic force and displacement were measured with a 25 N force detector and an inductive displacement transducer, respectively. Dry and hydrous NBS glass bars, typically 2 x 5 x 25 mm^3 in size, were measured from 173 K up to temperatures close to T_g. It was not possible to reach the glass transition temperature due to progressive viscous bending of the sample under the applied static load (see also discussion below). Loss data below 273 K could be affected by sample surface icing when operated in air. Such data were not further considered.

The mechanical loss spectra were evaluated with OriginPro2016. The spectra have been smoothed using a moving average of 15 data points. The average data scatter around the smoothed curves is $\Delta\tan\,\delta = \pm 5 \cdot 10^{-4}$. For clarity the lowest point of each spectrum was shifted to zero.

Table 3.2: Viscosity data of nominal dry NBS glass (NBS0-0.1 MPa) and hydrous NBS glasses (NBS1, NBS3c and NBS5c).

	NBS0-0.1MPa			NBS1			NBS3c			NBS5c	
run	T [K]	$\log \eta$ [η in Pa · s]	run	T [K]	$\log \eta$ [η in Pa · s]	run	T [K]	$\log \eta$ [η in Pa · s]	run	T [K]	log [η in Pa · s]
1	834	12.75	1	715	12.04	1	615	11.07	1	534	12.45
	839	12.46		720	11.81		625	10.66		539	12.09
	844	12.22		725	11.56		615	11.15		534	12.29
	849	12.00		730	11.35						
	853	11.71		716	11.86	2	607	11.62	2	546	11.11
	859	11.46					612	11.42		556	10.65
	864	11.23	2	704	12.75		607	11.73		546	11.23
	869	11.01		715	12.13						
	874	10.80		720	11.84						
	879	10.60		725	11.59						
				730	11.37						
2	837	12.57		716	12.02						
	847	12.13									
	857	11.61	3	707	12.52						
	866	11.12		717	12.04						
	876	10.69									
			4	708	12.37						
				723	11.74						
				733	11.30						
A_{vis}	-29.8 ± 0.5			-23.2 ± 1.7			-25.2 ± 3.7			-35.5 ± 5.0	
$B_{vis} \times 10^{-4}$	3.55 ± 0.04			2.52 ± 0.12			2.24 ± 0.22			2.55 ± 0.27	
T_{12}	850			716			600			538	

Notes. A_{vis} and B_{vis} are the Arrhenian parameters derived from the equation $\lg(\eta) = A_{vis} + B_{vis} / T$. T_{12} is the isokom temperature (see text for details).

3.3 Results

3.3.1 Glass transition temperature

Results of T_g and T_f determination are already reported in Bauer et al. [52] but are discussed here in more detail in view of relaxation processes in the glasses. Although heating and cooling rates during DTA are smaller than the quench rates applied during synthesis, significant difference between the fictive temperature T_f and the glass transition temperature T_g was only observed for sample NBS5 with 20 K lower value for T_f (table 3.2). The good agreement of the data is probably due to the relatively small differences in the cooling/heating rates by at most a factor of 5

(except for the rapidly quenched sample NBS8), and to effects of fictive pressure. While the isobarically quenched synthesis products represent a fictive pressure of 500 MPa, during the first upscan of DTA the glasses are relaxed to ambient pressure. Increasing fictive pressure shifts the onset of enthalpy relaxation towards higher temperature [78]. This counteracts the effect of faster cooling after synthesis compared to heating during DTA.

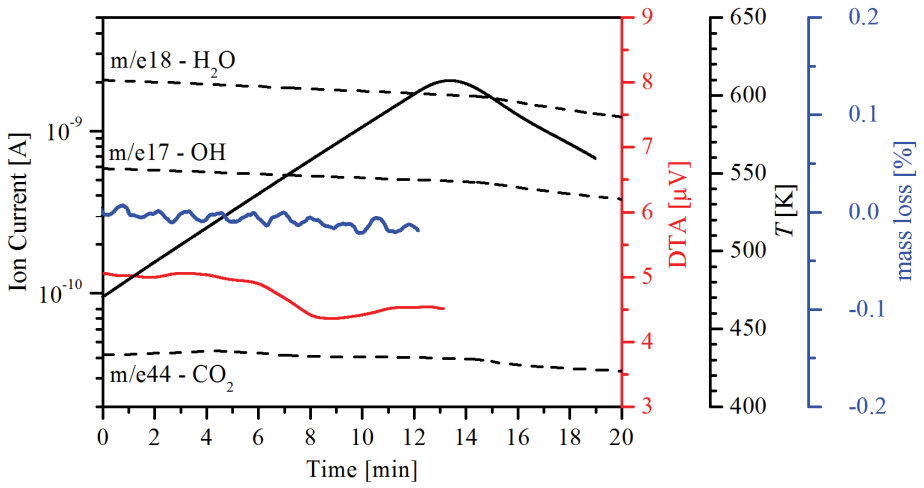

Figure 3.1: Records of DTA-TG-MS measurements on sample NBS5. The solid red line is the DTA signal showing the onset of the glass transition endotherm upon ca. 6 min of heating which corresponds to a T_g of 529 K. Black dashed lines show the ion currents of the mass channels m/e17 (OH), m/e18 (H_2O) and, for comparison, m/e44 (CO_2) during DTA measurement (red line). The solid black line represents the temperature evolution during experiment, and the blue line represents the mass change of the sample during the analysis.

No significant change in sample mass was observed for the hydrous sample NSB5 even for temperatures exceeding 600 K, i.e. 50 K higher than the measured T_g (figure 3.1). In addition, the simultaneously recorded ion currents for the masses 18 (H_2O) and 17 (OH) show no changes during DTA measurement. Both results give evidence for negligible water loss during heating. The very good reproducibility of T_g values determined from three heating cycles supports this statement.

3.3.2 Viscosity

The viscosity of anhydrous and hydrous NBS glasses with water contents up to 5 wt% H_2O was measured in the range of $10^{10.60}$ - $10^{12.75}$ Pa·s. An

example of an experimental record of temperature and viscosity is shown in fig. 3.2 for a run with NBS5c at temperatures just above T_g. Only a small increase in viscosity of ~0.1 log units between the first and the last temperature step ($T_I = T_{III}$) has been observed, indicating that only a marginal amount of water was lost during the viscosity measurement on this water-rich sample.

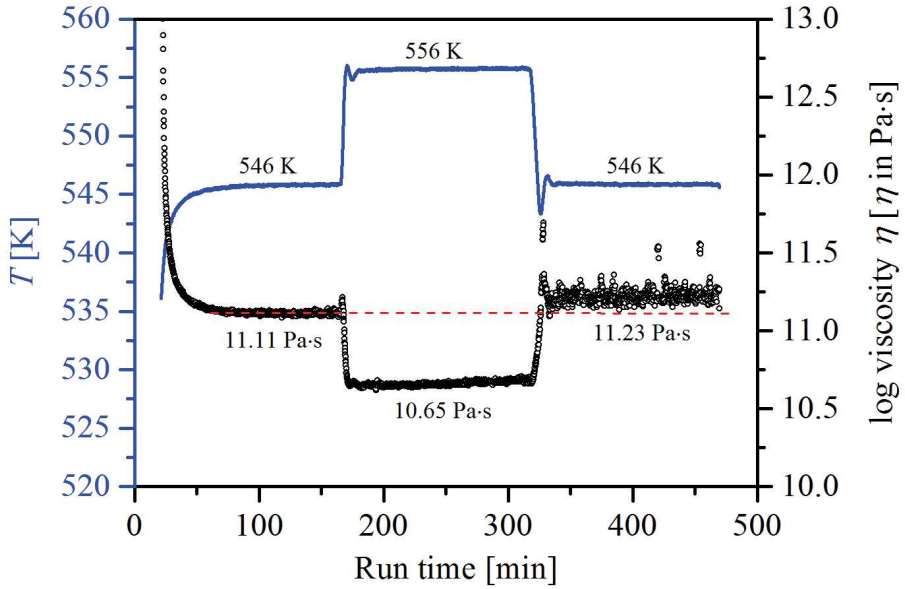

Figure 3.2: Sphere penetration experiment of NBS5c. The temperature is marked with a blue line (left ordinate) Temperatures of the steps I, II, and III are 546 K, 556 K, and 546 K, respectively. The corresponding viscosities (11.11 Pa · s, 10.65 Pa · s and 11.23 Pa · s) are marked with black dots (right ordinate). The red line is intended as visual guide to facilitate the comparison of viscosities between the first and last temperature step.

Data for two samples of NBS1 processed in four measurement series are in perfect agreement (table 3.2, figure 3.3). For instance, the viscosity in the first run is $10^{11.35}$ Pa · s at 730 K, $10^{11.37}$ Pa · s at 730 K in the second run, and $10^{11.30}$ Pa · s at 733 K in the last run. These data demonstrate high reproducibility of measurements and confirm absence of water loss during high temperature treatment of water-poor glasses. The dependence of viscosity on temperature is presented in figure 3.3. The largest temperature range was probed with the anhydrous NBS glass. Within this T-range the data are well described by an Arrhenian equation

$$log(\eta) = A_{vis} + \frac{B_{vis}}{T}, \tag{3.2}$$

The number of data points and the T-ranges are smaller for hydrous samples, but straight line behavior is evident also in these cases. The Arrhenian parameters A_{vis} and B_{vis} as well as the derived T_{12} data of the measured samples are given in table 3.2.

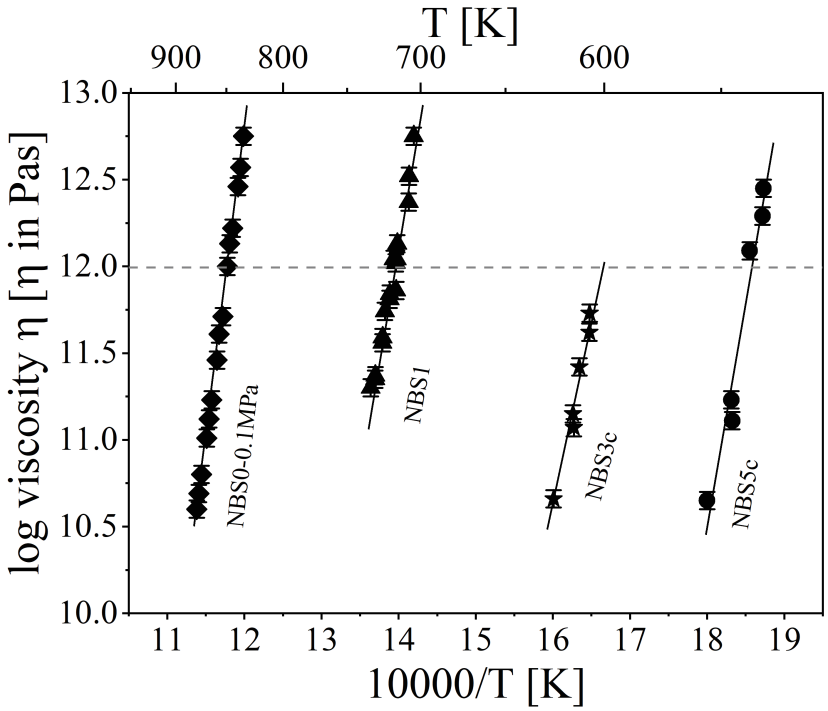

Figure 3.3: Viscosity vs. reciprocal temperature of hydrous and anhydrous NBS glasses. Solid lines are the best linear fit of eq. 3.1 through the data. The dashed line is intended for the determination of the isokom temperature T_{12} for which the Newtonian viscosity is 10^{12} Pa $\cdot$ s ($T_{12} \approx T_g$).

3.3.3 Internal friction

Figure 3.4 shows the smoothed mechanical loss spectra of a nominal dry NBS glass and glasses containing between 0.23 and 4.70 wt% H_2O. The figure exemplary shows internal friction data for $f = 7.125$ s^{-1}. Although slightly shifted in temperature, data for other frequencies were similar in shape and are not shown here. As already mentioned, the maximum of the α-relaxation peak is not accessible by the experimental technique, and only its low temperature flank can be probed. Nevertheless, a shift of the α-relaxation peak towards lower temperature upon hydration is evident, consistent with DTA and viscosity measurements.

In the spectrum of the nominally dry sample NBS0-0.1MPa a sub-T_g

relaxation peak at ~313 K can be seen. With the addition of water, this peak slightly shifts towards higher temperatures and decreases significantly in its height until it diminishes at 0.50 wt% H_2O. On the other hand, a broad shoulder develops at 650 K after the addition of 0.23 wt% H_2O (figure 3.8). The height of this relaxation mode increases and the peak shifts towards lower temperature with further addition of water.

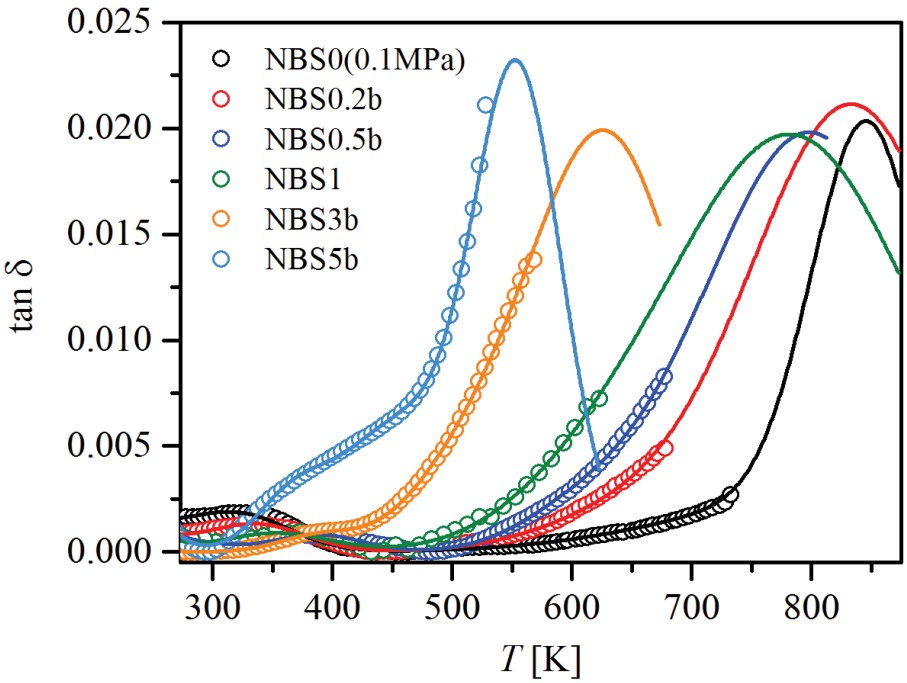

Figure 3.4: Mechanical loss (tan δ) as a function of temperature for $f = 7.125$ Hz for the uncompressed nominal dry and hydrous NBS glasses. Symbols represent the measured data points. The cumulative fit curve is shown for better visualization (solid lines). See also figure 3.7 for better resolved spectra.

3.4 Discussion

3.4.1 α-relaxation mechanism in oxide glasses

T_g measured by DTA and the isokom temperature T_{12} derived from sphere penetration viscometry are in very good agreement (figure 3.5). For comparison T_g and T_{12} data of different silicate [79], [80], borate [50], and aluminosilicate glasses [80]–[83] are shown in figure 3.5. The latter ones are particularly suitable for comparison with borosilicate glasses

due to structural similarities. In aluminosilicate glasses with sufficient alkali and alkaline earth elements for charge compensation, aluminum is predominantly coordinated by four oxygens. Only minor amounts of five-fold and six-fold coordinated aluminum have been detected by NMR spectroscopy in virtually completely polymerized glasses, such as albite or anorthite (25 CaO, 25 Al_2O_3, 50 SiO_2 mol%) glass [72]–[75], [84]–[87]. With the addition of water, aluminum is still preferentially tetrahedrally coordinated, and only a minor increase of higher coordinated Al species has been found [84], [85], [87], [88]. As in the case of aluminosilicate and boroaluminosilicate glasses silicon favors strongly the four-fold coordination state in borosilicate glasses, regardless of the added water [49], [88]–[90]. In contrast, a considerable change in boron coordination by hydration was observed for borosilicate glass [52]. In anhydrous NBS glass 88% of the boron is tetrahedrally coordinated. After the addition of 3 wt% H_2O basically all three-fold coordinated boron is transformed into four-fold coordination.

The effect of H_2O on T_g for NBS is very similar to another alkali-rich silicate glass, phonolite, [81] as indicated by the nearly parallel trends in figure 3.5. A stronger initial decrease of T_g upon hydration is visible for albite and rhyolite glasses compared to phonolite glasses. As discussed in Bouhifd et al. [81] and previous studies on the effect of water on aluminosilicate glasses e.g. [76], [77], the influence of water is more pronounced on polymerized glasses than on glasses already containing some non-bridging oxygen (NBO). This is easy to explain by the relative change in the abundance of broken T-O-T bonds with addition of water. For polymerized melts containing already 1 - 2 wt% H_2O, the effect of further addition of water on viscosity and glass transition temperature becomes similar to depolymerized melts.

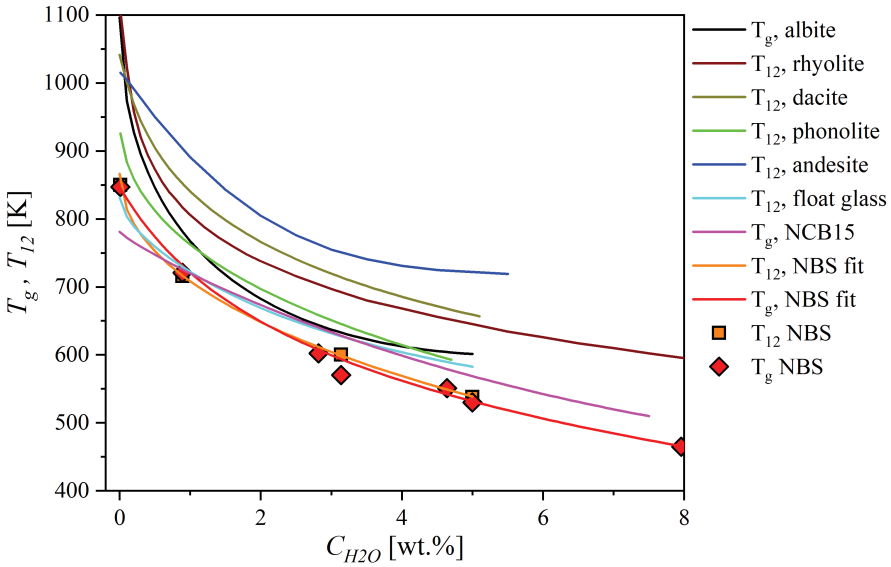

Figure 3.5: Dependence of the glass transition temperature on water content for silicate, aluminosilicate, borosilicate and borate glasses. T_g refers to results of DTA measurements, T_{12} was calculated from viscosity data. Lines represent calculations by viscosity equations for rhyolite and andesite, and trends based on experimental data for other compositions: albite [81], rhyolite [80], dacite [83], phonolite [81], andesite [82], float glass [91], NCB15 [50]. Albite, rhyolite, dacite, phonolite, and andesite are synthetic multicomponent aluminosilicate glasses of compositions representing those of natural igneous rocks. Chemical compositions of the anhydrous glasses are given in table 3.3).

The degree of depolymerization in glasses is often expressed by the ratio of non-bridging oxygen over tetrahedra cations (NBO/T). NBO/T of the glasses considered here is calculated considering the content of network modifier oxides (Na_2O + CaO + K_2O + MgO) and all network forming oxides (SiO_2, Al_2O_3, B_2O_3) and refers always to dry composition. For simplicity we assume for silica-rich glasses that all boron is 4-coordinated. Then, NBO/T is given as NBO/T=2·((*Na*$_2$O + K_2O + MgO + CaO) - (Al_2O_3 + B_2O_3))/ (SiO_2 + 2·*Al*$_2$O$_3$ + 2·B_2O_3). Data are included in table 3.2. Glasses containing significant amounts of iron (»1 wt%) are not considered due to the complex structural role of ferrous and ferric iron making an assignment to network former and network modifier ambiguous.

Table 3.3: Compositions of glasses reported in figure 3.5 (in mol%).

	NBS	albite	rhyolite	dacite	phonolite	andesite	float glass	NCB
SiO_2	74.03	75.30	82.78	69.49	65.40	62.46	71.39	
TiO_2			0.07	0.43	0.66	0.02	0.00	
Al_2O_3		12.07	8.07	12.67	12.72	13.41	0.44	
B_2O_3	9.97							74.71
FeO_{tot}			0.90			0.05	0.07	
MgO			0.05	3.74	3.10	8.65	5.79	
CaO			0.60	7.60	2.80	10.73	9.52	10.33
Na_2O	16.00	12.62	4.17	4.94	10.04	3.48	12.62	15.18
K_2O			3.36	1.14	5.28	1.20	0.16	
NBO/T	0.13	0.01	0.00	0.10	0.19	0.24	0.76	n.d.
Reference	[52]	[81]		[83]	[81]	[82]	[91]	[50]

n.d. = not defined

Data of dry albite glass [81] and rhyolite glass [80], which are completely polymerized (NBO/T $\approx$ 0), show a very steep decrease of the glass transition temperature at low water content but only a smooth dependence at high water contents. Slightly depolymerized systems (dacite, NBO/T = 0.10 [83]; phonolite, NBO/T = 0.19 [81]; andesite, NBO/T = 0.24 [82]) are initially less sensitive to addition of water while at high water contents the evolution with water content is rather similar to polymerized melts. It is worth noting that hydrous albite and rhyolite melts have even lower T_g than dacite and andesite melts with the same water content, pointing to a strengthening role of alkaline earth elements in the melt. The trend for NBS glass (NBO/T=0.13) fits well to aluminosilicate glasses.
At water contents >0.1 wt% the dependence of T_{12} on H_2O content is much weaker for float glass than for aluminosilicates and borosilicates, consistent with the high NBO/T of 0.76 [91]. At very low water contents there appears to be a stronger effect of water on float glass, but data show a relatively large scatter, probably due to uncertainty in water determination. The glass transition temperature of soda lime borate glass varies only slightly with water content in the whole H_2O range. This can be explained by weak B-O-B connections in borate glasses, resulting in already low viscosity in the anhydrous melt.

3.4.2 Effect of glass composition and water speciation on network depolymerization

The type and the species of the network forming cations, as well as the initial degree of polymerization are important parameters for the evolution of depolymerization upon hydration (see previous section). Another parameter influencing the depolymerization of hydrous glasses is the water species distribution. In contrast to water molecules, formation of hydroxyl group strongly decreases network connectivity. The stabilization of hydroxyl groups or molecular water depends strongly on the composition of the oxide glass system. OH groups dominate only at water contents ≤4 wt% in silicate [92] and aluminosilicate glasses [49], [93]. Boron strongly supports formation of hydroxyl groups in the glasses [49], [50]. For instance, 80% of the dissociated water species and only 20% molecular water are present at 8 wt% H_2O in soda lime borate glasses [50].
A three-component model to compare and to quantify the individual contributions of OH groups, molecular water and the dry glass on T_g was proposed by Tomozawa et al. [51]. Based on this model T_g of different glass compositions were compared in the study of Deubener et al. [40] using the reduced glass transition temperature $T_g^* = \frac{T_g}{T_g^{GN}}$, where T_g^{GN} is the glass transition temperature for a nominal dry glass containing 0.02 wt% total water:

$$T_g^* = \frac{1.01 \cdot c_G + 0.22 \cdot A_{OH} \cdot c_{OH} + 0.22 \cdot B_{H_2O} \cdot c_{H_2O_{mol}}}{c_G + A \cdot + c_{OH} + B_{H_2O} \cdot c_{H_2O_{mol}}}, \qquad (3.3)$$

where c_G, c_{H2Omol} and c_{OH} denote the weight fractions of anhydrous glass, of molecular water and of water dissolved as OH groups, respectively. Parameters A_{OH} and B_{H2O} describe the influence of hydroxyl groups and molecular water on the reduced glass transition temperature, respectively. T_g* data for various compositions plotted in Ref. [40] show large variation which reflect compositional effects but may be affected also by differences in water speciation measured on glasses at room temperature compared to the equilibrium speciation at T_g. In order to evaluate composition

effects on parameter A_{OH} and B_{H2O}, we consider only glasses, for which equilibrium concentrations of hydrous species could be calculated for T_g. The water speciation reaction can be expressed as [94]

$$H_2O_{(m)} + O_{(m)} = 2OH_{(m)}, \tag{3.4}$$

where O represent all network oxygen, i.e. all oxygen which is not bound to hydrogen and m denotes the melt state. Assuming ideal mixing of the H_2O, O, and OH species, the equilibrium constant K for the above reaction is

$$K = \frac{[OH]^2}{[O] \cdot [H_2O]}, \tag{3.5}$$

where brackets signify mole fractions of the species on a single oxygen basis [95]. The temperature dependence of K can be expressed by [95]

$$lnK = A_{ws} - \frac{B_{ws}}{T}, \tag{3.6}$$

where A_{ws} and B_{ws} are specific parameters for each melt composition. In table 3.4 the constants for eqn.(3.5) are summarized for the compositions of interest in our study. For rhyolite, different water speciation data are reported in literature, see [95]. In our calculations of T_g^* we have used the data based on in situ infrared spectroscopy of a simple rhyolite melt published in [96]. For albite and dacite, water speciation equations from [97] and [98] have been applied. New equations calculated for andesite, NBS, float glass and soda lime borate glass NCB15 are also reported in table 3.1. These equations were derived with the assumption that water speciation measured in glasses at room temperature represents the equilibrium speciation in the melt at the fictive temperature T_f of the glass [95]. For NBS and NCB15 T_f was directly measured by DTA. For andesite and float glass T_f was derived from viscosity-temperature relationships. According to Scherer [99] the melt is frozen in during quench at a specific viscosity depending on the cooling rate q of the experiment ($\log \eta = 11.3 - \log q$). The procedure is described in [95].

Table 3.4: Water speciation in melts, T_g determinations and results of T_g^* modeling using eqn. (3.2).

Composition	NBO/T	Water speciation ln K (eqn. 3.5)	Water speciation T range (K)	T_g	Data sources	T_g^* modelling (eqn. 3.2) A_{OH}	B_{H2O}	Ref.
albite	0.01	3.51 - 4065	/T 709 - 892	DSC	[81], [97]	86.2 ± 1.9	4.0 ± 1	this study
rhyolite	0.00	3.33 - 4210	/T 773 - 1073	Visc	[80], [96]	64.9 ± 1.7	3.4 ± 1	this study
dacite	0.10	2.88 - 3567	/T 753 - 863	Visc	[83], [98]	40.9 ± 2.0	2.5 ± 2	this study
NBS	0.13	2.14 - 1805	/T 465 - 722	DTA	this study	26.8 ± 1.9	7.1 ± 3	this study
andesite	0.24	3.86 - 4355	/T 749 - 911	Visc	Behrens unp. data, [82]	19.8 ± 0.8	0.0	this study
float glass	0.76	8.81 - 7091	/T 596 - 760	Visc	[91], [92]	23.4 ± 1.3	7.7 ± 1	this study
						22.9 ± 1.1	6.9 ± 1	[91]
soda-lime borate	n.d.	2.05 - 580	/T 509 - 675	DTA	[50], [100]	11.4 ± 0.2	0.0	this study
NCB15						11.7	1.8	[100]

Notes. NBO/T represents the nominal anhydrous glass. The B_{H2O} parameter is statistically not constrained. Fitting is sufficient with the A_{OH} parameter only. n.d. = not defined.

Figure 3.6a shows the reduced glass transition temperature as a function of the water content for selected silicate, borate, aluminosilicate and borosilicate glasses. A shift towards higher water contents with increasing melt depolymerisation is visible at intermediate T_g* values. For each glass composition, parameters A_{OH} and B_{H2O} were determined by fitting to eqn. (3.2). Fit parameters for float glass and soda lime glass based on water speciation calculated for T_g do not differ significantly from previous evaluation based on water speciation measured on the glasses. This demonstrates that the variations which can be seen in fig. 3.6a and b mainly originate from compositional effects and are not significantly affected by the fictive temperature. Fitting indicates that molecular water has little to negligible effect on T_g* for all glasses (table 3.4). An average of 3.7 ± 3.0 is obtained for the B parameter considering all data in table 3.4.

A systematic non-linear variation of the A_{OH} parameter as a function of NBO/T is evident from figure 3.6b with a strong increase of A with decreasing NBO/T below 0.20 and a roughly constant value of A_{OH} in the NBO/T range of 0.2 - 0.8. Thus, for aluminosilicates, borosilicates and silicates with intermediate degree of depolymerization the effect of water species on depression of T_g* can be estimated using $A_{OH} = 21$ and $B_{H2O} = 3.7$. However, data for other compositions are required to verify this trend.

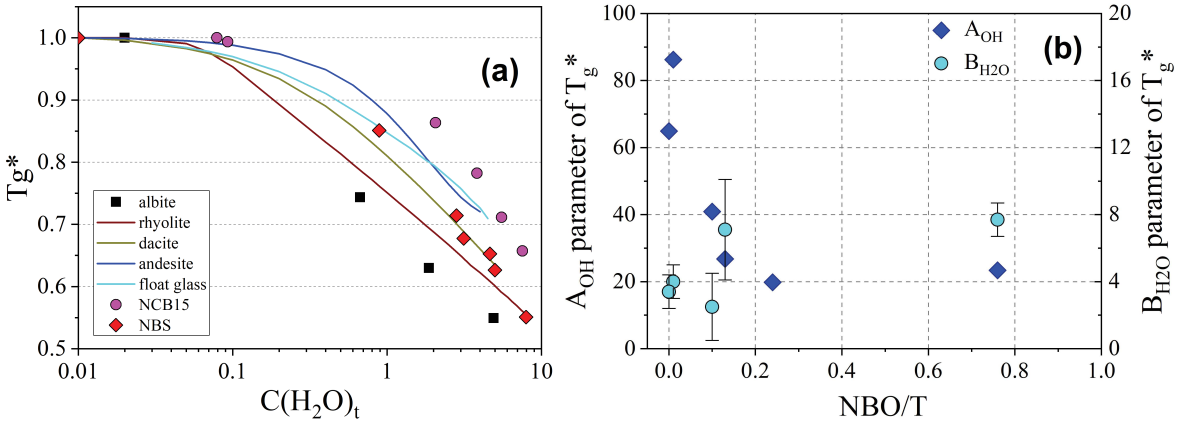

Figure 3.6: a) Reduced glass transition temperature T_g*=T_g/ T_g^{GN} vs. water content for selected oxide glasses. The weighting parameters A_{OH} and B_{H2O} for the determination of the reduced glass transition temperature and corresponding literature are listed in table 3.4 for the different compositions. b) Parameter A_{OH} and B_{H2O} in eqn.(3.2) vs. degree of depolymerization expressed as NBO/T. B_{H2O} is roughly constant in the NBO/T range of 0.13 – 0.77.

It is worth noting that the trend for silica-rich compositions cannot be transferred to borate glasses. NCB15 has a molar composition of 15 Na_2O – 10 CaO – 75 B_2O_3, and negligible NBO is present in the glass [44]. However, the A_{OH} value is very low with 11.4 ± 0.2, a consequence of weak B-O-B bonds in the glasses.

3.4.3 Effect of H_2O on internal friction

In order to separate contributions of different relaxation mechanisms, the mechanical loss spectra were deconvoluted into Gaussians as shown in figure 3.7. Gaussians have been chosen for fitting for the sake of simplicity and because of the smooth and broad temperature dependence of relaxation, which would not allow fitting more complicated models. In all cases three Gaussians were sufficient to reproduce the spectral features.

The peak at highest temperature is assigned to the α-relaxation [43], [55], [58], i.e. the structural relaxation at the glass transition. Due to technical difficulties, the α-relaxation peak is only poorly constrained by experimental data points. Because of the frequency dependence of α-relaxation, the temperature of the peak maximum, T_α, cannot be simply approximated by the T_g values listed in table 3.1. Knowledge of the shear

modulus (G_∞) would be required for an estimation of T_α from T_g (see [29]) but this value is not known for the NBS glasses. In the study on soda-lime silicate glasses Reinsch et al. [29] found that T_α is ca. 40 K higher than T_g at a frequency of $f = 7.125$ Hz. As an approximation, this relationship was used as a constraint for fitting of the α-peaks of NBS glasses. A second constraint in fitting of the α peaks was the assumption of similar peak heights (figure 3.4), following the schematic representation of internal friction peaks in alkali silicate glasses of Brückner [55].
We are aware that this fitting procedure induces an uncertainty in the determination of the temperature and peak height, especially for the β-mode, which appears as a shoulder of the α-relaxation. In order to estimate the influence of the evaluation method we compared two different approaches with different peak heights and temperatures of the α-relaxation mode for a water-rich (NBS5b) and a water-poor (NBS0.5b) sample. Peak height/temperature combinations were 0.05/590 K and 0.02/553 K for NBS5b, and 0.03/843 K and 0.02/798 K for NBS0.5b. For both water contents neither the height nor the temperature of the α-peak was found to have noticeable effect on the sub-T_g modes.
The low temperature peak at ~313 K in the dry NBS glass is attributed to γ-relaxation which is in line with internal friction measurements on different silicate glasses [55], [73], [101]. Its shift towards higher temperature and its decrease in height with the addition of water is consistent with observations on hydrous soda-lime silica glass [29] and sodium silicate glass [69]. Based on these trends, this γ-peak seems to disappear at > 1 wt% H_2O (see figure 3.8). A second sub-T_g relaxation peak at ≈650 K is clearly visible for the NBS glass with 0.23 wt%. Confirming the study of Reinsch et al. [29] on hydrous soda-lime silica glass and findings reported in the review of Day [58], this peak is attributed to a water induced β-relaxation process. Its height increases whereas its maximum temperature decreases with increasing water content (figure 3.8).
At 3 wt% water a new peak appears at similar temperature at which the γ-relaxation peak is observed in the spectra of water-poor glasses.

With increasing water content the height of this peak increases while its position shifts to lower temperature (figure 3.8), consistent with trends observed for β-relaxation peaks [58]. In the study of Reinsch et al. [29] on soda-lime silicate glasses a single β-relaxation peak was observed at water contents up to 0.24 wt%, and a second peak arises at water contents >1 wt%. The peak at higher temperature was attributed to OH groups (β_{OH}) and the one at the lower temperature flank to a mode related to molecular water (β_{H2O}). In the case of soda-lime silicate glasses it can be clearly distinguished between these two β-relaxation modes, whereas in the mechanical loss spectra of the NBS glasses in this work we observe only one broad β-relaxation peak at water contents <3 wt% (blue dashed line in fig. 3.7). Only upon further water addition it is possible to identify a second β-relaxation mode (3 wt% and 5 wt% H_2O in figure 3.7, dashed green line) and, consistent with [29], we attribute this mode to β_{H2O}.

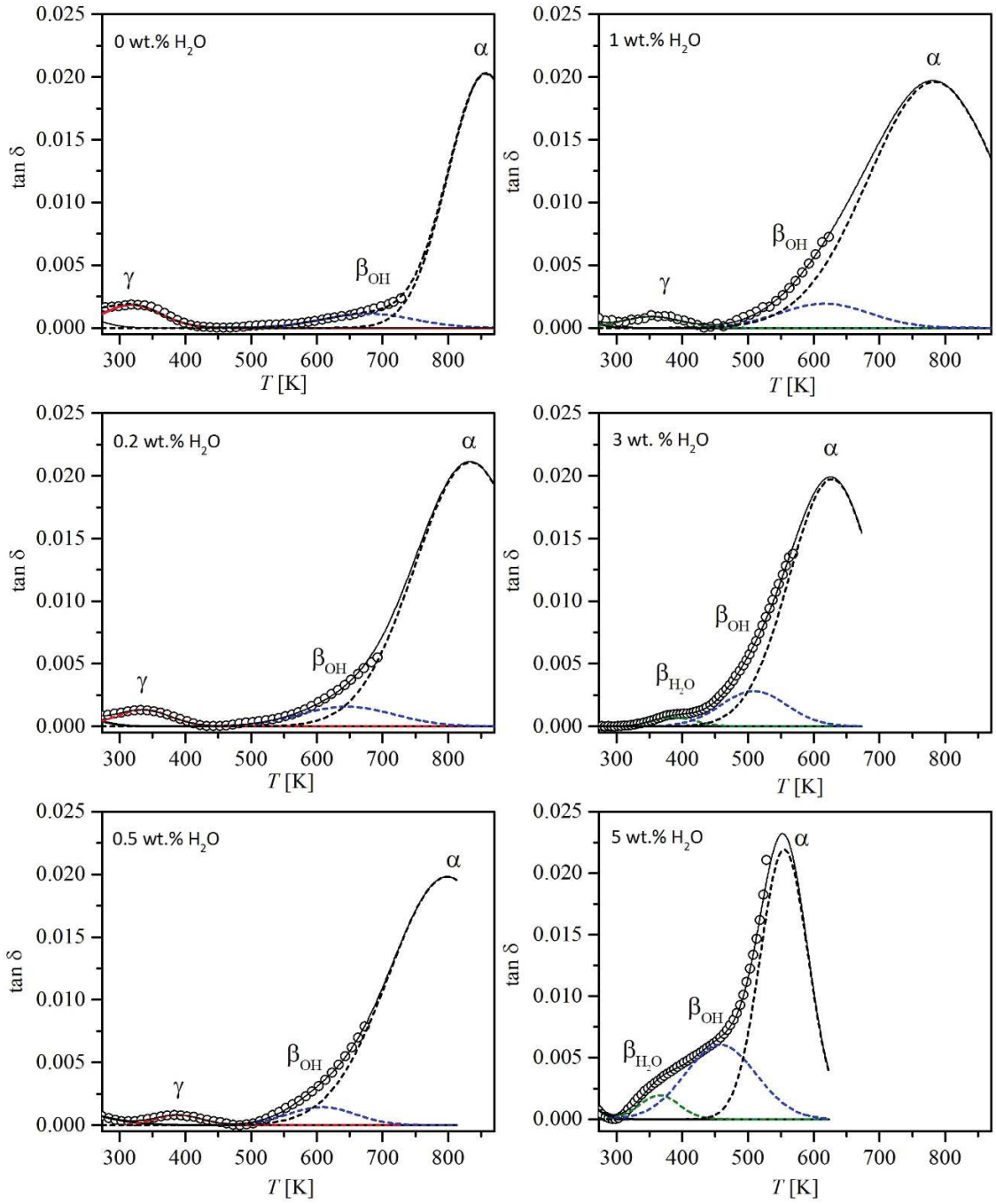

Figure 3.7: Deconvoluted mechanical loss spectra of anhydrous and hydrous NBS glasses at $f = 7.125$ Hz. Note the disappearance of the γ-peak above 0.5 wt% H_2O and the appearance of a second β-relaxation mode in NBS3b (see text for details). Color code for fitting curves: black – α; blue – β_{OH}, green – β_{H2O}; red – γ.

The derived peak heights as well as the peak temperature positions of the relaxation modes are plotted as a function of the total water content in figure 3.8a,b. The temperature of the β_{OH}-peak moderately decreases upon hydration. The trend is similar to the α-relaxation peak but less pronounced. At the same time the intensity of the β_{OH}-peak increases due to the increasing amount of OH groups in the glasses. The most pronounced increase is observed from 3 to 5 wt% H_2O (figure 3.8b). In this range of water contents, the β_{H2O}-mode appears, shifts slightly towards lower temperature and rises in height. In contrast, the γ-relaxation peak shifts strongly to higher temperature and decreases in intensity until it diminishes at ca. 1 wt% H_2O.

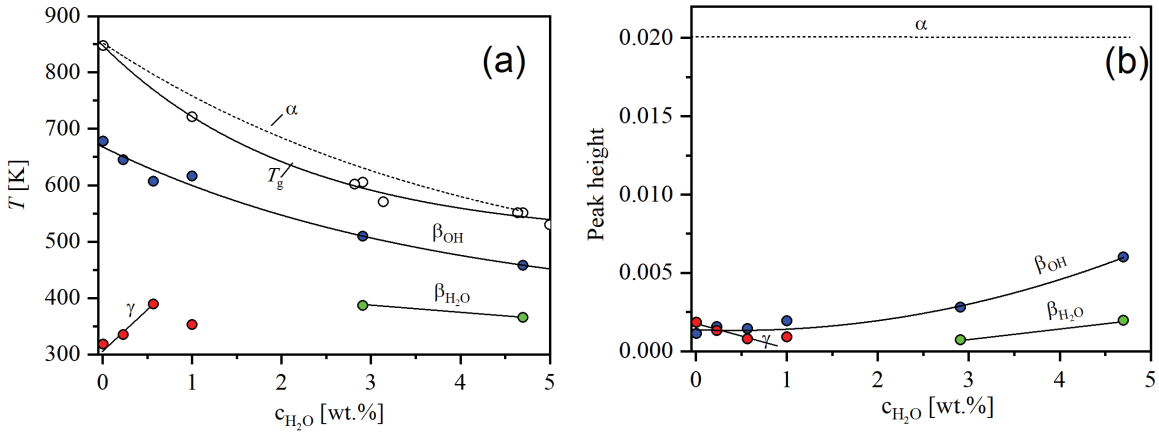

Figure 3.8: Temperature (a) and height (b) of DMA relaxation peaks (α, β_{OH}, β_{H2O}, and γ) vs. water content for f= 7.125 Hz. The dashed line illustrates the estimated peak temperatures and heights for the only partially measurable α-relaxation mode (see text for details). Lines are intended as visual guides. For comparison T_g values determined with DTA are presented in (a) for NBS glasses with similar water contents (open circles, NBS3 and NBS5, see table 3.1).

The derived data supports the assignment of the relaxation modes in the study of Reinsch et al. [29] and is consistent with the evolution of water species distribution in the NBS glasses [52]. OH groups are the dominating water species up to 7 wt% H_2O. Significant amounts of molecular water are first present at 3 wt% H_2O and increase strongly between 3 and 5 wt% H_2O. The newly appearing peak assigned to β_{H2O} may be caused by molecular water itself or by a cooperative movement with sodium comparable with relaxation modes in mixed alkali silicate glasses [43].

3.5 Conclusions

Different relaxation mechanisms are operative in oxide glasses, depending on composition and temperature. Water plays a particular role in these processes since it strongly enhances network relaxation and, thus, reduces glass transition temperatures. The three-component model proposed by Tomozawa et al. [51] and modified by Deubener et al. [40] is suitable to describe the influence of water species on the reduced glass transition temperature, T_g^* . While the parameter B_{H2O}, which weighs the influence of molecular water in the model, is small and roughly constant for a variety of glass compositions, the parameter A_{OH}, describing the influence of OH groups, depends strongly on composition, i.e. for highly polymerized silicate systems. At intermediate degree of polymerization a constant value of A_{OH} of 21 can be used to estimate T_g of hydrous silicate, borosilicate and aluminosilicate melts. However, it should be noted that this approach cannot be applied to oxide glasses with weak intertetrahedral bonding, e.g. borate glasses, for which the A_{OH} parameter is noticeably smaller. As shown by internal friction measurements, water not only affects the so called α relaxation but also the low temperature sub-T_g relaxation modes, which become more pronounced in sodium borosilicate glasses with increasing water content. Using water speciation data, these modes were assigned to β-relaxations involving OH groups and H_2O molecules. In water-rich glass regions, water induced β-relaxation processes can occur even close to room temperature. This may have implications for understanding the mechanisms of subcritical crack growth, i.e. water-related relaxation mechanisms may play a crucial role at crack tips and affect the velocity of crack propagation. Since β-relaxation mechanisms are operative even at room temperature in water-rich glasses, we expect major contributions of such processes to aging and fatigue of glasses, at least in near-surface regions of glasses being subject of hydration.

4

Density, elastic constants and indentation hardness of hydrous soda-lime-silica glasses

P. Kiefer[a], R. Balzer[b], J. Deubener[a], H. Behrens[b], T. Waurischk[c], S. Reinsch[c], R. Müller[c]

[a]Clausthal University of Technology, Institute of Non-Metallic Materials, 38678 Clausthal-Zellerfeld, Germany

[b]Institute of Mineralogy, Leibniz University Hannover, 30167 Hannover, Germany

[c]Federal Institute of Materials Research and Testing (BAM), 12489 Berlin, Germany

Abstract

The effect of structural water on density, elastic constants and microhardness of water-bearing soda-lime-silica glasses of up to 21.5 mol% total water is studied by buoyancy, ultrasonic echography and Vickers indentation. It is found that the Poisson's ratio and the water content are positively correlated, while density and the elastic moduli decrease with increasing water content. In parallel to the elastic moduli, Vickers hardness decreases by approximately 27% from the dry to the most hydrous glass. For small water fractions (< 3 mol%), the dependencies are non-linear reflecting the non-linear change in the concentrations of OH and H_2O molecules dissolved in the glass structure, whereas for higher water fraction linear dependencies are found. According to the concept of partial molar properties, water in the glass structure is mechanically soft and quasi incompressible with a Poisson's ratio close to 0.5. To distinguish the effect of structural water and environmental water, indentations were performed in toluene, nitrogen gas and air. Time-dependent softening was evident for testing dry glasses in humid atmospheres as well as for tests of hydrous glasses in dry atmospheres. The results indicate that the response times of dissolved water species are effectively equal in both scenarios.

4.1 Introduction

Water is a common trace constituent of conventional soda-lime-silica glasses that enters into the network structure when melted in atmospheres containing steam [102]. In industrial glasses the total water content is typically assumed to be 40 mol water per m^3 melt for air-gas-fired glass furnaces and >70 mol water per m^3 melt for oxygen-gas fired furnaces, i.e. 0.03-0.05 wt% [103], [104]. Using an electrical resistance furnace for melting in air, which complies with standard laboratory conditions, a slightly lower water content is reported (on average 0.02 wt%) [40]. The dissolution of water into the glass melt can be formally described on basis

of the reaction between a bridging oxygen of the glassy network with a H_2O molecule of the steam forming two OH groups in the melt [94]. Thus, the total dissolved water content under equilibrium conditions is proportional to the square root of the water vapor pressure. The range of concentrations of dissolved water in soda-lime-silica glasses can be slightly broadened by bubbling with dry or wet gases at ambient pressure [105]. On the other hand, several wt% of water can be dissolved in soda-lime-silica melts at high confining pressures [91], [92], [106].
Assuming an ideal behavior of the oxygen-bearing species in the melt, the concentrations of silanol groups (Si-OH), bridging oxygen (Si-O-Si) and water molecules (H_2O) are predicted by the reaction, i.e. Si-O-Si + H_2O = 2 Si-OH. As for liquid silicates the temperature derivative of the reaction constant is generally positive, cooling the glass melt favors formation of H_2O molecules [107]. The resulting H_2O-to-OH ratio is frozen-in at the glass transition, i.e. the corresponding fictive temperature, leading to a higher OH content for rapidly quenched glasses [95]. Evidence for the presence of OH groups and H_2O molecules in the interior of soda-lime-silica glasses comes inter alia from near-infrared spectroscopy [91], [92], [106], low temperature static ^{1}H NMR spectroscopy [92] and dynamic mechanical analysis [29]. In contrast, water speciation is more complex at the surface of soda-lime-silica glasses, as humidity interacts with adsorbed hydrous species and triggers multicomponent diffusion processes of OH-groups, water molecules and counteracting ions, such as Na^+, leading to concentration gradients within a hydrous dealkalized surface region [108]. For hygroscopic sodium silicate glasses a strong decrease in density, Young's modulus and hardness has been reported, which was based on the deleterious effect of water in depolymerizing the glass network and the increased plastic deformability of hydrous glasses at room temperature [38], [109], [110]. While the dependencies in density and in the elastic constants were linear up to a total water content of about 12 wt%, Knoop hardness decreased gradually at first, then proceeded more rapidly, and then gradually again [109]. The effect of water dissolution on physical properties was also studied for natural aluminosilicate glasses [111]–[113]

where the apparent linear dependence in decreasing the molar volume and the elastic moduli with the total water content up to 12–13 wt% was confirmed. These studies show that the effect was independent on water speciation and the connectivity of the silicate network as the partial molar volume of water in silicate glasses was constant with the initial composition of the nominal anhydrous base glass.

In contrast for soda-lime-silica glasses that exceed standard industrial water limits only slightly (< 0.1 wt%) an increase in density and Young's modulus with the concentration of water was reported [37], [114], [115]. Besides the stiffening effect of elastic properties by structural water, indentation hardness was found to be environmentally sensitive [116]–[121]. Surface softening of soda-lime-silica glasses was evident with increasing the holding time of the indent in water-bearing atmospheres whereas in water-free environments such as vacuum, distilled toluene hardness was the highest and constant with the time during which the maximum load was maintained. First, Kranich and Scholze [118], [119] attributed the effect to the elastic recovery of the glass after indentation, as the hardness under load, which was observed through an inverted microscope, was load- and time-independent and practically equal to the hardness measured in liquid water. Later, the effect was reported to occur also during loading [122]. Finally, Tomozawa [123] explained that environmental sensitivity of microhardness originates from diffusion of water molecules from the environment (water content of the test liquid, atmospheric moisture) into the deformed glass volume under the indent. Under tensile stresses, water molecules are capable to relax strained Si-O-Si bonds leading to an compressive surface stress after unloading, that can be used to strengthen soda-lime-silica glass fibers [28] whereas under compressive stresses the effect weakens the surface after indentation. In this approach, however, the role of dissolved water species that are already present in the glass structure remains unclear.

Considering the above issues and the technical importance of soda-lime-silica glass, the influence of dissolved water on the micromechanical properties is still poorly understood. Thus, the main aim of this study

was to explore the effect of dissolved water for concentrations exceeding standard industrial limits and by that to shed light on the role of the different water species in a depolymerized network structure where calcium ions are present to prevent the silicate network to be readily soluble. In particular, density, elastic constants and indentation hardness were studied for a commercial multicomponent soda-lime-silica glass, which was re-melted in a high confining pressure (500 MPa) to enrich the water content up to 7.8 wt%.

4.2 Experimental

4.2.1 Glass preparation

For the syntheses of hydrous glasses containing up to 7.8 wt% water, commercial microscope slides were used. The molar composition of the microscope slide glass (MSG) was $SiO_2/Na_2O/CaO/MgO/Al_2O_3/K_2O/(Fe_2O_3/TiO_2)$ = 73.2/13.3/6.6/6.2 /0.5/0.2/(0+) as analyzed by X-ray fluorescence (Axios, PANalytical). Oxides within brackets present a nominal molar amount <0.05.
The slides were crushed and ground to a powder with an agate mortar. Glass powders and distilled water were filled step-wise in cylindrical platinum capsules of 6 mm diameter and 30 mm length to provide a homogeneous distribution of water in the glass. The water-to-glass powder ratio was calculated to prepare hydrous glasses of nominal total water content of 0, 1, 2, 4, 6, 8 wt%. The powder-water mixtures were slightly compacted with a steal piston and subsequently sealed with a PUK welding device (PUK^3 professional plus, Co. Lampert). All syntheses were carried out in an internally heated pressure vessel (IHPV) using argon as pressure medium at 500 MPa and 1673 K for 20 h. A detailed description of the apparatus is provided in [124]. After isobaric quenching the glasses at an initial cooling rate of approximately 200 K min^{-1}, pressure relieve and removing the platinum mantle, bubble- and crystal-free glass cylinders were obtained. Glass cylinders were then

cut into sections of approximately 1–3 mm thickness for mechanical experiments and approximately 0.3 mm for optical spectroscopy. Surfaces were polished (diamond < 1 μm). The glasses were named accordingly to display the nominal water content in wt% and the synthesis pressure in MPa, e.g., 4W-MSG500 = 4 wt% water, 500 MPa.

4.2.2 Density and molar volume

The density ρ of the glasses was determined at room temperature using the Archimedean buoyancy with water as an immersion liquid. The error of this method (based on repetitive measurements) was $\leq$0.2. The molar volume of the hydrous glasses is calculated using:

$$\overline{V} = \frac{M_{H2O}x_W + M_{MSG}x_{MSG}}{\rho}, \tag{4.1}$$

where M_{H2O} and x_W are the molecular weight and mole fraction of water (OH-groups and water molecules), respectively. M_{MSG} is the molecular weight of nominal dry microscopy slide glass and x_{MSG} its mole fraction.

4.2.3 Water content and water speciation

The total water content C_W was determined by a bulk extraction method (pyrolysis and subsequent Karl-Fischer titration (KFT)). Two measurements of each glass (10–20 mg) were conducted and the data were averaged. In addition to KFT, near infrared (NIR) spectroscopy was used to determine the concentrations of water molecules C_{H2O} and hydroxyl groups C_{OH} in the hydrous glasses. Infrared spectra were recorded with a Fourier Transform Infrared (FTIR) spectrometer (Bruker IFS88, Karlsruhe, Germany) coupled with an infrared microscope (Bruker IR scope II, Karlsruhe, Germany) that is equipped with a mercury-cadmium-tellurium (MCT) detector. For NIR-measurements a tungsten light source and a CaF_2 beam splitter were used. Spectra were recorded in the range of 2,000–11,000 cm^{-1}. Three measurements at different spots of each glass (double polished platelets from top and bottom part of the

prepared cylinder, uncertainty in thickness was ±2 μm) were analyzed and the data were averaged. A detailed description of the KFT and NIR experiments is provided elsewhere [50], [125].

4.2.4 Elastic constants

Room temperature ultrasonic measurements were performed by a pulse-echo method using a pulse-receiver instrument (Echometer 1077 Karl Deutsch). Ultrasonic velocities U_l and U_s were determined from the specimen height h of two parallel faces (1 μm diamond, polished) and the delay time Δt_l and Δt_s between successive signals using 4–12 MHz and 5 MHz transducers for longitudinal (l) modes and for shear (s) modes, respectively [126], [127]:

$$U_l = \frac{2h}{\Delta t_l} \; and \; U_s = \frac{2h}{\Delta t_s}. \tag{4.2}$$

From the ultrasonic velocities elastic constants are calculated by [128]:

$$L = \rho U_l^2, \tag{4.3}$$

$$G = \rho U_s^2, \tag{4.4}$$

$$K = L - \frac{4}{3}G, \tag{4.5}$$

$$E = \frac{9KG}{3K + G}, \tag{4.6}$$

$$\nu_P = \frac{E}{2G} - 1, \tag{4.7}$$

with ρ = density, ν_P = Poisson's ratio and L, G, K and E = longitudinal, shear, compression and Young's modulus, respectively. The error of this method (based on repetitive measurements) was $\leq 0.15\%$ and $\leq 0.25\%$ for the longitudinal and shear ultrasonic velocity, respectively.

4.2.5 Hardness

Glass surfaces were indented with a Vickers diamond under load control at 1.96 N using a universal hardness testing machine (ZwickRoell ZHU2.5, Ulm, Germany). The load was applied within 5 s (loading ramp), held for various times between 1–300 s (holding time) and removed within 5 s (unloading ramp), which results in a nominal (un)loading rate of 0.39 N s^{-1}. The regime was selected on basis of an initial parameter study and led to a crack-free indentation of the MSG glass. The length of the indent diagonals was measured using an inverted microscope (Leica DM-ILM, Wetzlar, Germany) positioned directly below the sample. The microscope was equipped with a 20x objective (Leica N Plan L, Wetzlar, Germany) and a monochrome camera (Pixelink PL-D725MU-T, Ottawa, Canada) to allow for acquisition of images. Diagonals were measured "under load" (during the holding time at which the maximum load was maintained) and after completely unloading the sample. Ten indents per data point were performed to provide statistical significance. Indentation was done in different environments. A first series was acquired in a glovebox (MBraun Labmaster 130, Garching, Germany) in a dry nitrogen gas atmosphere of approximately 300 ppm_v water volume fraction (= 30 Pa vapor partial pressure) at 25 °C. The second series was measured in a cleanroom with a constant humidity of approximately 9300 ppm_v water volume fraction (= 942 Pa vapor partial pressure) at 18 °C. Humidity in the glovebox was monitored with a dew point sensor (Michell Instruments Easydew EA2-TX, Ely, UK) connected to a data acquisition module (Ahlborn Almemo 8590-9, Holzkirchen, Germany). In the cleanroom the monitoring of humidity was carried out with a FHAD462 sensor connected to an Almemo 2470-2S data acquisition module (both Ahlborn, Holzkirchen, Germany). A third series of indents were performed in anhydrous toluene (Sigma Aldrich) of 10 ppm_v H_2O. Vickers hardness is given by [129], [130]

$$H_v = \frac{P}{2.157 \times 10^{-3} a^2}, \tag{4.8}$$

where H_V is Vickers hardness (GPa), P is the applied load (N), and a is the average half diagonal of the indent (μm).

Slides of the base glass and polished sections of the hydrated glasses were stored for approximately 20 days in the dry nitrogen gas atmosphere of the glove box before hardness tests were conducted. Other samples were stored in the cleanroom for the same time before testing under these environmental conditions. N_2 gas stored samples were used for the series of hardness tests performed in liquid toluene.

4.3 Results

4.3.1 Water content and speciation

Figure 4.1A shows the baseline corrected spectra of hydrous MSG glasses in the range of 6000–4000 cm^{-1}. As discussed by Withers and Behrens [93] the choice of baseline is crucial for the spectra evaluation and hence for the determination of the linear molar absorption coefficient.

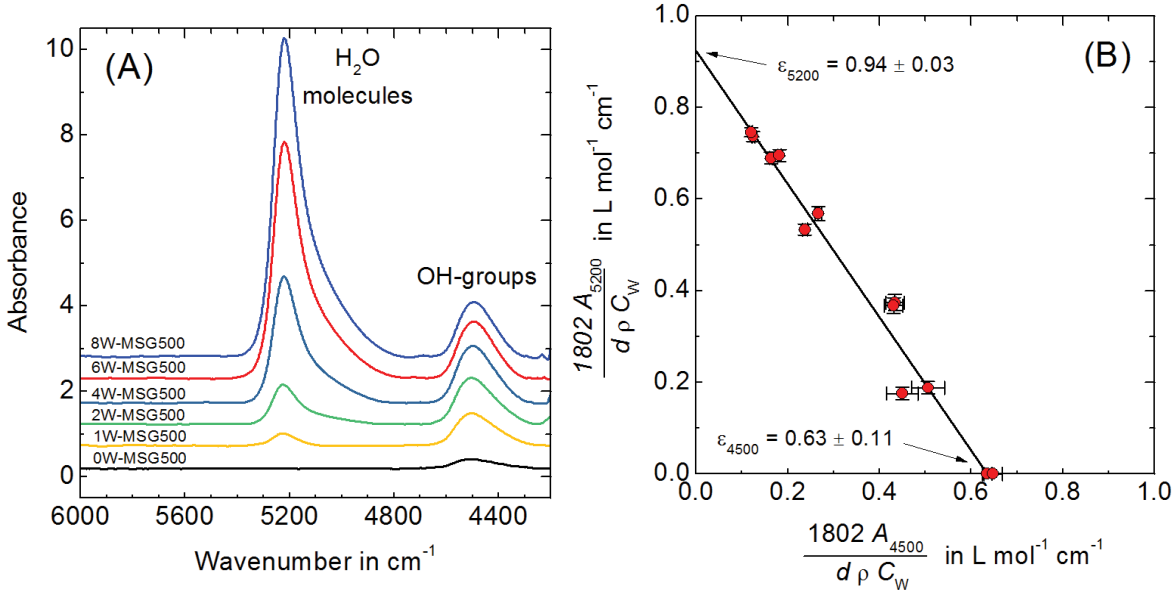

Figure 4.1: Baseline corrected spectra of the hydrated MSG glasses in the NIR range (A) and calibration plot for the determination of the linear molar absorption coefficients of the bands at 5200 and 4500 cm^1 (B). Note that the NIR spectra are scaled to the same thickness of 0.3 mm and plotted with an offset for clarity. The absorption coefficients ϵ_{5200} and ϵ_{5200} were determined from the intercepts with the axes by fitting eq. 4.11 through the data.

For our glasses, we chose a tangential baseline as it revealed the highest reproducibility. The bands near 5200 cm^{-1} and at approximately 4500 cm^{-1} are assigned to the combination of stretching and bending vibration modes of water molecules and of terminal OH-groups (silanols), respectively [95], [114].
NIR spectroscopy requires to transfer measured peak intensities into concentration quantities. Following the Lambert-Beer law, the concentration of the two different water species in wt% from peak height (absorbance, A) are given by [92]

$$C_{H2O} = 1802 \frac{A_{5200}}{d\rho\epsilon_{5200}} \tag{4.9}$$

and

$$C_{OH} = 1802 \frac{A_{4500}}{d\rho\epsilon_{4500}}, \tag{4.10}$$

where ρ is the density (g L^{-1}), d is the thickness (cm), ϵ_{5200} and ϵ_{4500} are the linear molar absorption coefficients (L mol^{-1} cm^{-1}) of bands at 5200 and 4500 cm^{-1}, respectively. If one assumes that the total water content C_W in the hydrous glass is represented by the sum of both contributions, the linear molar absorption coefficients of the OH-band and molecular water band can be derived from combining eqs. (4.9) and (4.10) in form of the linear equation [92]

$$\frac{1802 A_{5200}}{\rho C_W} = \epsilon_{5200} - \frac{\epsilon_{5200}}{\epsilon_{4500}} \times \frac{1802 A_{4500}}{d\rho C_W}, \tag{4.11}$$

where C_W is the total water content as determined by KFT. Figure 4.1B shows that a linear dependence is evident when plotting the right-hand side of eq. 4.11 versus the term 1802 $A_{4500}/(d\rho C_W)$. A regression analysis through the MSG data results in the linear molar absorption coefficients $\epsilon_{5200} = 0.94 \pm 0.03$ L mol^{-1} cm^{-1} and $\epsilon_{5200}= 0.63 \pm 0.11$ L mol^{-1} cm^{-1}, which are similar to those reported by Stuke et al. [92] for soda-lime-silica and float glass applying a similar calibration. Absorption coefficients were used to determine the contents of H_2O molecules C_{H2O} and OH groups C_{OH} from NIR absorbance, density

data and eqs. (4.8-4.9). In case of the dry base glass (0W-MSG0) and its re-melt under 500 MPa confining pressure (0W-MSG500), water is predominately dissolved as OH-groups. Their content was determined from the absorbance near 2850 cm^{-1} and using the linear molar absorption coefficient $\epsilon_{2850} = 50.8$ L mol^{-1} cm^{-1} following the approach developed by Behrens and Stuke [106] (not shown). The spectroscopic data as well as the density of the glasses were compiled in table 4.1.

Table 4.1: Water contents and DTA results of samples used in this study.

Glass	ρ (g L^{-1})	C_W (wt%)	C_{OH}+C_{H2O} (wt%)	C_{OH} (wt%)	C_{H2O} (wt%)	M (g mol^{-1})	x_W	$\overline{V}$ (cm^{-3} mol^{-1})
0W-MSG0	2467(5)	-	0.039(1)	0.039(1)	-	59.131	0.0013	23.84
0W-MSG500	2485(5)	-	0.23(1)	0.23(1)	0.00(1)	58.875	0.0075	23.69
1W-MSG500	2484(5)	1.05	0.98(6)	0.77(6)	0.21(2)	57.888	0.0315	23.30
2W-MSG500	2480(5)	1.75	1.87(6)	1.17(5)	0.70(3)	56.759	0.0589	22.89
4W-MSG500	2451(5)	3.92	3.85(6)	1.52(5)	2.33(6)	54.398	0.1162	22.19
6W-MSG500	2418(5)	5.81	5.90(8)	1.54(3)	4.36(8)	52.153	0.1708	21.57
8W-MSG500	2376(5)	7.77	7.71(9)	1.47(4)	6.24(9)	50.319	0.2153	21.18

Inspection of table 4.1 shows that the IHPV synthesis with an increasing addition of water led initially to an increase in the content of the OH groups, whereas at higher C_W H_2O molecules are predominant. The trends of C_{OH} and C_{H2O} with total water content that are illustrated in figure 4.2 are in agreement with water speciation data of other hydrated soda-lime-silica glasses of previous studies [91], [92], [106]. One should stress here that density and therefore also molar volume of hydrous soda-lime-silica glasses decrease with increasing water content. The dependence will be analyzed in detail in section 4.4.1.

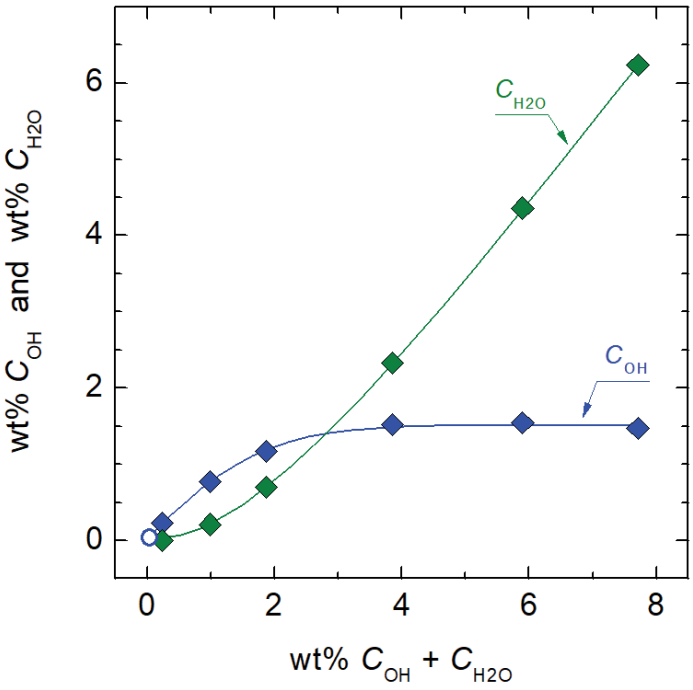

Figure 4.2: Contents of OH groups and H_2O molecules in hydrous soda-lime-silica glass. The error bars of the water species do not exceed the size of the symbols. Symbols indicate synthesis pressure (circle = 0.01 MPa, diamond = 500 MPa). Lines are intended as visual guides.

4.3.2 Ultrasonic velocity

Figure 4.3 shows the dependence of the ultrasonic velocity on the mole fraction of total water. A positive deviation from a linear trend is indicated by the data. The dissolution of water in the soda-lime-silica glass led to a slight increase in the ultrasonic velocity for longitudinal and shear modes at first and then to a continuous decrease for higher water fractions. For instance, the longitudinal velocity of the pressurized re-melt of the anhydrous base glass (0W-MSG500) was 5895 ± 9 m s^{-1}, U_l of the glass with the total water fraction 0.0315 (1W-MSG500) was 5966 ± 9 m s^{-1}, whereas U_l of the glass with the highest water content (8W-MSG500) was 5787 ± 9 m s^{-1} (table 4.2). The dependence of the elastic moduli went in line with the ultrasonic velocities and will be analyzed in section 4.4.2.

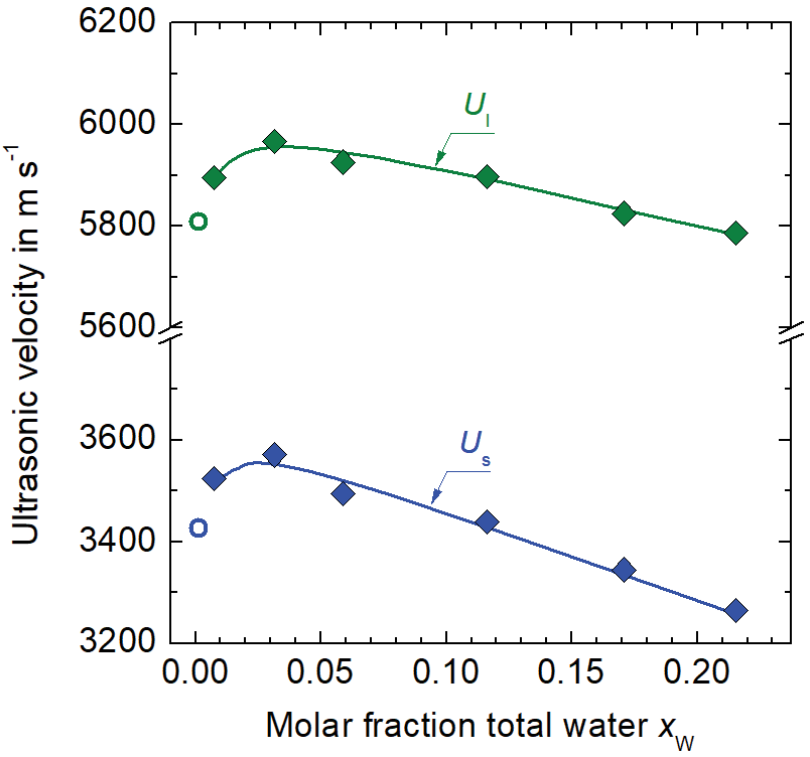

Figure 4.3: Dependence of the ultrasonic velocity for longitudinal U_l and shear modes U_s on the mole fraction total water x_W. The error bars of the velocities do not exceed the size of the symbols. Symbols indicate synthesis pressure (circle = 0.01 MPa, diamond = 500 MPa). Lines are intended as visual guides.

Table 4.2: Ultrasonic velocities U_l and U_s (eq. 4.2) and elastic constants L, G, K, E and ν_P (eqs. 4.3–7) of the anhydrous and hydrous glasses. Numbers in parentheses give uncertainty of the last digit.

Glass	U_l (m s^{-1})	U_s (m s^{-1})	L (GPa)	G (GPa)	K (GPa)	E (GPa)	ν_P (GPa)
0W-MSG0	5808(9)	3426(9)	83.2(3)	29.0(2)	44.6(1)	71.4(4)	0.233(4)
0W-MSG500	5895(9)	3524(9)	86.4(4)	30.9(2)	45.2(1)	75.4(5)	0.222(4)
1W-MSG500	5966(9)	3571(9)	88.0(4)	31.5(2)	46.0(1)	77.0(5)	0.221(4)
2W-MSG500	5926(9)	3495(9)	87.1(5)	30.3(2)	46.7(2)	74.7(2)	0.233(4)
4W-MSG500	5897(9)	3439(9)	85.2(4)	29.0(2)	46.6(2)	72.0(5)	0.242(4)
6W-MSG500	5825(9)	3345(9)	82.0(5)	27.1(2)	46.0(2)	67.9(5)	0.254(4)
8W-MSG500	5787(9)	3265(9)	79.6(5)	25.3(2)	45.8(2)	64.2(5)	0.267(5)

4.3.3 Microhardness

The dependence of the Vickers hardness on the total water content of the glasses for testing in two different environments is shown in figure 4.4. H_V is found to evolve in line with the elastic moduli. Again, the data let us believe that a slight positive deviation from the linear trend

is evident leading to a more rapid decrease in H_V for glasses of higher water content. The hardness of the hydrous glasses in toluene, which had the lowest water content (10 ppm_v) of the tested environments, was the highest, the hardness in N_2 gas of the glove box (p_{H2O} = 30 Pa ≈ 300 ppm_v) was lower and the hardness "under load" that corresponds to the hardness in liquid water [118], [119], was the lowest.
The hardness in toluene and under load was constant with the time of the holding (not shown), whereas the hardness in the N_2 gas and in air were found to be time-dependent. A decrease in hardness with increasing time of holding the maximum load is evident from figure 4.4B. From inspection of table 4.3 it can be seen that the hardness of the dry base glass 0W-MSG-0 was lower in air (p_{H2O} = 942 Pa) than in the dry N_2 gas (p_{H2O} = 30 Pa) and decreased somewhat faster with the holding time.

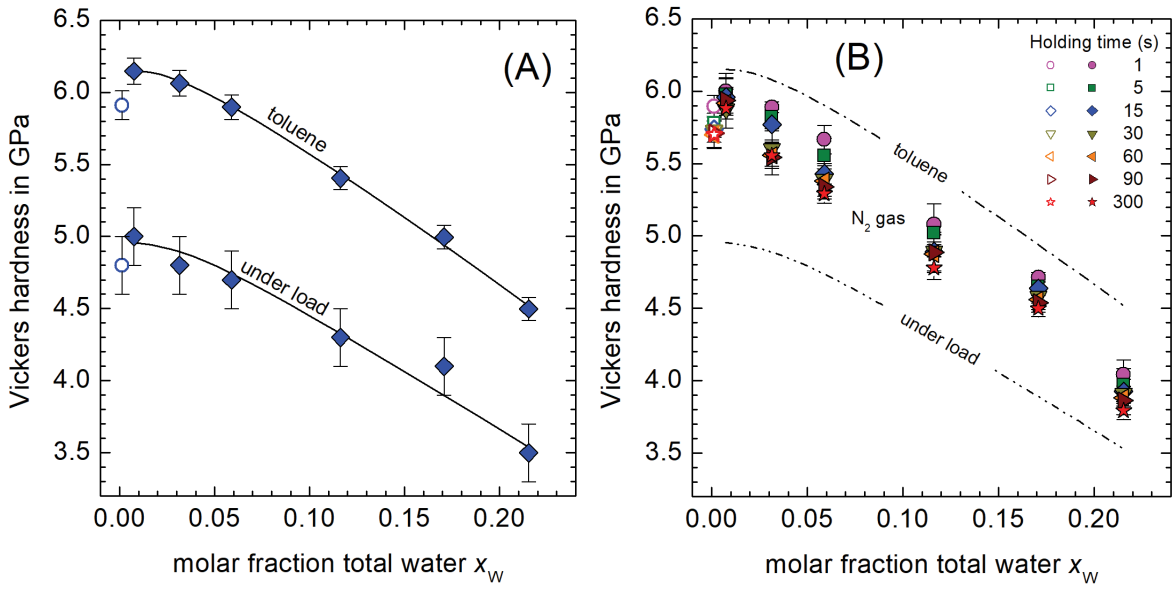

Figure 4.4: Dependence of the Vickers hardness on the water content of the hydrous soda-lime-silica glasses using a load of 1.96 N and two different environments. Part (A) shows the hardness in liquid toluene (water content = 0.001%) after unloading (upper curve) and the in N_2 gas of p_{H2O} = 30 Pa under load (lower curve). Part (B) illustrates the Vickers hardness after unloading in N_2 gas (p_{H2O} = 30 Pa) for different holding times. For comparison, the lines of toluene and under load measurements are added. Pressure of glass synthesis: open symbols = 0.01 MPa, full symbols = 500 MPa. Lines are intended as visual guides.

Table 4.3: Vickers hardness H_V (Load = 1.96 N) for indentation in different media (p_{H2O} = partial water pressure) and holding times. Numbers in parentheses give uncertainty of the last digit.

Indentation parameter			Glasses						
Media	p_{H2O} (Pa)	Holding time (s)	0W-MSG0 H_V (GPa)	0W-MSG500 H_V (GPa)	1W-MSG500 H_V (GPa)	2W-MSG500 H_V (GPa)	4W-MSG500 H_V (GPa)	6W-MSG500 H_V (GPa)	8W-MSG500 H_V (GPa)
Toluene	1*	1–300	5.91(10)	6.15(9)	6.06(9)	5.90(8)	5.41(8)	5.00(8)	4.50(8)
N_2 gas	30	1	5.89(7)	6.00(8)	5.89(4)	5.67(10)	5.08(14)	4.72(3)	4.04(10)
Air	942	1	5.83(8)		-		-	-	-
N_2 gas	30	5	5.78(7)	5.98(14)	5.82(8)	5.55(12)	5.02(6)	4.65(4)	3.97(11)
Air	942	5	5.72(12)		-		-	-	-
N_2 gas	30	15	5.74(9)	5.96(6)	5.77(11)	5.43(7)	4.99(14)	4.64(5)	3.93(8)
Air	942	15	5.55(10)		-		-	-	-
N_2 gas	30	30	5.73(12)	5.88(7)	5.60(12)	5.39(7)	4.89(13)	4.58(4)	3.91(5)
Air	942	30	5.50(8)		-		-	-	-
N_2 gas	30	60	5.70(9)	5.92(17)	5.56(9)	5.38(11)	4.88(13)	4.56(9)	3.88(6)
Air	942	60	5.51(10)		-		-	-	-
N_2 gas	30	90	5.71(3)	5.94(9)	5.54(12)	5.34(8)	4.89(13)	4.54(5)	3.86(10)
Air	942	90	5.28(12)		-		-	-	-
N_2 gas	30	300	5.70(10)	5.88(13)	5.55(9)	5.29(6)	4.78(8)	4.50(5)	3.79(6)
Air	942	300	5.33(8)					-	-
Under load									
N_2 gas	30	1–300	4.8(2)	5.0(2)	4.8(2)	4.7(2)	4.3(2)	4.1(2)	3.5(2)

Key: *The water content of toluene was 10 ppm_v.

4.4 Discussion

4.4.1 Density and molar volume

High precision measurements of the density of soda-lime-silica glasses with a water content < 0.3 mol% were provided by Scholze et al [114]. They found that water, which dissolves predominately as OH-groups, increases the density slightly by +3.82 g L^{-1} per mol% water. The increase in density was linked with the decrease in the mean distance in hydrogen bonding (O-H $\cdot\cdot\cdot$ O) with increasing total water content of the glasses. The positive compositional effect on density was confirmed by a later report of McMillan and Chlebik [37]. If one assumes that the MSG glass of this study is affected by the same density increase (up to 1 mol% total water), the additional increase in density due to compression using the synthesis pressure of 500 MPa can be estimated as 0.036 g L^{-1} MPa^{-1}. The OH-dependent increase and the pressure-dependent increase in density are both illustrated in figure 4.5A by black dotted lines and a vertical double-headed arrow, respectively.

For a total water content > 1 mol%, density is found to decrease strongly in accordance with an earlier study [106] performed at various synthesis pressures (figure 4.5A). At this level of hydration water molecules are becoming more and more dominant (tab. 4.1) and the dependence of the molar volume $\overline{V}$ of the hydrous glasses on the molar fraction of total water x_{H2O} can be analyzed (figure 4.5B). Assuming a regular solution between water molecules and the silicate glass, partial molar fractions can be derived from the method of tangents on the molar volume curve [38]. If the small effect of OH-groups on the molar volume for fractions < 0.01 is neglected, $\overline{V}(x_W)$ is well described by the linear equation 23.68 ± 0.06 cm^3 mol^{-1} - 12.1 ± 0.5 cm^3 mol^{-1}× x_W, which results in a partial molar volume of water in hydrous soda-lime-silica glasses up to $x_W = 0.215$ of approximately $\overline{V}_{H2O} = 11.6 \pm 0.6$ cm^3 mol^{-1}.

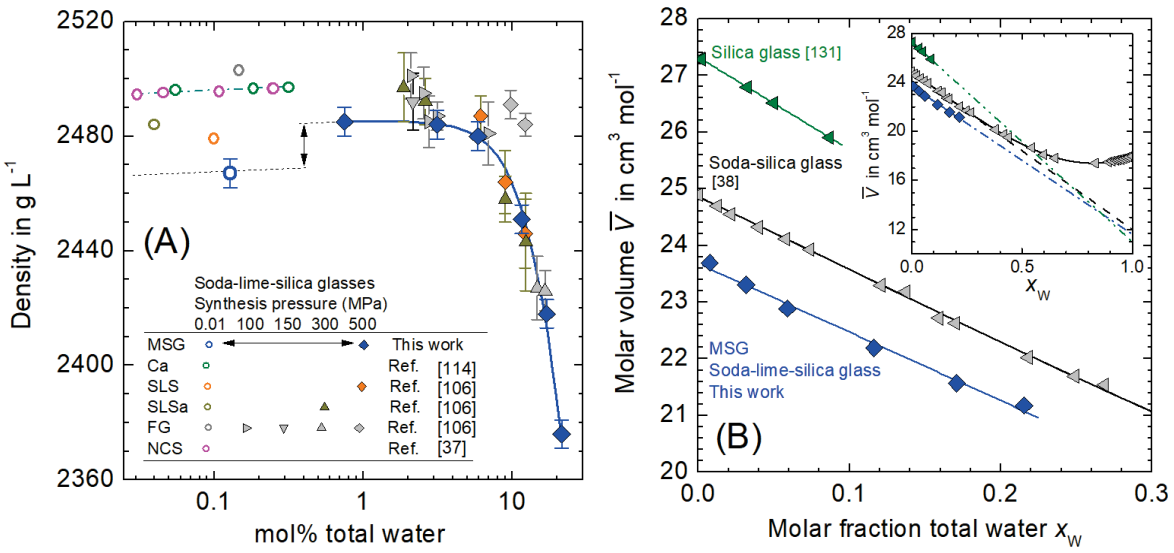

Figure 4.5: Density of different soda-lime-silica glasses as a function of mol% total water (A) and dependence of the molar volume on the molar fraction of total water for silica, soda-silica and soda-lime-silica glasses (B). Solid lines in are best linear fits through the data, dashed and dashed dotted lines in (A) illustrate the OH-dependent increase in density whereas in (B) these lines are extrapolations to approximate $\overline{V}_{H2O}$ from the intercept with the molar volume axis at $x_W = 1$. The analyzed molar compositions of the nominal dry base glasses are: soda-lime-silica: "Ca" = $SiO_2/Na_2O/CaO$ = 74.0/15.9/10.1 [114], "SLS" = $SiO_2/Na_2O/CaO/(Al_2O_3/Fe_2O_3/K_2O)$ = 73.4/15.5/10.1/(0+) [106], "SLSa" = $SiO_2/Na_2O/CaO/(Al_2O_3/Fe_2O_3/K_2O)$ = 74.1/15.8/10.2/(0+) [106], "FG" = $SiO_2/Na_2O/CaO/MgO/Al_2O_3/K_2O/(Fe_2O_3)$ = 71.4/12.6/9.5/5.8/0.4/0.2/(0+) [106], "NCS" = $SiO_2/Na_2O/CaO$ = 73.8/15.5/10.7 (by batch) [37]; soda-silica: SiO_2/Na_2O = 75/25 (by batch) [38]; silica: SiO_2 ≤100 [131]. Oxides within brackets present a nominal molar amount <0.05.

The volume, which water occupies in hydrous soda-lime-silica glasses, is found to be similar to those in hydrous silica glasses for $x_W < 0.09$ [131] and hydrous soda-silica glasses for $x_W < 0.27$ [38] as pointed out by the insert of figure 4.5B. For all three glass types the occupied volume resembles that of densest molecular form of H_2O that is ice VII ($\overline{V}_{H2O} = 12.3 \pm 0.6$ cm^3 mol^{-1} [111], [112]. $\overline{V}_{H2O}$ has been collected for a series of natural aluminosilicate glasses and found to be independent on water speciation and the connectivity of the silicate network, i.e. the number of non-bridging oxygen per network forming tetrahedron of the anhydrous base glass [113]. The former means that volume changes accompanied with the equilibrium reaction Si-O-Si + H_2O = 2 Si-OH are rather small, whereas the later indicates that dissolution of water is very efficient with respect to the packaging of the silicate glass, i.e. H_2O takes less than half of the partial molar volume of a dry silicate glass. Thus, the decrease in both density and molar volume of the hydrous soda-lime-silica glasses with > 1 mol% total water is related to an increase in a densely packed hydrous volume fraction of lower weight.

4.4.2 Elastic constants

Figure 4.6 shows the dependence of the elastic constants on the total water fraction. The data indicate a positive deviation from the linear trend of the elastic moduli at low water content. In particular, synthesis of the nominal dry re-melt at 500 MPa pressure resulted in $E = 75.4 \pm 0.5$ GPa. The synthesis with about 3 mol% total water yield $E = 77.0 \pm 0.5$ GPa and the one with approximately 21.5 mol% water yield $E = 64.2 \pm 0.5$ GPa, that is a decrease of >16% with respect to the initial value. In contrary to the dependence of the elastic moduli, the Poisson's ratio seems to be constant at first and then increases to $\nu_P = 0.267$. However, with respect to the uncertainty in the ν_P data a non-linear dependence cannot established beyond doubt. Using the same solution model as for the molar volume, one can define partial molar elastic constants for the fraction of dissolved water in the hydrous soda-lime-silica glasses [112].
Figure 4.6A and 4.6B show that the elastic moduli and the Poisson's

ratio are linear functions of water content up to the highest concentration investigated but the linear approximation overestimates and underestimates, respectively, the compositional dependence at small water fractions ($< 3\%$). The situation is pointed out in figure 4.6C and 4.6D, which show the compositional dependence in logarithmic scales. For a water content dominated by OH-groups, Limbach et al. [115] provide elastic constants of soda-lime-silica glasses. Their data show a slight increase in the Young's modulus and vaguely decreasing values of ν_P in agreement with the increase in density (figure 4.5A) that was originated by the change from weak to strong hydrogen bonds [114]. For hydrous compositions that are dominated by water molecules (>3 mol% total water), however, the linear behavior indicate that water speciation is apparently ineffective. For these glasses the partial molar constants of water are $\overline{L}_{H2O} = 41 \pm 4$ GPa, $\overline{E}_{H2O} = 11 \pm 7$ GPa, $\overline{K}_{H2O} = 41 \pm 1$ GPa, $\overline{G}_{H2O} = 1 \pm 3$ GPa and $\overline{\nu_P}_{H2O} = 0.45 \pm 0.06$ as determined by linear regression through the data.

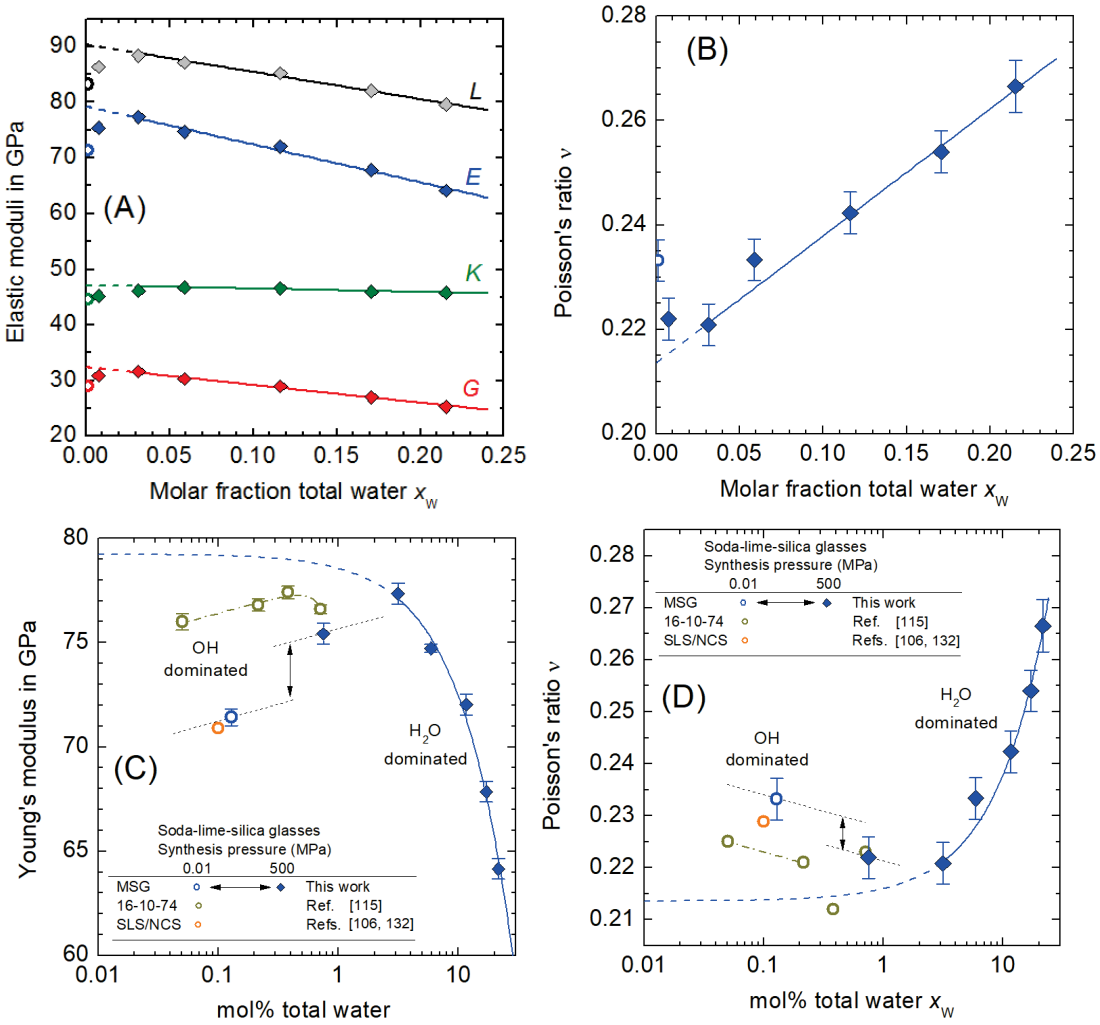

Figure 4.6: Dependence of the elastic moduli L, E, K, and G (A) and the Poisson's ratio ν_P (B) on the molar fraction of total water. The error bars of the elastic moduli do not exceed the size of the symbols. Symbols indicate synthesis pressure (dots = 0.01 MPa, diamonds = 500 MPa). Lines are linear regressions through the data for $x_W > 0.03$. The compositional dependence on logarithmic scales is exemplarily illustrated for the Young's modulus and Poisson's ratio in (C) and (D), respectively. The latter are intended to highlight the effect of dissolved water on elasticity for a water speciation dominated by the portions of hydroxyl groups (OH) and water molecules (H_2O) as indicated by NIR spectroscopy. Thin dotted and dash dotted lines indicate compositional trends and compaction effects (double-headed arrow) of OH-dominated glasses, respectively. Thick solid and dashed lines are best fits through the hydrous glass data dominated by water molecules from (A) and (B) and their extrapolation towards lower total water fractions. The molar composition (by batch) of the nominal dry glass "16-10-74" is $SiO_2/Na_2O/CaO$ = 74.0/15.9/10.1 [115]. The "SLS" glass of Ref. [106] is equal to "NCS" of Ref. [132].

4.4.3 Microhardness

The environmental-sensitivity of microhardness has been explained by diffusion of water molecules from the environment (water content of the

test liquid, atmospheric moisture) into the deformed glass volume under the indent, which leads to a time-dependent softening effect [123]. In contrast, hardness is highest and appears to be constant with time when tested in water-free environments such as under vacuum or in toluene [119], [121]. An independence of hardness on holding time is also achieved if diagonals were measured under load and thus preventing elastic recovery of the glass after completely unloading the sample [119]. Under these conditions, hardness is lowest and the value corresponds to hardness measured in water [119]. Thus, it seems to be beneficial to analyze the time-dependent response of the glass against environmental water on basis of the reduced hardness M_H :

$$M_H(p_{H2O}, x_W, t) = \frac{H_V(p_{H2O}, x_W, t) - H_V(p_{H2O}, x_W, \infty)}{H_V(p_{H2O}, x_W, 0) - H_V(p_{H2O}, x_W, \infty)}, \qquad (4.12)$$

where $H(p_{H2O},\ x_W,\ 0)$ is the initial hardness that is measured under vacuum or in toluene and $H(p_{H2O},\ x_W,\ \infty)$ is the stationary hardness that is measured under load or in water. It is expected that a plot of M_H versus holding time (log scale) leads to a sigmoidal shaped curve, which follows a stretched exponential function [133]. However, for the narrow range in holding times figure 4.7 shows that M_H can also be approximated by the linear function:

$$M_H(p_{H2O}, x_W, t) = A + B\ lg(t_{pH2O,x_W}), \qquad (4.13)$$

where A and B are adjustable parameters and t_{pH2O,x_W} is the holding time. The indices p_{H2O} and x_W specify the environmental vapor pressure and the water content of the glass, respectively. The characteristic time of the response τ is the time at which M_H is reduced to 0.5. In case of the base glass (0W-MSG0) with $x_W = 0.0013$ the decrease in hardness with time is flatter when tested in N_2 gas ($p_{H2O} = 30$ Pa) and steeper for air testing ($p_{H2O} = 942$ Pa) (figure 4.7A). Using eq. 4.13 the characteristic time of the softening is approximated to be shorter ($\tau = 128$ s) in air and longer ($\tau = 2{\times}10^6$ s) in dry nitrogen gas (figure 4.7B). Such trend in

environmental-sensitivity can be derived also for dry silica glass, using indentation data for 200, 2188 and 15000 Pa vapor partial pressure [118], [119]. However, the conclusion that silica glass is more environmentally sensitive could not be proven convincingly as the silica glass tested in Refs. [118], [119] has a lower water content than 0W-MSG0.

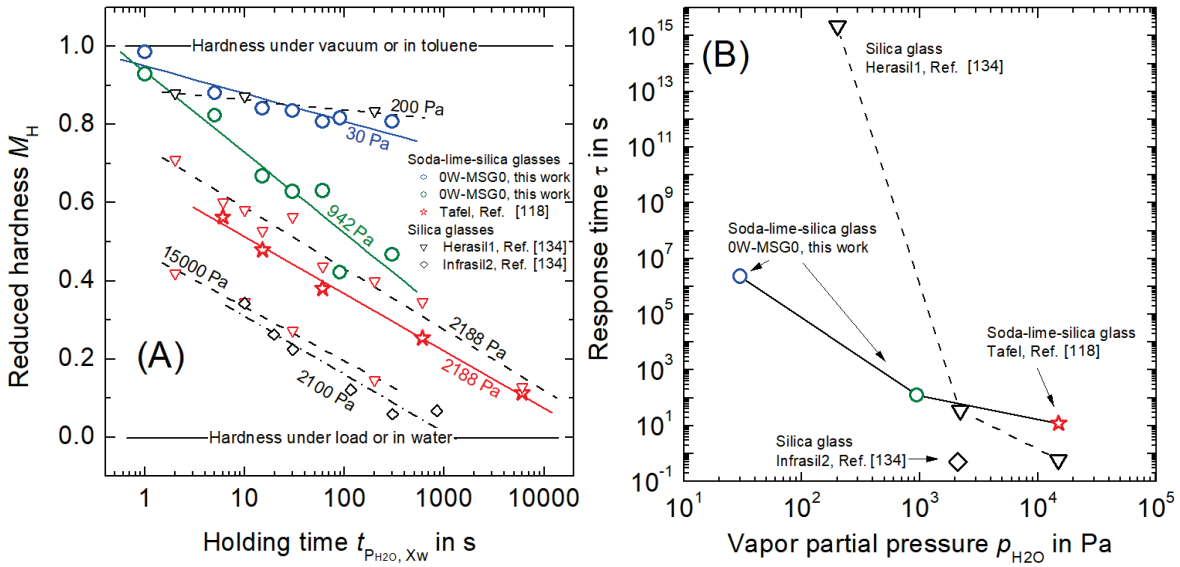

Figure 4.7: Reduced hardness as a function of the holding time (load = 1.96 N (200 gf)) for different environmental vapor pressures (p_{H2O} as indicated) (A) and characteristic response time vs. environmental vapor pressure (B). Lines in part (A) are best fits of eq. 4.13 through the data. Line in Part (B) is intended as visual guide. The analyzed compositions of the nominal dry base glass "Tafel" is $SiO_2/Na_2O/CaO/MgO/Al_2O_3/K_2O/SO_3/Fe_2O_3$ = 72.7/13.3/7.6/4.0/1.5/0.6/0.2 0.1 (wt%) [118], [119]. The water content x_W of the base glasses are: 0.0013 (0W-MSG0, tab. 4.1), 0.000267 ("Herasil1" [134]), 0.000017 ("Infrasil2" [134]). The water content of the commercial soda-lime-glass "Tafel" [118], [119] was assumed to be equal to the used microscope slide glass 0W-MSG0. It has to be noted that reduced hardness was based on hardness tests in toluene and under load for 0W-MSG0, in toluene and in water for "Infrasil2", under vacuum and under load for "Herasil1", and under vacuum and under load for "Tafel", respectively.

The hydrous soda-lime-silica glasses prepared in this study show a similar M_H dependence with holding time although the environmental vapor pressure was kept constant in this series of indentations (figure 4.8). With increasing x_W reduced hardness and the corresponding response time decrease noticeably. Comparing figure 4.7B and 4.7B indicates effectively equal response times in both scenarios. That would mean that initially dissolved water species have the same mobility under the imprint than those formed by dissolved water from the environment. Although the

actual species concentrations at the glass surface and under the imprint during softening are unknown, it seems reasonable that water molecules are playing the governing role in the time-dependent softening process.

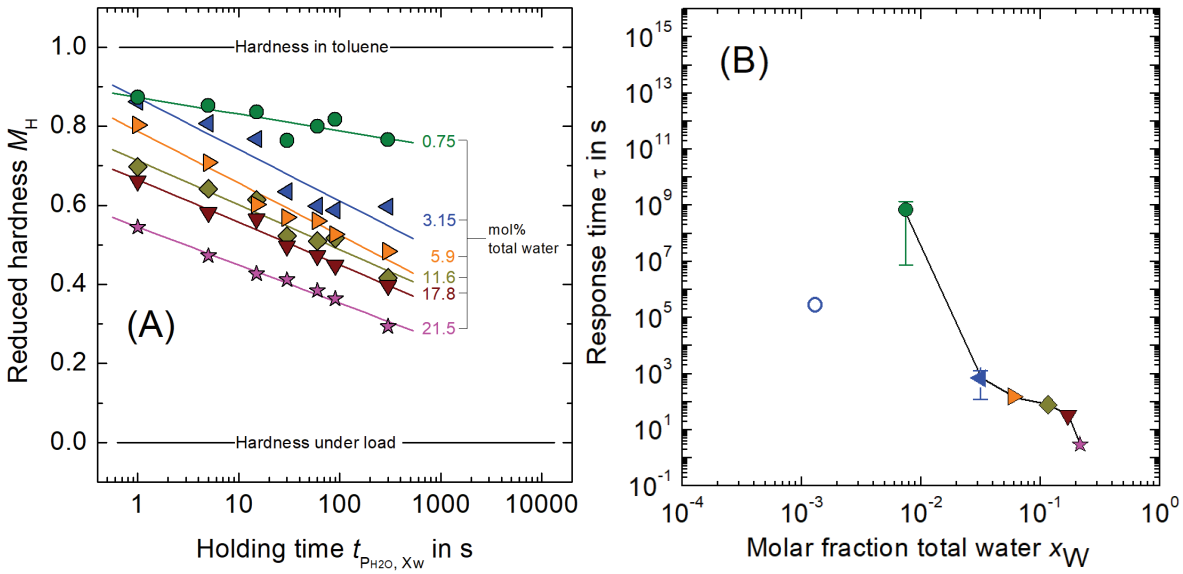

Figure 4.8: Reduced hardness as a function of the holding time (load = 1.96 N (200 gf)) for hydrous soda-lime-silica glasses of different initial water contents (x_W as indicated) (A) and the dependence of the characteristic response time on the initial molar fraction of total water (B). Vapor partial pressure was 30 Pa for all indentations. Symbols indicate synthesis pressure (circle = 0.01 MPa, full dot, full triangle, full diamond and full star = 500 MPa). Lines in part (A) are best fits of eq. 4.13 through the data. Line in Part (B) is intended as visual guide.

4.5 Conclusions

The results of our study show that dissolved water strongly affects the micromechanical properties of soda-lime-silica glasses. Water decreases the stiffness of the glass as the Young's modulus decreases by more than 20% and the Poisson's ratio increases towards the limiting value of 0.5 for pure H_2O. For hydrous glasses, where the water fraction is dominated by H_2O molecules ($x_w > 0.03$), the dependencies of the elastic constants on the total water content are linear up to the highest concentration investigated but the linear approximation overestimates and underestimates, respectively, the compositional dependence at small water fractions ($< 3\%$). The deviation reflects the change in the concentrations of OH groups and H_2O molecules, which are representative for progressive

hydration. As molecular water is light and densely packed in silicate glass structure, bulk modulus remains nearly unchanged, whereas molar volume, density and the ultrasonic velocity decreases. The occurrence of a time-dependent softening effect in hydrous glasses under constant environmental moisture demonstrates that water species, most probably water molecules, are capable to relax stressed silicon-oxygen bonds effectively. Their diffusivity is efficiently high so that equal time scales can be assigned to softening caused by migration of external and internal water molecules.

5

Statistical analysis of propagation rates of indentation-induced radial cracks in soda-lime-silica glass

P. Kiefer[a], J. Deubener[a], R. Müller[b], H. Behrens[c]

[a]Clausthal University of Technology, Institute of Non-Metallic Materials, 38678 Clausthal-Zellerfeld, Germany

[b]Federal Institute of Materials Research and Testing (BAM), 12489 Berlin, Germany

[c]Institute of Mineralogy, Leibniz University Hannover, 30167 Hannover, Germany

Abstract

Due to the stochastic nature of crack nucleation by Vickers indentation, a statistical analysis of propagation rates of 185 radial cracks was performed. Crack growth was observed directly using a video camera with high image acquisition rate. It is found that propagation rates are controlled by the environmental reactions at the crack-tip shortly after their initiation (< 1 s). Calibration of the stress intensity K_I showed that the residual stress factor χ and the exponent n of the equation $K_I = \chi P c^{-n}$ (with P = load and c = crack length) are broadly distributed among the 185 analyzed cracks, ranging from 10^{-16} to 10^4 and from 0.1 to 5, respectively. For the most frequent crack, the equation holds $K_I = 0.052 P c^{-1.47}$. The results show that correlations of indentation-induced crack length to stress intensity necessitate the use of statistically significant data that are calibrated by the environmental reactions at the crack-tip.

5.1 Introduction

Fatigue effects can lead to significant reductions in strength of glasses as the fracture stress-to-load duration ratio depends sensitively on the atmospheric water content, i.e. the relative humidity (RH) [7], [10], [11]. Complex stress dependent phenomena and reactions of water at the crack-tip are discussed to contribute to stress corrosion of glasses [135]–[138], which include the subtle interplay between hydration, hydrolysis, condensation, ion-exchange [139], stress enhanced water diffusion [26], [140] and glass dissolution [26], locally changed glass viscosity [141] and moduli [27], [42], [110], fast and stress dependent alkali diffusion and leaching [142] and resulting compressive stress generation [143]. This situation is further complicated by the uncertain crack-tip environment, which may be affected by water absorption/desorption kinetics, cavity effects [144], capillary condensation [145], [146], and locally enhanced alkali concentration and corrosion. Further, water is also found to promote stress relaxation under load, which has been utilized for forming surface

compressive layers as a novel strengthening method [28]. Since all these phenomena are restricted to the very close vicinity of the crack tip, they are difficult to study. However, experimental curves of the subcritical crack growth rate dc/dt (c = crack length and t = propagation time) in glasses exhibit typically four characteristic regions (0, I, II, and III [12], [147], [148]) with increasing stress intensity K_I (if plotted in logarithmic scales) enabling the fracture strength to be predicted from slow crack growth observations [149], [150]. For region I of the $\lg(dc/dt)$ versus $\lg(K_I)$ diagram where the complex reaction between atmospheric water and glass at the crack-tip controls the crack growth [12], K_I can be estimated from eq. 5.1 [151], [152]:

$$\frac{dc}{dt} = AK_I^m. \tag{5.1}$$

The parameters A and m of eq. 5.1 are constants, which depend on the environmental condition of the fatigue experiment and the chemical resistance of the glass, respectively. Even though eq. 5.1 is of empirical nature, recent ab initio calculations for the Si-O bond rupture confirm that the basic kinetic dependence of crack growth rate on stress intensity of eq. 5.1 is valid [153], [154].

Because of the stochastic nature of crack nucleation by Vickers indentation, however, this method cannot be applied to crack propagation without careful statistical considerations. Further, the complexity of Vickers cracking patterns and their related stress fields make it difficult to conclude on the stress intensity factor K_I at the crack-tip, which controls the crack propagation. Estimation of K_I, however, could be based on averaged c or dc/dt data fitted with fundamental laws of crack propagation. For that case, the fracture driving force for a propagating crack of the radial crack system is described by the empirical generalization [33], [129], [155]–[158]:

$$K_I = \chi P c^{-n}, \tag{5.2}$$

where c is the crack length measured from the center of the indent, P is the load χ is a residual stress factor accounting for both the elastic-plastic

properties of the glass and the angular position along the crack front while n is the crack length exponent ($n > 0$). While the scale factor A and growth exponent m of eq. 5.1 can be determined directly from stress intensity calibrated specimens such as double cleavage drilled compression (DCDC) [159] and double cantilever beam (DCB) [21], their determination is impeded due to the unknown stress field at the crack tip initiated by Vickers indentation [160]. However, if A and m are known from DCDC or DCB experiments for the glass under consideration, they can be used to calibrate the growth data of Vickers induced cracks under the same environmental conditions. In that case, it is useful to express K_I of eq. 5.1 by eq. 5.2, which reads

$$\frac{dc}{dt} = A(\chi P c^{-n})^m = A\chi^m P^m c^{-nm} \tag{5.3}$$

and after taking the logarithm one has

$$\frac{lg\left(\frac{dc}{dt}\right)}{m} = \frac{lg(A)}{m} + lg(\chi P) - n\ lg(c). \tag{5.4}$$

From a plot of the left hand side of eq. 5.4 versus lg(c) one finds the residual stress factor χ (from the intercept) and exponent n (from the slope) for each crack. Here we present an attempt to use statistically significant crack growth data for the above calibration procedure. Particularly, the aim of the study is to analyze how far the residual stress factor χ and the crack length exponent n of each crack deviate from their average value. Therefore, 185 radial cracks induced by Vickers indentation were grown in commercial soda-lime-silica glass under the same environmental condition as for a prior crack growth experiment using a double cantilever beam (DCB). For each crack and within the first minute after nucleation, 1800 data points of the decreasing crack propagation rate dc/dt with increasing crack length c are recorded.

5.2 Experimental

Propagation of indentation-induced cracks was studied on commercial soda-lime-silica glass surfaces. For this purpose, as received microscope slides according to ISO 8037/1 (IDL, Nidderau) were used. Glass slides were cut into pieces of 5×20 mm, ultrasonicated in ethanol and dried with dust free wipes. The glass composition is 72.56 SiO_2, 0.77 Al_2O_3, 0.02 Fe_2O_3, 6.95 CaO, 6.40 MgO, 12.65 Na_2O, 0.63 K_2O and 0.02 TiO_2 (in mol%) as analyzed by X-ray fluorescence (Axios, PANalytical).
Glass surfaces were indented with a Vickers diamond under controlled load at 14.72 N using a universal hardness testing machine (ZHU 2.5, Zwick Roell). The load was set within 5 s (loading ramp), held constant for 15 s and removed within 5 s (unloading ramp) which results in a nominal (un)loading rate of 2.94 N s^{-1} (figure 5.1). The regime was selected on basis of an initial parameter study and led to a high initiation crack probability of the microscopy glass in dry environments. Crack propagation was observed from below through a long distance objective at a magnification of 20x (N PLAN L, Leica) of an inverted microscope (DM-ILM, Leica) and recorded with a 5.3 megapixel CMOS sensor of a monochrome camera (PL-D725MU-T, PixelInk). For each indent a video was recorded at 30 frames per second (fps) for about 60 s (≈ 1800 frames). Uncompressed capturing and subsequent decomposition in single video frames were performed using TroublePix and BatchProcessor software (Norpix), respectively. Each image was analyzed using a self-written MatLab (Mathworks) code, which gauges the rim of the indent and the position of the crack tip from the same grey scale threshold value. Simultaneously, the center of the indent was determined, which serves as a basis for the crack length calculation. After the crack was initiated and detectable for the software, the crack length c of each image was measured by taking the Euclidean distance between the pixel of the center of the indent and the pixel determining the crack tip.
Indenter and camera were referenced to a synchronized time tag. The tag was set to the end of the unloading ramp of the indenter, which was

$t_0 = 0$ in the timescale of the image acquisition (figure 5.1). We note that initiation of radial cracking can deviate from t_0. In case of delayed cracking (radial crack appears at $t > t_0$) the delay time $\delta = t$ - t_0 was recorded.

The above setup was implemented in a glove box (labmaster130, MBraun) that allows for the adjustment of atmospheric water. During our experiments, the water content was adjusted to 650 ppm_v H_2O, which equals a relative humidity of 1.18%. Humidity was monitored using a dewpoint transmitter (Easydew, Michell Instruments). RH was adjusted to meet the environmental conditions of a prior DCB experiment of Wiederhorn [12] on a microscopy slide glass of similar composition. Wiederhorn [12] found that the glass obeys eq. 5.1 for growth rates between $\approx 7\times10^{-8}$ and 3×10^{-6} m s^{-1} (region I). In particular eq. 5.1 holds for $m = 24.45$ and $\lg(A) = -0.46$ (dc/dt in m s^{-1} and K_I in MPa $m^{1/2}$) [147]. 57 indents were set under these conditions at the surface of the microscopy slide. Indentation generated in total 185 radial cracks after 60 s of recording, which resulted in a crack initiation probability of 81% [161]. Under these conditions other crack types were not observed.

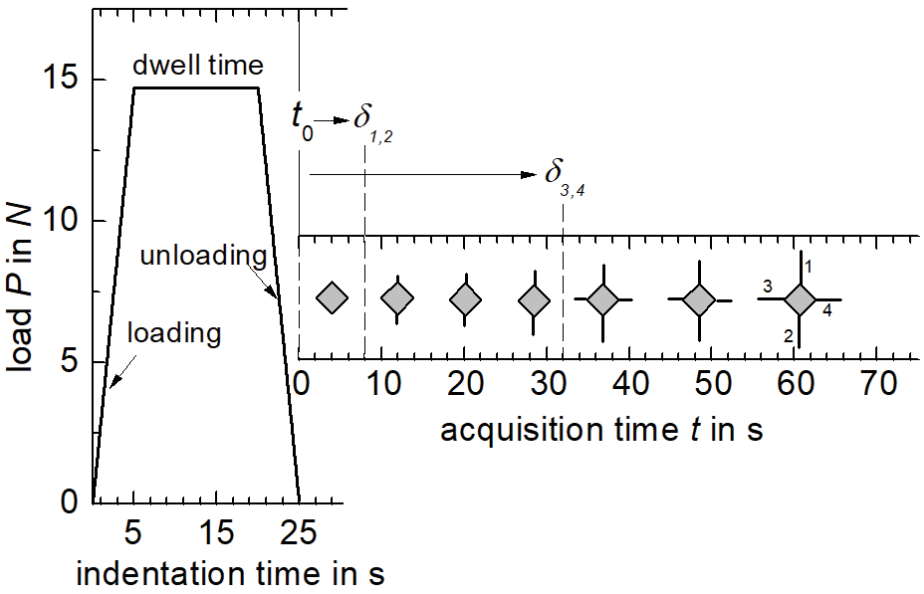

Figure 5.1: Schematic load-time curve of the Vickers indentation to initiate radial cracks. The image acquisition is triggered at the end of the unloading ramp at t_0. Exemplary cracking of crack numbers 1 and 2 at the delay time $\delta = t$ - $t_0 = 8$ s and of crack numbers 3 and 4 at $\delta = 32$ s.

5.3 Results

Figure 5.2 shows selected frames out of three video segments as an example for instantaneous and delayed cracking after Vickers indentation. Cracking of two radial cracks occurred between frame 49 and 50 at the horizontal corners of the first indent (figure 5.2a), which coincided with the end of the unloading ramp at t_0. These cracks were assigned to be instantaneous within the resolution limit of recording (1/30 s). At frame 107, a third crack at the bottom corner became first observable. This crack is delayed by $\delta = 1.90$ s. Finally, the fourth corner crack appears at frame 136 ($\delta = 2.87$ s). At the second indent, three instantaneous cracks are evident while the fourth crack is popping-in at $\delta = 0.23$ s (figure 5.2b). The third indent shows that radial cracks can be formed also at the faces of the indent near to the corner (figure 5.2c). All cracks have grown during the video capture of about 60 s as illustrated by the bottom image of figure 5.2b. Between the frames 46 and 1850 the crack tip has moved by ca. 10 μm. The visible length of radial cracks is $l = c$ - a, where a is the half diagonal of the indent before cracking and c is the crack length from the center of the indent.

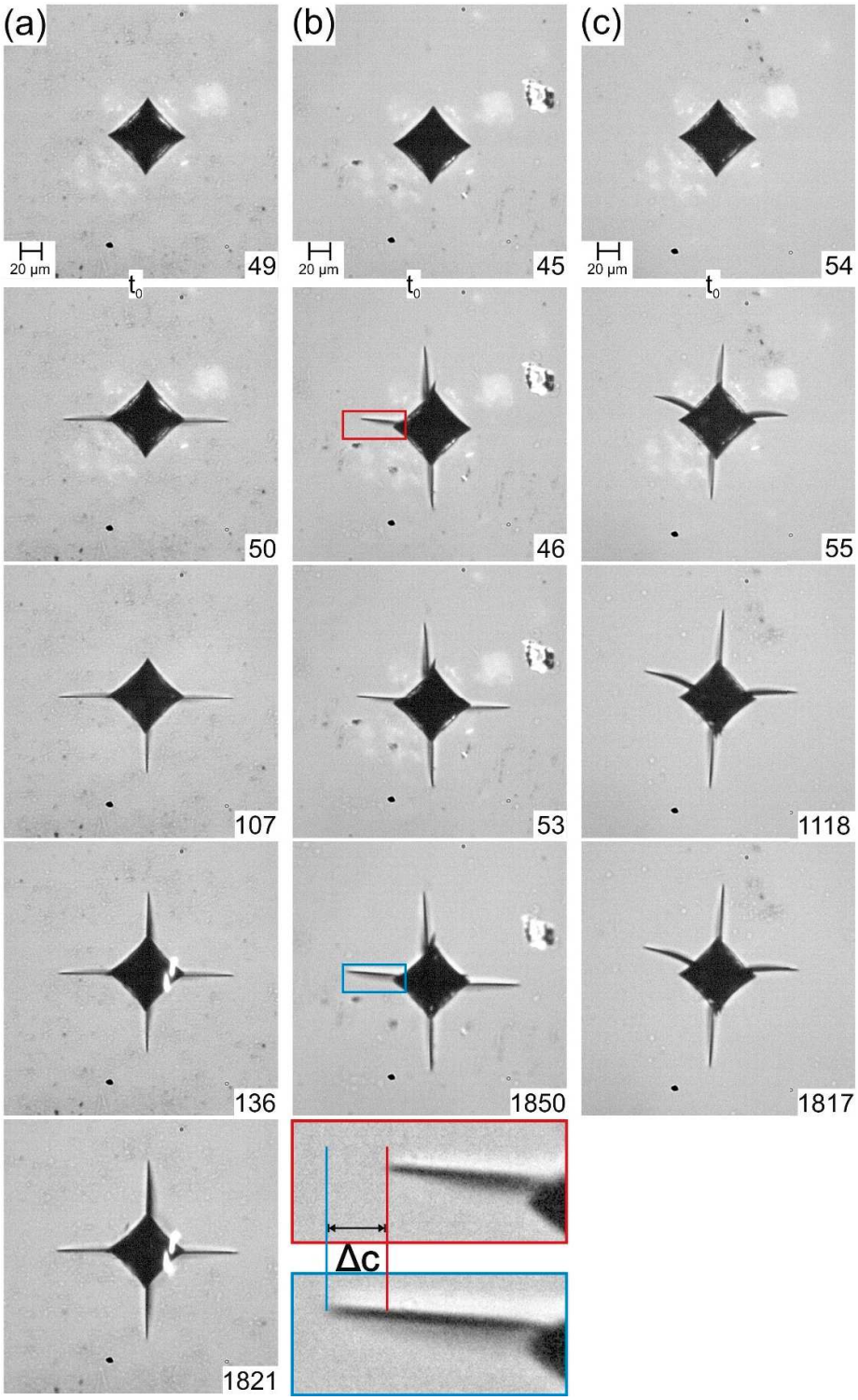

Figure 5.2: Selected frames out of three recorded videos after indentation at 14.72 N. The end of the unloading ramp, i.e. t_0 was between frames 49 and 50 for indent (a), between 45 and 46 for indent (b) and between 54 and 55 for indent (c). The figure illustrates instantaneous radial cracking (frames 50 (a), 46 (b) and 55 (c)) and the appearance of delayed radial cracks (frames 107 (a), 136 (a) and 53 (b)). The bottom images of (b) highlight the propagation of the crack tip between frames 46 and 1850 (Δt = 60.13 s) at higher magnification. Note that radial cracking occurred at the corner of indents (a) and (b) but also at the faces of the indent (c).

Figure 5.3 shows the results of the data processing with the Matlab script for the 12 radial cracks of figure 5.2. During the first seconds after crack nucleation a strong increase in crack length is evident, which then decreases with increasing propagation time. A linear time dependence of the form [146], [162]–[164]

$$lg(c) = lg(S_1) + S_2 lg(t - \delta), \tag{5.5}$$

where S_1 and S_2 are adjustable parameters is evident, when plotting the crack length versus propagation time (t - δ) in logarithmic scales. To capture the important patterns of the propagating crack, the parameters S_1 and S_2 of each crack were determined by linear regression through the data. This procedure resulted in smoothed crack length data of the form

$$c = S_2(t - \delta)^{S_1}, \tag{5.6}$$

from which the crack propagation rate dc/dt of the 185 cracks were derived by taking the first derivative with respect to the propagation time

$$\frac{dc}{dt} = S_1 S_2 (t - \delta)^{S_2 - 1}. \tag{5.7}$$

One should stress that some cracks show noticeable deviation (arrow) from the linear trend at an early stage < 1 s (figure 5.3B and 5.3D), which indicate possible crack interaction (crack B and crack T of indent 1 were delayed). On the other hand, the 4 cracks of the third indent obey the linear trend starting from the first frames (figure 5.3F), although crack L and crack R are curved and have grown at the faces of the indent (figure 5.3C). Crack patterns and the quality of the linear fits shown in figure 5.3, with regression coefficients R^2 from 0.88 to 0.95, are typical of all 185 analyzed cracks.

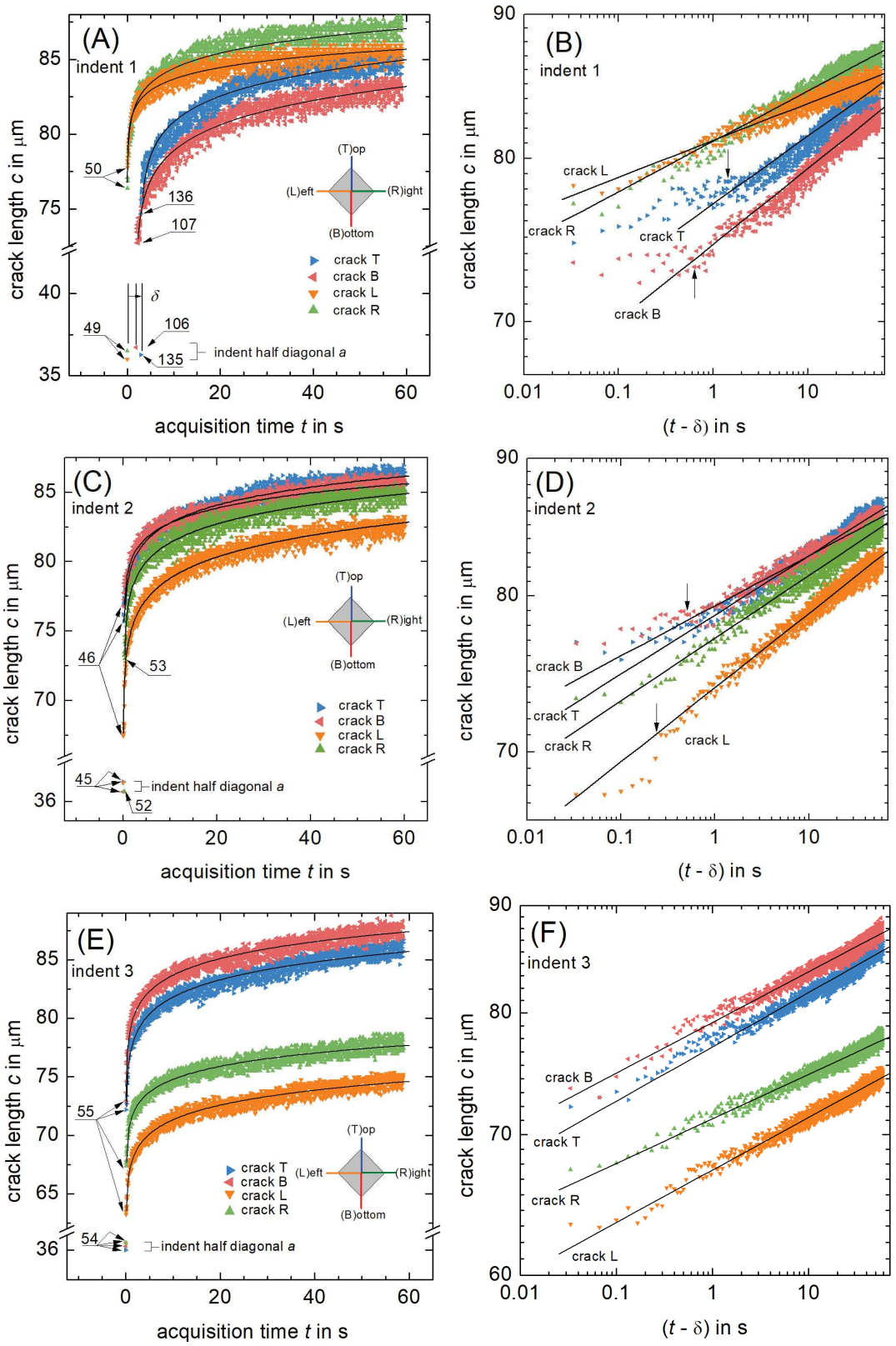
(A)
indent 1
crack length c in µm
acquisition time t in s
50
136
107
49
106
135
δ
indent half diagonal a
(T)op
(L)eft
(R)ight
(B)ottom
crack T
crack B
crack L
crack R
(B)
indent 1
(t - δ) in s
(C)
indent 2
46
53
45
52
(D)
indent 2
(E)
indent 3
55
54
(F)
indent 3

Figure 5.3: Time dependence of the crack length c of the 12 radial cracks of figure 5.2. Each data point equals an analyzed frame of the video sequence. The scatter of the crack length data is mainly caused by the lateral resolution of the camera system. Numbers of selected frames are indicated in correspondence to those in figure 5.2. Compact lines of parts B, D and F are best linear fits of eq. 5.5 to the lg(c) versus lg(t - δ) data. Regression coefficients R^2 are 0.92, 0.93, 0.88, 0.92 (part B), 0.93, 0.92, 0.96, 0.95 (part D) and 0.94, 0.95, 0.95, 0.92 (part F) for T, B, L and R cracks, respectively. The received average crack length is also illustrated in parts A, C and E by black lines. Arrows indicate deviation from the linear trend. Radial cracks are labelled according to their position at the top, bottom, left and right corner of the indent with T, B, L and R, respectively.

Figure 5.4 shows that the majority of radial cracks (≈76%) are visually initiated within 5 seconds ($\delta \leq$5 s) after completely unloading the sample, but sporadic cracking occurred also at a delay of up to 49 seconds. 43 cracks (= 19%) are not formed within the recording time and another waiting time of 1 hour without recording. Resolving the first 5 seconds in greater detail (insert of figure 5.4) reveals that (quasi)instantaneous cracking ($\delta \leq$0.1 s) is for the applied indentation protocol and the prevailing environmental conditions and the most frequent response of the material.

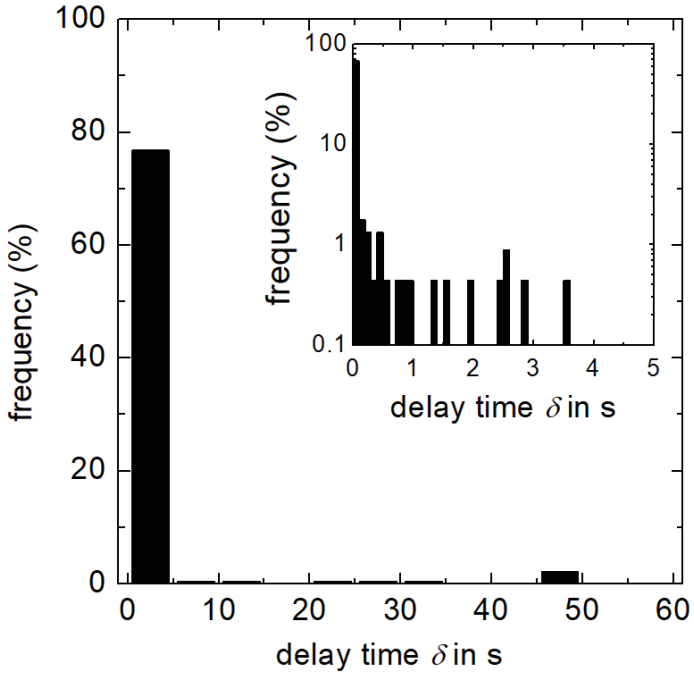

Figure 5.4: Frequency distribution of the delay time δ of radial cracking during the first minute after completely unloading the glass. The insert shows the delay of up to 5 s in greater detail. Note the crack initiation probability was 81% after 60 s. Bin size of the frequency distribution is 5 s and for the insert 0.1 s.

The crack propagation rates of the 185 recorded cracks are found to be relative broadly distributed (figure 5.5). The temporary velocity at 5 s of propagation is covering a range from 9.7×10^{-8} m s^{-1} to 2.7×10^{-6} m s^{-1}, which is a factor of approx. 28 between the slowest and the fastest crack. At the end of the acquisition time (t - δ = 60 s), crack velocity had decreased to 8.4×10^{-9} m s^{-1} for the slowest and to 5.9×10^{-7} m s^{-1} for the fastest crack while the factor between both increased to 71.

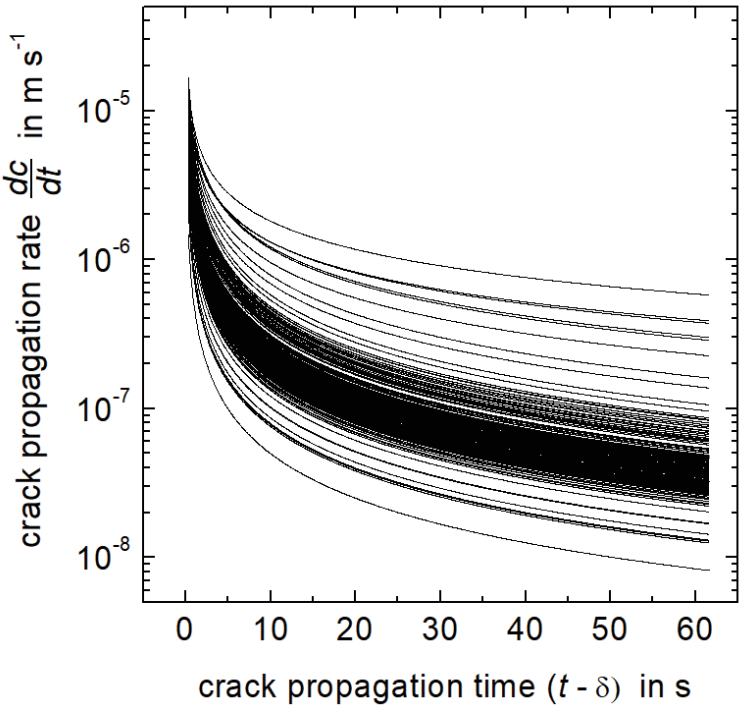

Figure 5.5: Crack propagation rate dc/dt of eq. 5.7 versus propagation time t - δ of the 185 analyzed radial cracks.

A similar broad distribution among the analyzed cracks is obtained, when the propagation rate is evaluated for constant crank length. Figure 5.6 shows lognormal distributed propagation rates with a decreasing mean value for increasing crack length. For instance, temporary velocities from 0.03 to 11.18 μm s^{-1} for 80 μm long cracks were determined. We note that not all cracks reached a length of 80 μm in the acquisition time such as cracks L and R of indent 3 (figure 5.3E). Thus, with increasing length the number of cracks reduces. For instance, at 85 and 90 μm only 117 and 54 cracks, respectively were evaluated. We further note that due to the limited image acquisition rate of 30 fps, propagation rates of some other cracks at a length of 70 μm were not resolvable. Thus, they are

found to pop-in with $c > 70$ μm as shown for cracks L and R of indent 1 in figure 5.3A.

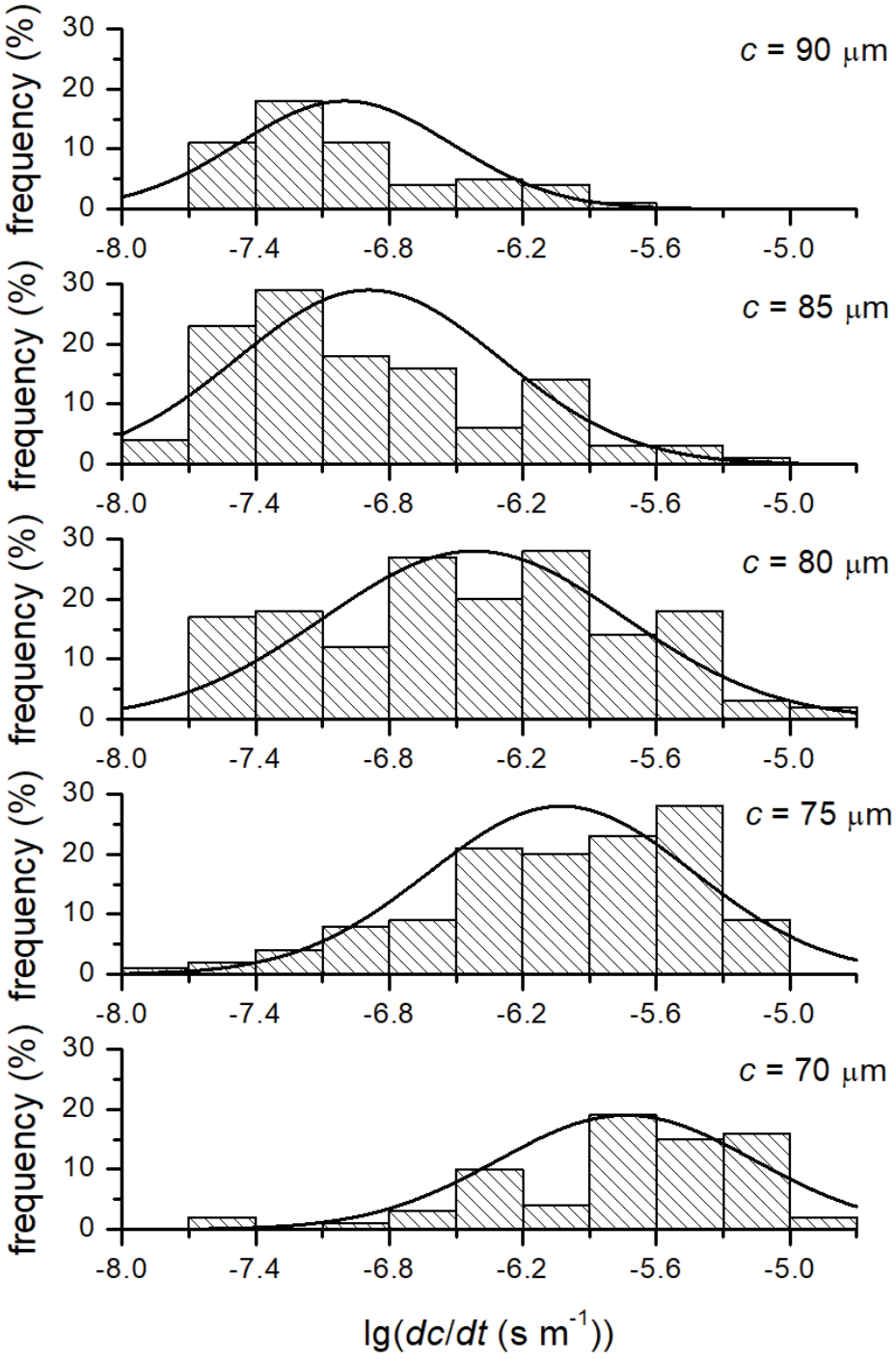

Figure 5.6: Distribution of the crack propagation rate for selected crack lengths of 70, 75, 80, 85 and 90 μm. Bin size = 0.3. Lines indicate a lognormal distribution. Note that distributions are normalized by the total number of cracks (185).

5.4 Discussion

Wilantewicz and Varner [165] reported that the initiation time of median radial cracks depends on the maximum load, the displacement rate and the holding time. In particular, they found that cracks begin to initiate relatively sooner on the unloading cycle as the total contact time increases (the total contact time t_{total} is the sum of the loading, hold and unloading periods). Using their data for soda-lime float glasses indented in air, cracking is predicted to appear preferentially during the unloading ramp (t_i/t_{total} = 0.8–0.9) which is earlier than observed in this study (figure 5.4). In another indentation study of Lawn et al. [166], the delay time of radial cracking was found to depend on the environmental condition. For low contact periods, the waiting time increased in the order water, air, nitrogen gas. Further, Bechgaard et al. [167] reported on environmental sensitivity of crack delay times. In their experiments, initiation of radial cracks in calcium aluminosilicate glasses was shorter when tested in humid atmospheres, but proceeded within 24 hours after indentation. In view of the above, we assume that humidity shortens the waiting times and that the pop-in of cracks is delayed in our study with respect to the predictions of Wilantewicz and Varner since indentation is performed under dry conditions of approx. 1% RH. Further, regarding incompleteness of crack initiation, we cannot exclude radial cracking after the recording time of 60 s and another waiting time of 1 h without recording. Delayed cracks with $\delta > 3660$ s would lead to an increase of the crack initiation probability, which is 81% (185 radial cracks out of 57 indents) for waiting 61 minutes. Thus, statistical analysis of our study misses possible contributions of some latecomers.

Shortly after their initiation, subcritical crack growth (SCCG) of the analyzed radial cracks appears to follow a common trend, i.e. the deceleration of propagation speed with increasing time and length seems to be self-similar but broadly distributed for t - δ = 0–60 s and c = 70–90 μm ($c/a \approx$ 2.0–2.5) (figure 5.5 and figure 5.6). The potential source of the scatter in the SCCG data, is not really understood at the

moment. The influence of residual fabrication stresses can be excluded as birefringence pattern (polariscope inspection) in the as-received glass were not detectable. On the other hand, the variation in the number and location (corner vs. faces) of instantaneous and delayed cracks per indent can lead to an interplay of inhomogeneous stress fields of multiple cracks growing at the same time. Thus, small changes in the time of crack nucleation can lead to different stress intensity at the crack tip and to variations in the propagation rate. This effect can be seen from cracks L and R compared with T and B of indent 1 (figure 5.2A). Cracks L and R are visible at the same time (for the camera acquisition rate of 30 fps). Their propagation rates are found to be similar and quite different to those of the later cracks T and B (figure 5.3A). Differences in SCCG are also evident, if one compares cracks T and B with L and R of the third indent (figure 5.2C). As these cracks initiate at the same time, their propagation rates seem to depend also on small changes in the nucleation position. One should note that radial cracks nucleate as median cracks in the densified zone below the surface (near to the indenter tip) as recent in-situ side views by X-ray tomography [168] and digital holographic tomography [169] pointed out. To what extent the delay in nucleation of median cracks depend on chemical reactions with water molecules of the environment is unclear. The propagation speed of the initial median crack is very high ($>10^3$ m s^{-1}) as one can approximate from the indenter half-diagonal (close to 36 μm) and the image acquisition speed of the camera (30 fps). Thus, initially the growth rate of the median crack corresponds to region III of Wiederhorn's $\lg(dc/dt)$ versus $\lg(K_I)$ diagram but decreases considerably during propagation towards the glass surface. If observed from below by an indenter microscope (as in this study), this early stage cannot be viewed. The crack becomes first visible, when its front reaches the surface at a radial position $c > a$.

For $c > a$ and shortly (t - $\delta < 1$ s) after their initiation, crack propagation rates are found to be of the same order of magnitude as those of Wiederhorn's DCB specimen ($< 3\times10^{-6}$ m s^{-1} [12]), which justifies the assumption that SCCG is controlled by the same environmental reactions

at the crack-tip in both experiments (region I). Thus, the scale factor A and growth exponent m (eq. 5.1) of the DCB experiment of Wiederhorn, was used to calibrate the SCCG data of this study as the environmental conditions (RH≈1%) and the glass composition (soda-lime-silica glass – microscopy slide) are nearly identical. Therefore, the left hand side of eq. 5.4 versus lg(c) was plotted to find the residual stress factor χ (from the intercept) and exponent n (from the slope) for each crack. In order to aid clarity, figure 5.7 shows only these dependencies for the 12 cracks of figure 5.3.

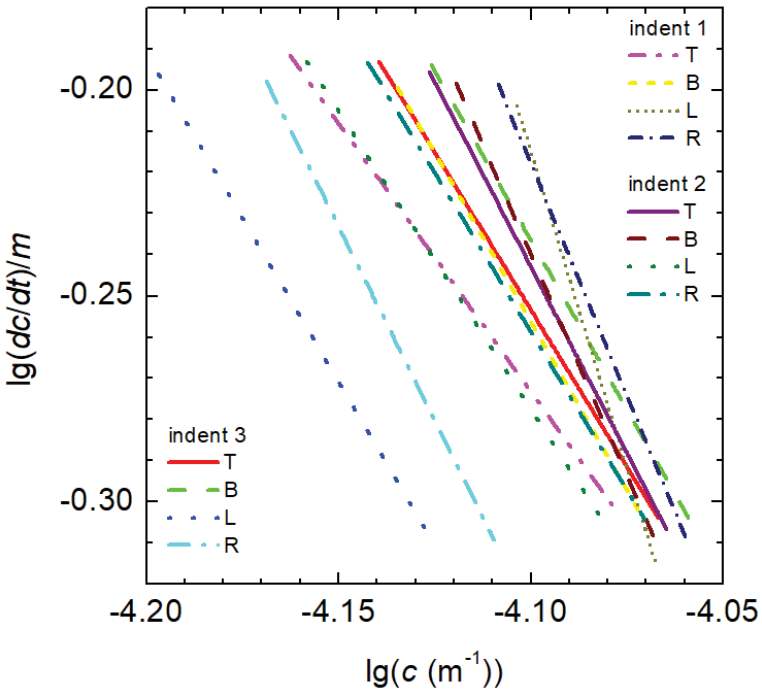

Figure 5.7: Lg(dc/dt)/m versus lg(c) of the 12 radial cracks of figure 5.3. The figure illustrates the calibration of propagation rates using eq. 5.4 and m = 24.45 and lg(A) = -0.46 (dc/dt in m s^{-1} and K_I in MPa m$^{1/2}$) [12].

Figure 5.8 shows that the residual stress factor χ and crack length exponent n is broadly distributed among the 185 cracks analyzed. Assuming that the crack initiation is Weibull distributed [170], the most frequent crack has n = 1.47. In case of the residual stress factor χ, the distribution is heavy-tailed as the shape parameter (Weibull modulus) is greater than 0 but less than 1. Taking the median value (= 0.052) instead of the modal, the fracture driving force of soda-lime silica glass at 1% RH can be expressed by the equation $K_{I(RH=1\%)} = 0.052Pc^{-1.47}$. The

Weibull plots (figure 5.8B and figure 5.8D) clearly stress that cracks of low and high χ and n are present that are hardly covered by the assumed distribution type. Including these outliers, χ spreads > 20 orders of magnitude and also for n values between 0 and 5 are evident, which is the most striking feature of figure 5.8. It emphasizes that residual stresses at the crack-tip can be very different from crack to crack as cracks of the same length are propagating with different temporary velocities even under constant environmental conditions.

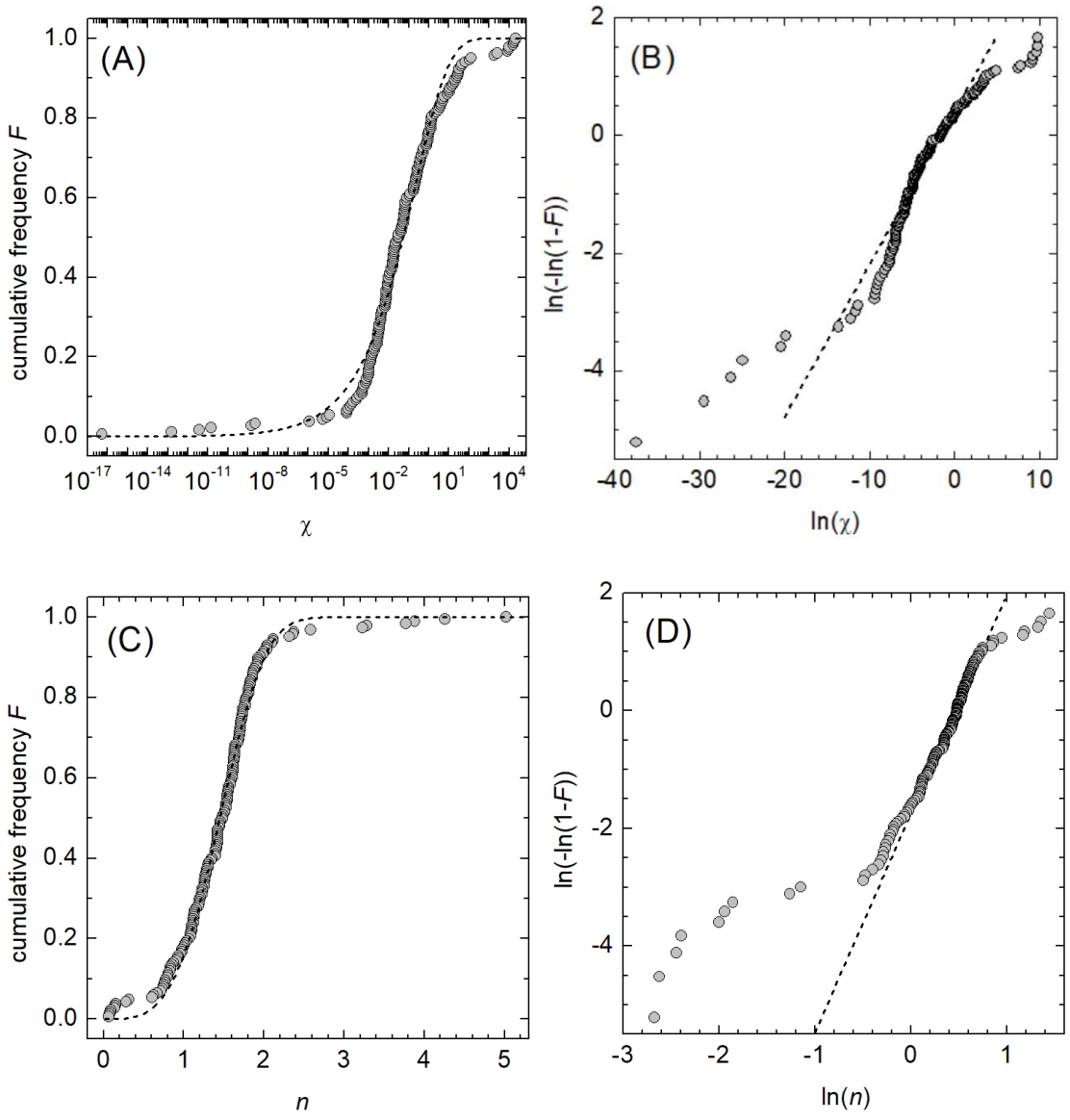

Figure 5.8: Cumulative distributions of the residual stress factor χ (A) and crack length exponent n (C) of eq. 5.1 for the 185 analyzed cracks. Parts (B) and (D) show Weibull plots of cumulative frequencies. Dashed lines are the best fit through the data with shape factor (Weibull modulus) 0.259±0.005 (χ), 3.72±0.04 (n), scale factor 4.7±0.2 (χ), 0.624±0.001 and regression coefficient 0.9806 (χ), 0.9934 (n).

Crack length data have been used as a measure of the critical stress intensity K_{IC} arresting the crack. More than 20 different equations of type:

$$K_{IFT} = K_{IC} = \chi_B P c_{max}^{-n}, \tag{5.8}$$

are compiled in the literature (see, e.g., Refs. [33], [157], [158]), where K_{IFT} is the indentation fracture toughness, χ_B is the residual stress factor at the crack-tip and c_{max} is the crack length on arrest. Most frequently, for median radial cracks those of Anstis et al. [171], Miyoshi [172] and Niihara [173] are used, which have $n = 3/2$ and $\chi_B = 0.0016(E/H_V)^{1/2}$ [171], $0.0018(E/H_V)^{1/2}$ [172] and $0.0309(E/H_V)^{1/2}(E/H_V)^{2/5}$ [173], respectively. For other radial crack types, such as Palmqvist cracks (crack opens at the corner of the indent with length $l = c$ - a), $n = 1/2$ and $\chi_B = 0.0123P^{-1/2}(E/H_V^{-1/4})^{2/5}$ [173] are proposed. All these equations use numerical calibration constants that result from a forced fitting of indentation induced crack length data of a different set of brittle materials. Two concerns need to be addressed when applying eq. 5.8 to crack length data of soda-lime-silica glasses. Firstly, our analysis clearly indicate that shortly (≈1 s) after indentation SCCG obeys region I, that is crack propagation is controlled by the reaction between atmospheric water and glass at the crack-tip. Secondly, we show that crack propagation rates are broadly distributed even when a constant indentation protocol is used. Hence, applicability of eq. 5.8 seems to be restricted to indentation testing in water-free environments, such as vacuum and toluene and the use of statistical significant data. The environmental sensitivity of eq. 5.8 goes in line with the observation that the "arrest" length c_{max} of indentation-induced radial cracks increases and K_{IFT} apparently decreases with increasing humidity, when a stress calibration is not performed [163]. Further, if χ_B in eq. 5.8. is expressed by the hardness-to-Young's modulus ratio [171]–[173] another environmental dependency becomes effective as softening (an increase of the indent diagonals) is reported for hardness tests in humid atmospheres [119], [174]–[176]. On the other hand, our results show that indentation toughness methodology can be used for

probing fracture susceptibility, in small-scale glass specimens [32], if environmental influences can be ruled out and calibrated residual stress factors are used.

5.5 Conclusions

SCCG of median radial cracks in a soda-lime-silica glass is broadly distributed when induced by Vickers indentation. Averaging the crack propagation rates over a statistical significant number of cracks appears to be a promising approach to determine stress intensity at the crack-tip with higher accuracy. The results show that the validity of $K_{IC(c_{max})}$ relations used to determine the indentation fracture toughness is questionable as the propagation rates, even under dry conditions of 1% RH, are controlled shortly after nucleation (< 1 s) by environmental reactions at the crack-tip.

6

Automated analysis of slow crack growth in hydrous soda-lime silicate glasses

P. Kiefer[a], M. Maiwald[a], J. Deubener[a], R. Balzer[b], H. Behrens[b], T. Waurischk[c], S. Reinsch[c], R. Müller[c]

[a]Clausthal University of Technology, Institute of Non-Metallic Materials, 38678 Clausthal-Zellerfeld, Germany

[b]Institute of Mineralogy, Leibniz University Hannover, 30167 Hannover, Germany

[c]Bundesanstalt für Materialforschung und -prüfung (BAM), 12489 Berlin, Germany

Abstract

To explore the impact of ambient and structural water on static fatigue, the initiation and growth of 3279 Vickers induced median radial cracks were automatically recorded and analyzed. We find that humidity is more efficient in initiating cracks and promoting their growth than water, which is dissolved in the glass structure.
In particular for slow crack growth ($< 10^{-6}$ m s^{-1}), tests in dry nitrogen showed a considerable decrease in the crack growth exponent with increasing water content of the glasses. On the other hand, if tests were performed in humid air, the crack exponent was independent of the water content of the hydrous glasses, while stress intensity decreased slightly. These observations indicate that water promotes the processes at the crack-tip regardless of its origin. However, ambient water is more efficient.

6.1 Introduction

Water is omnipresent at glass surfaces. In particular at the crack-tip, where vapour and liquid water (due to capillary condensation) can react with the stressed glass network. However, the glass-water interaction is complex and not adequately understood, although the control of such environmental reactions at the crack-tip is essential for improving the practical strength and the endurance limit of glassy products.
The basic idea of studying hydrous glasses is to create a situation where water species (hydroxyl groups and water molecules) are already present in the glass structure and to confront them with environmental water molecules reacting at the crack-tip. This approach requires several steps. Firstly, water-containing glasses must be synthesized to shed light on the influence of dissolved H_2O on the glass structure. The structural effects depend on the composition as was shown by previous studies on borate [50], borosilicate [24], [52], silicoborate [177], phosphate [178], aluminosilicate [179], and soda-lime silicate glasses [175]. Secondly,

volumetric and mechanical properties of hydrous glasses need to be investigated. Due to their technical importance, these investigations were carried out on soda-lime silicate glasses [175]. For a microscope slide glass, it was found that density, elastic moduli and Vickers hardness decrease with increasing water content, whereas the Poisson's ratio and the water content of the hydrous glasses are positively correlated. On the one hand, the trends reported by previous work reflect the non-linear change in the concentrations of hydroxyl groups and water molecules in the glasses. On the other hand, the properties were found to be environmentally sensitive, if the glass surface was involved, e.g., during indentation hardness measurements. It was observed that for dry glasses in humid atmospheres and for hydrous glasses in dry atmospheres, the indent size changed with the duration of the indentation, indicating that water was capable to relax stressed bonds in both scenarios. Particularly, the response times of dissolved water species coming from the environment and those being dissolved in the glass structure were found to be effectively equal. Recently, the hydrous glass approach was applied to capture stable crack growth in a nominal dry (0.13 mol% H_2O) and a hydrous microscope slide glass (17.08 mol% H_2O) using the double cantilever beam (DCB) technique [36]. Under vacuum, crack propagation rates $> 10^{-7}$ m s^{-1} in the hydrous glass were shifted to higher stress intensity, whereas under humid environment (air) crack propagation rates of the hydrous glass were shifted to lower stress intensity with respect to the dry glass. The apparent toughening effect of the dissolved water in the glass under vacuum was explained by higher energy dissipation during fracturing. Water-related internal friction bands observed in dynamic-mechanical spectroscopy studies [29], [36] supported this idea. With respect to the behavior in air, it was suggested that the dissipation mechanism was overwhelmed by environmental water, which led to the weakening, i.e. a decrease in stress intensity [36].

With this background, the hydrous glass approach was employed in this study with respect to the subcritical growth of Vickers induced

median radial cracks. A series of 5 microscope slide glasses with water contents ranging from 0.75 to 17.08 (mol%) was tested in two different environments (dry N_2 gas and air) to explore water-dependent effects. In spite of the limitations due to unknown amplitude of the residual stress field in this case, the technique of indentation allowed, in principle, automated experiments as well as automated data processing and analysis [35]. Thus, to demonstrate statistical significance, the growth of in total 3279 cracks was recorded (= 6.165 million frames) and automatically analyzed to determine the mean crack length within the first minute of propagation of each glass with high accuracy.

6.2 Experimental

6.2.1 Preparation of hydrous glasses

Samples of hydrous soda-lime silicate glasses from a previous study were used [175]. These were synthesized from commercial microscope slides (MSG) with a molar composition $SiO_2/Na_2O/CaO/MgO/Al_2O_3/K_2O/(Fe_2O_3/TiO_2)$ = 73.2/13.3/6.6/6.2 /0.5/0.2/(0+) as analysed by X-ray fluorescence (Axios, PANalytical). Oxides in parentheses were present in a nominal molar amount <0.05. Hydration was performed using an internally heated pressure vessel (IHPV) in which welded Pt-capsules were placed. Samples were heated to 1673 K at a pressure of 500 MPa for 20 h. The Pt-capsules were filled with powder of the crushed MSG glass and the required amount of water. Details of the hydration procedure using the IHPV apparatus were provided in [124]. The water contents were analyzed using Fourier transformed infrared spectroscopy and Karl-Fischer-titration. The results of these characterizations were published in [175]. Two platelets of approximately 20×5×1 mm^3 in size with diamond polished surfaces (< 1 μm) were prepared from each hydrated glass for placing Vickers indentation. The glasses were labelled 0W-MSG500 (0.75; 0), 1W-MSG500 (3.15; 0.214), 2W-MSG500 (5.89; 0.374), 4W-MSG (11.62; 0.605)

and 6W-MSG500 (17.08; 0.739). The names refer to the nominal water content in wt% and the synthesis pressure in MPa, e.g., 4W-MSG500 = 4 wt% water, 500 MPa. The first value in parentheses behind the name indicates the analyzed water content in mol%, while the second value is the ratio $c_{H2O}/(c_{OH} + c_{H2O})$ where c_{H2O} and c_{OH} represent the contents of water dissolved as molecules and hydroxyl groups, respectively, in the glass structure [175].

6.2.2 Automated data processing of Vickers induced crack growth

To initiate radial crack growth in the hydrous glass samples, the surfaces were indented with a Vickers diamond under a fixed load of 17.66 N using an universal hardness testing machine (ZHU 2.5, Zwick&Roell, Ulm, Germany). The automated protocol included a loading and unloading step of 5 s each (resulting in an (un)loading rate of $\pm$ 3.53 N s^{-1}) and a dwell time of 15 s (figure 6.1). Crack initiation and propagation were observed through a long distance objective at a magnification of 20x (N PLAN L, Leica, Wetzlar, Germany) of an inverted microscope (DM-ILM, Leica, Wetzlar, Germany) and recorded with a 5.3 megapixel CMOS sensor of a monochrome camera (PL-D725MU-T, PixelINK, Ottawa, Canada). The microscope was positioned directly below the hardness tester and the tip of the Vickers diamond was aligned to be parallel to the optical axis of the microscope. To increase the stiffness of the experimental setup, a steel plate with a thickness of 20 mm replaced the original microscope table. For each of the 62–143 indents per sample a video was recorded at an acquisition rate of 30 frames per second for durations of 60 s (=1800 frames) or 65 s (=1950 frames). The start of the image acquisition was triggered by a LabView script at the beginning of the unloading ramp ($t = 0$). The videos were recorded without any compression as .seq files using the TroublePix software (Norpix, Montreal, Canada). Decomposition of the videos into single Tagged Image File Format (.tiff) files was carried out using the BatchProcessor software

(Norpix, Montreal, Canada). Each .tiff image was automatically analyzed via a self-written MatLab code (Mathworks, Natick, MA, USA) that was capable to measure the Euclidean distance between the center of the indent and the tip of the corner cracks for each crack of the single images. The detection of the crack tip was performed using the grey scale values. Lengths determined by the automated analysis were in excellent agreement (< 2 μm) with scanning electron microscope (SEM) measurements.

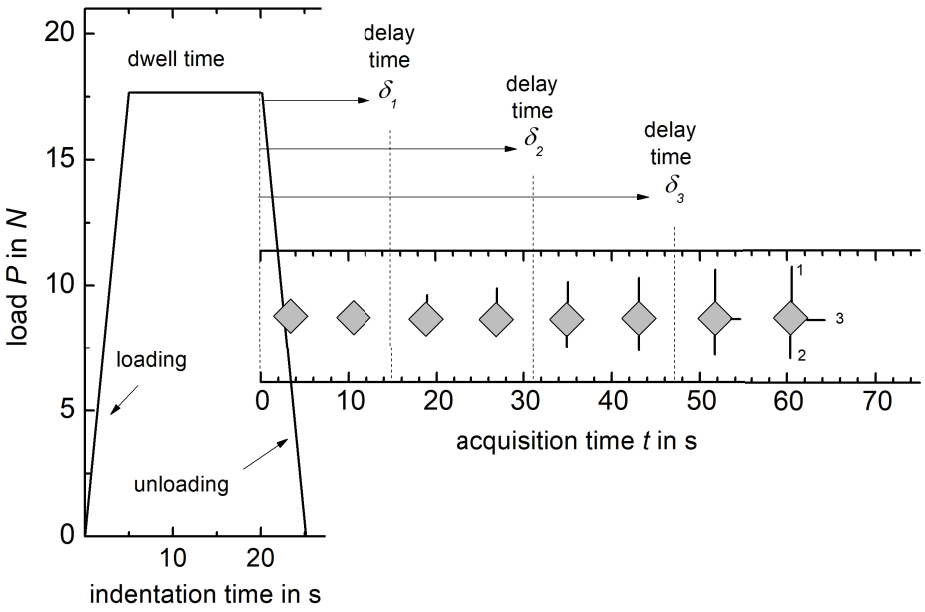

Figure 6.1: Scheme of the load-time curve of the Vickers indentation. Automated image acquisition was triggered at the start of the unloading ramp. Radial cracks at the corner of the indent were observed to grow after a delay time δ.

To study the impact of humidity, the measurements with the above setup were carried out in two different environments. On the one hand, the indentations were conducted in a glovebox (labmaster130, MBraun, Garching, Germany) providing a dry nitrogen atmosphere with a H_2O partial pressure $p_{H2O} \leq 30$ Pa at 25 °C. On the other hand, the second platelet of each specimen was measured in a cleanroom with a constant humidity of 942 Pa vapor pressure at 18 °C. Humidity in the glovebox was monitored with a dew point sensor (Michell Instruments, Easydew EA2-TX, Ely, UK) connected to a data logger (Ahlborn, Almemo 8590-9, Holzkirchen, Germany). In the cleanroom humidity was monitored using

a FHAD462 sensor connected to an Almemo 2470-2S data logger (both Ahlborn, Holzkirchen, Germany).

6.3 Results

Table 6.1 summarizes the total number of median radial cracks that were initiated during Vickers indentation and counted at the end of the video acquisition of the series in dry environment at 60 s and of the series in humid environment after 65 s, respectively. Representative images of Vickers induced cracks and their growth by video capturing were presented in a previous paper [35]. According to Wada et al. [161], the probability of crack initiation was determined by the crack number-to-corner number ratio, with 4 corners per indent z of the Vickers diamond. Inspection of table 6.1 reveals that the probability of crack initiation was higher for each glass when tested under the humid conditions of the cleanroom. Under the dry conditions of the glovebox, the frequency of initiated cracks first decreases with the water content to about 48% (4W-MSG500) and then increases to approximately 82% for the glass with the highest water content. Under humid conditions, the probability of crack initiation does not depend significantly on the water content of the glass.

Table 6.1: Total number of cracks initiated after 60 s (N_{60s}) and 65 s (N_{65s}), number of indents (z) and the probability of crack initiation F_{60s} and F_{65s}.

Glass	Vapor pressure p_{H2O} = 30 Pa			Vapor pressure p_{H2O} = 942 Pa		
	N_{60s}	z	F_{60s}	N_{65s}	z	F_{65s}
0W-MSG500	183	62	0.736	402	126	0.796
1W-MSG500	294	121	0.606	339	111	0.762
2W-MSG500	324	135	0.599	339	118	0.717
4W-MSG500	259	135	0.479	370	121	0.763
6W-MSG500	467	143	0.815	302	92	0.819

In order to analyse a possible delay in crack initiation in more detail, cumulative frequency functions $F(\delta)$ were generated for each glass (figure 6.2). This was done by arranging the delay of each crack in ascending order ($\delta_1 \leq \delta_2 \leq \delta_3 \leq ... \leq \delta_N$, the minimum first and the maximum last) followed by relating its rank number R_i to the total number of possible

cracks ($4z$). With the commonly used median rank approximation of Bernard and Bosi-Levenbach [180] one has:

$$F(\delta) = \frac{R_i(\delta_i) - 0.3}{4z + 0.4} for\ i = 1, ..., 4z, \tag{6.1}$$

For example, F = (1-0.3)/(4×62+0.4) = 0.0028 for the first crack (δ = 1.03 s) of 0W-MSG500 (p_{H2O} = 30 Pa), while F = (183-0.3)/(4×62+0.4) = 0.736 for the latest crack (δ = 59.87 s). Under humid conditions, cracks initiation for all glasses occured almost completely while unloading ($\delta < 5$ s). When tested in dry nitrogen gas, differences in the temporal evolution of crack initiation between the nominally anhydrous and hydrous glasses were evident. With increasing water content, crack initiation becomes increasingly delayed and often occurs after the unloading is completed ($\delta > 5$ s). In summary, figure 6.2 clearly shows that humidity shortens the delay time.

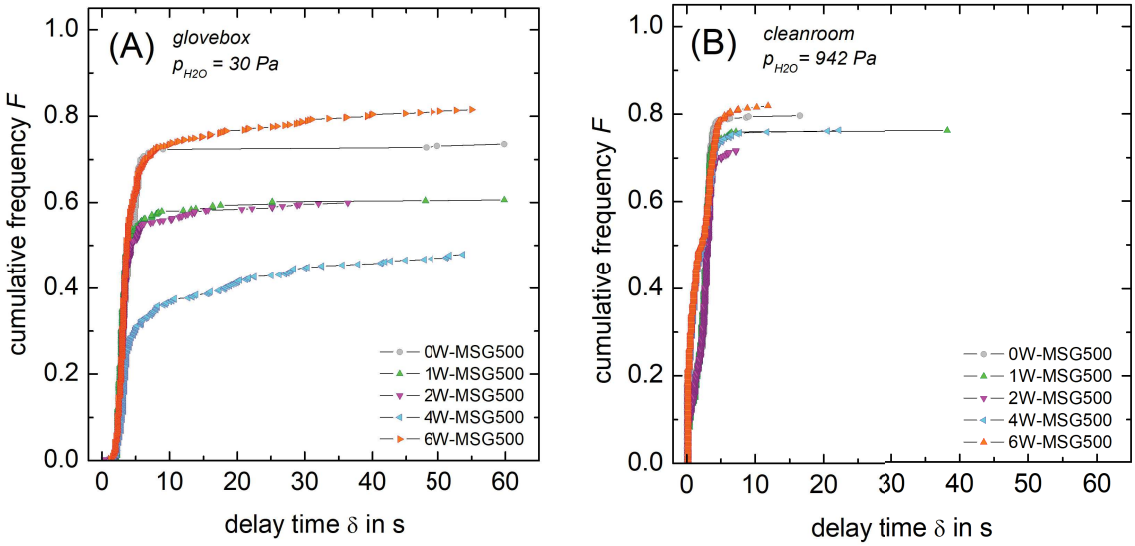

Figure 6.2: Cumulative frequency distribution $F(\delta)$ of the number of initiated cracks tested in dry (A) and humid (B) environments. Lines connecting data points are intended as visual guides.

In order to analyze crack growth in detail, the propagation time (t - δ) was calculated by subtracting the delay δ from the acquisition time t for each crack. Figure 6.3 primarily shows that the crack length strongly depends on the H_2O partial pressure, which has been noted already in previous studies [163], [176]. After 55 s, cracks reached about 70–120 μm under dry conditions, whereas in the humid environment,

crack lengths in the range 100–160 μm were detected. Further, large differences in the initial propagation rates from crack to crack are evident, leading to a broad distribution of crack lengths already shortly after their initiation (< 5 s). This feature underlines the demand of analyzing crack propagation using large data sets with $N > 200$ [35].

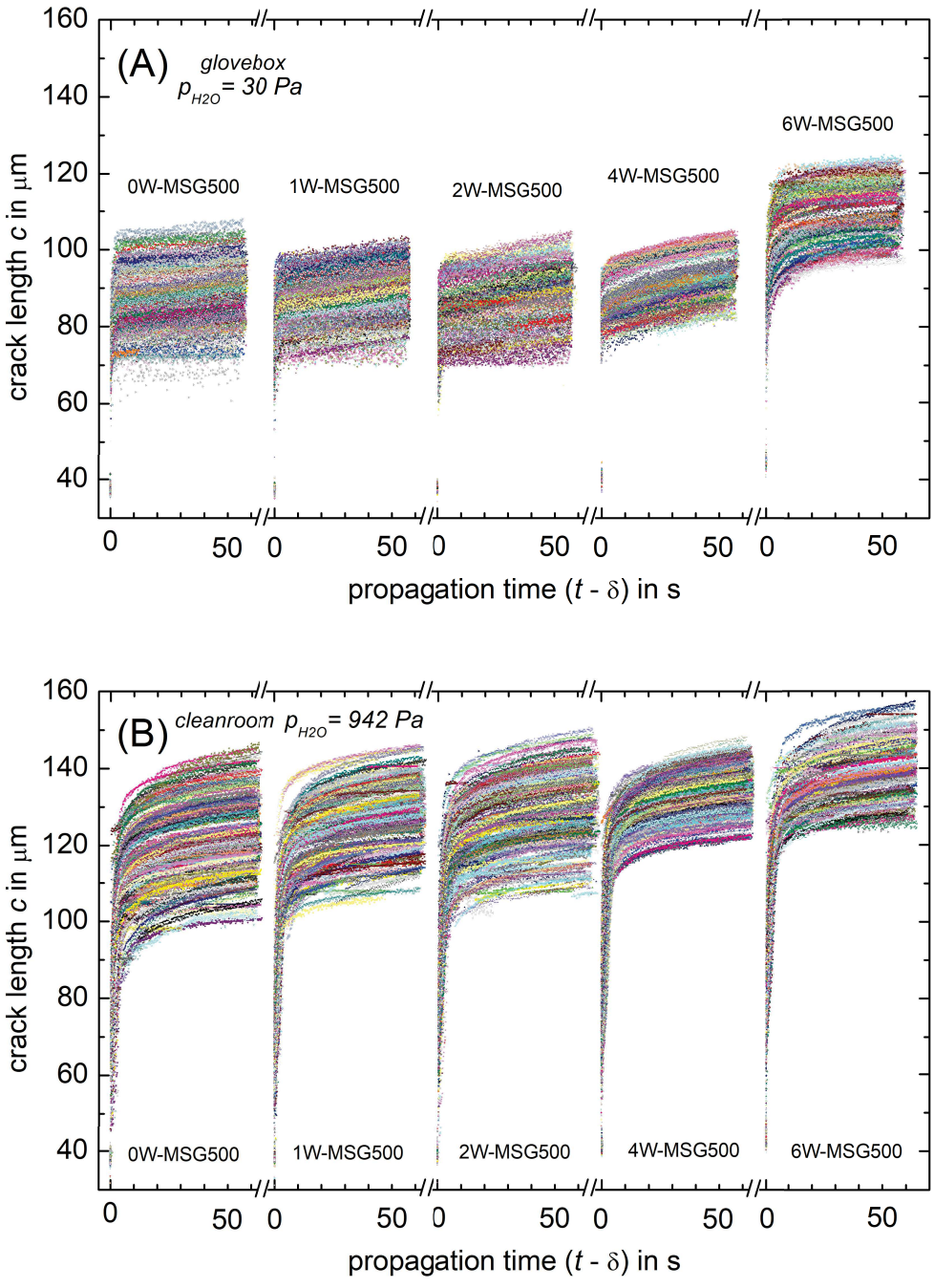

Figure 6.3: Length versus propagation time of cracks grown in hydrous glasses in 30 Pa partial pressure of H_2O (A) and in 942 Pa partial pressure of H_2O (B).

Figure 6.4 exemplarily shows cumulative distribution functions of the crack length c_{50s} (t - δ = 50 s). Cumulative frequency analyses using CumFreq (www.waterlog.info/cumfreq.htm) software indicated that c_{50s} were consistent with a Weibull distribution for all glasses and environments. Two-parameter Weibull distributions ($F = 1 - \exp[-(c_{50s}/c_m)^{\beta}]$ with scale parameter c_m and shape parameter β) were fitted using the OriginPro 2019 software (OriginLab, Northampton, MA, USA) with median-rank regression (MRR) and maximum likelihood estimators (MLE). For MRR, data series were generated by arranging the length c_{50s} of each crack in ascending order while simultaneously relating its rank number R_i to the total number N of observed cracks. For $F(c_{50s})$ one has:

$$F(c_{50s}) = \frac{R_i(\delta_i) - 0.3}{N + 0.4} for\ i = 1, ..., N. \tag{6.2}$$

MLE does not make use of data sorting, which could lead to self-correlation of the data. In this case, data points in figure 6.4 were plotted according to median ranks and the lines according to the MLE solutions. Graphs of the confidence interval of figure 6.4 were used to give preference for either MRR or MLE solutions. Results of the fitting procedure were compiled in table 6.2. These fitted Weibull distributions were found to be negatively skewed and of small tail. It is noteworthy that independent from the fitting procedure a few short and long cracks outside the 95% confidence interval are present in most hydrous glasses (figure 6.4B). One should note that a more rigorous analysis of fracture data requires unbiasing factors, which must be calculated for any specific Weibull distribution, see e.g. ASTM C1239-06a. The unbiased MLE treatment improves the size of the confidence intervals, whereas for large datasets it affects only marginally the fit parameters c_m and β.

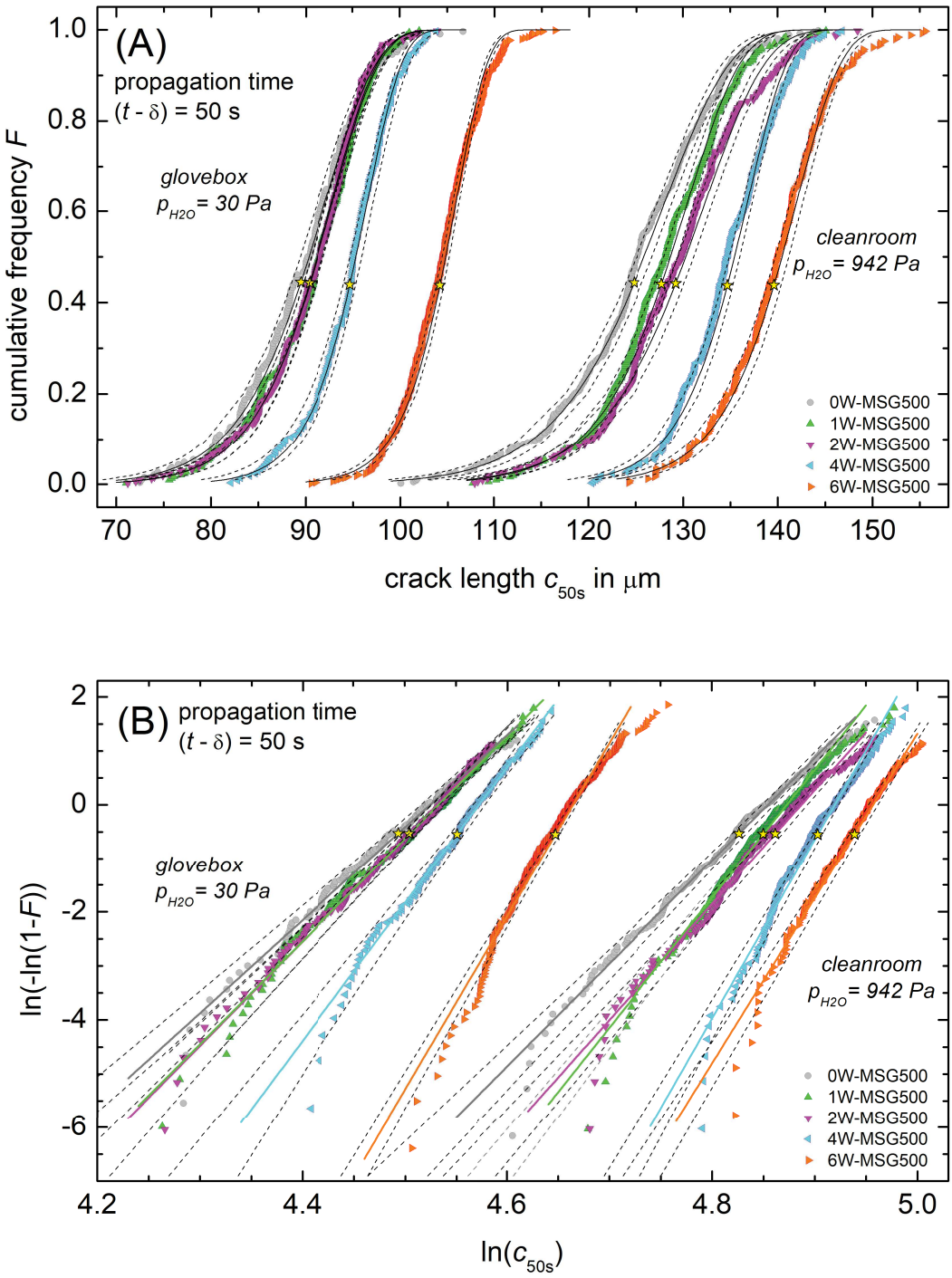

Figure 6.4: Cumulative frequency F of the crack length c_{50s} in dry and humid environments (A). Part (B) shows corresponding Weibull plots of cumulative frequencies. Solid lines are the best fit (MRR and MLE) through the data with parameters compiled in table 6.2, while dotted lines are 95% confidence intervals. Yellow stars indicates the mean crack length c_{av}.

Table 6.2: Scale parameter c_m, shape parameter β , skewness parameter K, standard deviation σ and mean length c_{av} of Weibull distributed crack lengths c_{50s} (propagation time t - δ = 50 s). The skewness parameter K calculates as $K = (c_{av}$ - $c_m)/\sigma$. Weibull distributions were fitted using median-rank regression (MRR) and maximum likelihood estimators (MLE).

Glass	Vapor pressure p_{H2O} = 30 Pa						Vapor pressure p_{H2O} = 942 Pa					
	c_m (μm)	β	$-K$	σ (μm)	c_{av} (μm)	Method	c_m (μm)	β	$-K$	σ (μm)	c_{av} (μm)	Method
0W-MSG500	92.26	17.23	0.39	6.40	89.46	MRR	128.32	19.08	0.39	8.09	124.77	MRR
1W-MSG500	93.04	19.08	0.39	5.87	90.47	MLE	130.69	23.89	0.41	6.66	127.75	MRR
2W-MSG500	92.94	19.31	0.39	5.80	90.39	MLE	132.57	21.32	0.40	7.53	129.26	MRR
4W-MSG500	96.76	25.43	0.41	4.65	94.71	MLE	136.95	33.28	0.42	5.08	134.70	MRR
6W-MSG500	106.04	32.34	0.42	4.05	104.25	MRR	142.15	30.67	0.42	5.71	139.62	MRR

Distributions of randomly selected propagation times indicated that the small skewness of the Weibull distributions of figure 6.4 is typical, i.e. $-K$ is nearly constant (0.39–0.41). Hence, the mean length c_{av} instead of the modal length c_m of cracks was taken to simplify the evaluation of the crack propagation rate within these limits. Figure 6.5 shows that the crack growth is largely influenced by the humidity. After 50 s of propagation, cracks have reached mean lengths in the range of 90–104 μm at low H_2O partial pressure and 125–139 μm under higher p_{H2O}. Within the two series, a trend of longer cracks at higher water content of the glasses is evident.

A two-phase exponential growth model was used to describe the dependence of average crack length on propagation time since a single-phase power-law [146], [162]–[164] noticeably overestimates the early stage $(t - \delta) \leq 5$ s of most tests in higher humidity. The fitting procedure was carried out for c_{av} data of each glass and testing environment of figure 6.5, which resulted in smoothed crack length data of the form:

$$c_{av} = c_\infty + S_1 exp\left[-\frac{(t-\delta)}{t_1}\right] + S_2 exp\left[-\frac{(t-\delta)}{t_2}\right], \qquad (6.3)$$

where c_∞, S_1, t_1, S_2 and t_2 are adjustable parameters. The mean crack propagation rate ν_{av} was derived by taking the first derivative with respect to the propagation time:

$$\nu_{av} = \frac{dc_{av}}{dt} = -\frac{S_2}{t_2} exp\left[-\frac{(t-\delta)}{t_2}\right] - \frac{S_1}{t_1} exp\left[-\frac{(t-\delta)}{t_1}\right] \qquad (6.4)$$

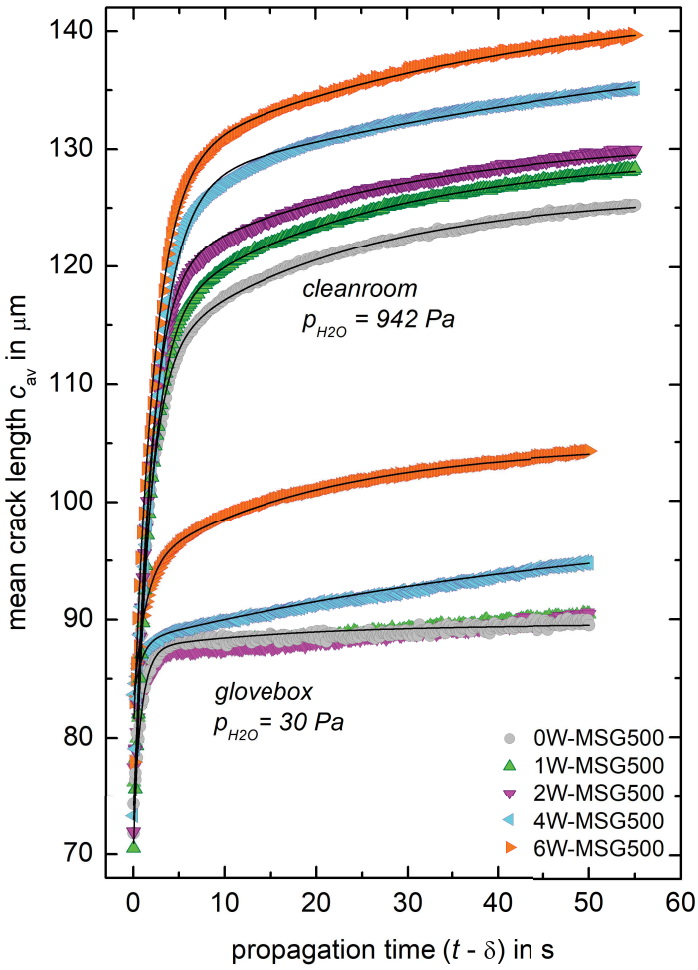

Figure 6.5: Mean crack length c_{av} as a function of the propagation time (t - δ). Solid lines are best representation of data as fitted by equation 6.3 with R^2=0.977-0.999.

6.4 Discussion

Figure 6.2 highlights the environmental sensitivity of crack delay times. To check if an additional influence of the water speciation on crack delay is present, crack initiation probabilities for δ = 1, 2, 3, 6 and 60 s were extracted from figure 6.2 and plotted versus the ratio of dissolved water molecules to total water content of the hydrous glasses (figure 6.6). On one hand, figure 6.6 shows that the influence of the water speciation is almost constant with time, i.e. the crack initiation probability develops almost uniformly. On the other hand, figure 6.6A indicates a lower probability of crack initiation of glasses in which dissociated H_2O and water molecules are present in equal fractions. The latter would imply that OH-groups

delay cracking while water molecules speed up cracking. Reasons for this compositional effect need to be addressed in a future work. However, one has to note that similar patterns have been found for density and mechanical properties of hydrous glasses, where OH initiated an increase in the elastic moduli, whereas the trend caused by water molecules was the opposite [175]. Further, one has to stress that this analysis is limited to a time maximum of one minute, which rules out effects taking place during longer observation times. For instance, Bechgaard et al. [167] reported that initiation of radial cracks in calcium aluminosilicate glasses was shorter when tested in humid atmospheres, but proceeded within 24 hours after indentation.

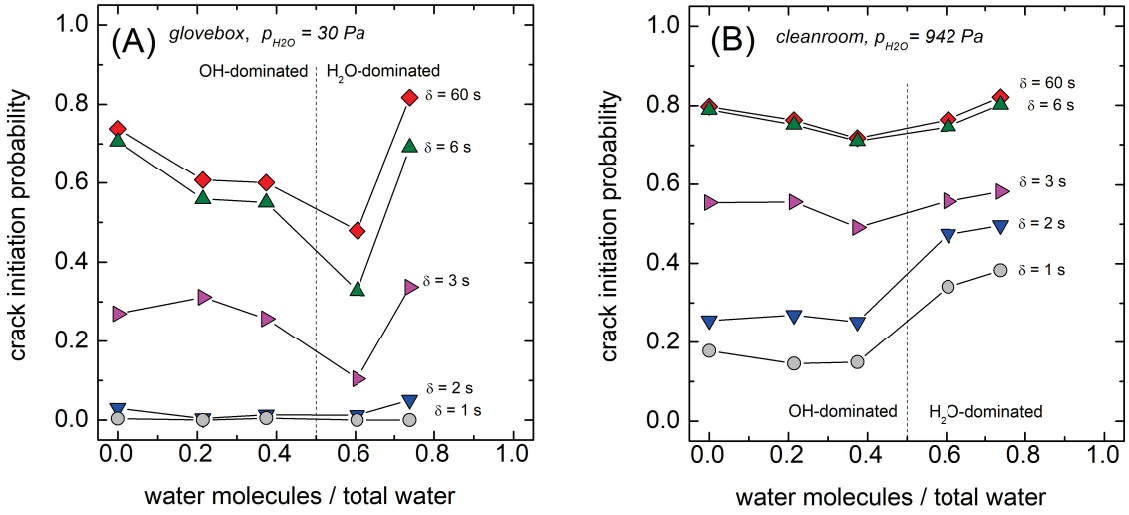

Figure 6.6: Temporal evolution of the crack initiation probability as a function of the water speciation in low (A) and high (B) humidity.

The stress intensity K_I at the tip of median radial cracks, which are induced by Vickers indentation, can be approximated as [33], [129], [155]–[158]:

$$K_I = \chi P c^{-m}, \tag{6.5}$$

with χ = residual stress factor, P = load and m = crack length exponent. A recent attempt to calibrate K_I of 185 single cracks revealed

that χ and m are broadly distributed. Mean values and standard deviations of the m and χ distributions comprising 185 cracks were = 1.47±0.44 and 0.052±31.3, respectively [35]. The value of the mean exponent (1.47 ≈ 3/2) confirmed theoretical considerations for a point loading indenter [129], [155], [156]. In contrast, the value of the residual stress factor χ is specific and accounts for the elastic-plastic properties of the glass, the angular position along the crack front and the environmental condition of the fatigue experiment. As humidity levels and glass compositions of this study differ from that of [35], $\chi = 0.052$ is not applicable here and χ remains a tunable parameter. If one assumes that the residual stress factor χ scales with the square root of the Young's modulus-to-hardness ratio $(E/H_V)^{1/2}$ [171], [172] and setting $\chi_B = \chi(E/H_V)^{-1/2}$, equation 6.5 can be rewritten as:

$$\frac{K_I}{\chi_B} = \left(\frac{E}{H_V}\right)^{1/2} P c_{av}^{-3/2} \tag{6.6}$$

The calibration factor χ_B accounts now mainly for the environmental reactions at the crack-tip. Thus, an interrelation between stress intensity K_I/χ_B and the mean crack propagation rate v_{av} can be established by plotting v_{av} calculated with equation 6.4 versus the right-hand side of equation 6.6. For the determination of K_I/χ_B, Young's modulus E of each hydrous glasses was taken from a previous study [175] and hardness was calculated using the mean value of the half diagonal length a of the Vickers indent as recorded for $t < \delta$. (For instance, see data points at $t - \delta \approx 0$ of figure 6.2A for a, while Vickers hardness is $H_V = P/(2.157\times10^{-3}a^2)$ in units of H_V (GPa), P (N), and a (μm). Figure 6.7 shows that in this Wiederhorn diagram [12], [147], humidity clearly shifts the lines towards lower stress intensity values and within the two series, K_I/χ_B decreases with increasing water content of the glasses. Figure 6.7 also displays that the slope n ($n = \lg(\nu_{av})/\lg(K_I/\chi_B)$) of the lines is affected by the testing conditions. For the series tested under high p_{H2O} (942 Pa), it is found that n = 20–27, whereas for the glasses tested in low humidity, n increased from 23 to 88 with decreasing water content (table 6.3). Noticeably, the hydrous glass 4W-MSG500 shows two segments. A first segment at the

early stage of the crack propagation ($\nu_{av} > 2 \times 10^{-7} m\ s^{-1}$) of $n = 68$ and a second segment at the later stage of $n = 16$. Values of n in the range from 16 to 27 were reported for crack growth, which is controlled by the reaction of water molecules of the environment with the glass at the crack-tip (so called stage I reactions) [12], [147], [181]. In contrast, higher values are typical for water-independent crack propagation (stage III reactions) [12], [20], [147], [181].

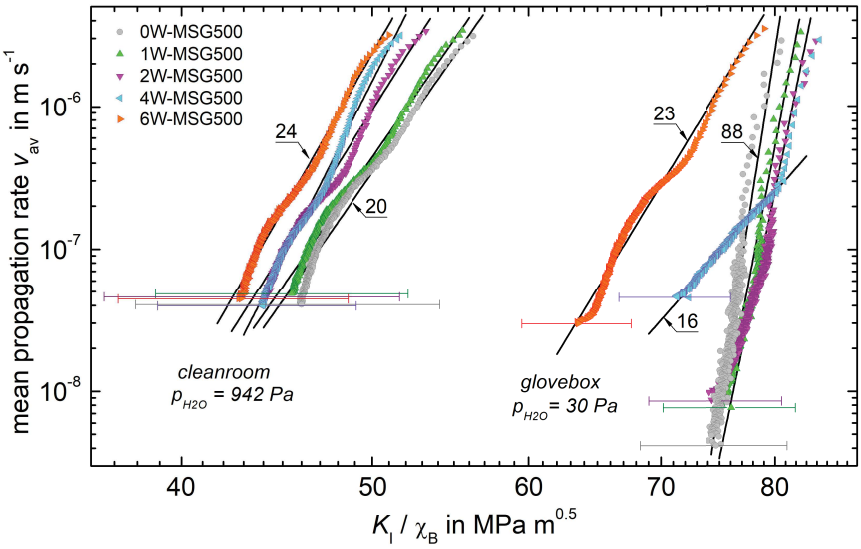

Figure 6.7: Mean crack propagation rate v_{av} versus uncalibrated stress intensity K_I/χ_B. Lines of slope n (as indicated) are best linear fits through data. Error bars show standard deviation of the crack length distributions of table 6.2

Based on this classification, one can assign 0W-MSG500, 1W-MSG500 and 2W-MSG500 to stage III reactions at low p_{H2O} of the glove box (30 Pa), while the more hydrous glasses 4W-MSG500 (at least at low propagation rates) and 6W-MSG500 show already stage I reactions. This implies that for hydrous glasses of high water contents, dissolved water promotes crack growth in a similar way as water molecules originating from the gas phase. One explanation for this would be that water readily escapes from the freshly fractured surface of hydrous glasses increasing the p_{H2O} of the vapor at the crack tip similar to the stress-induced emission of sodium during the fracture of anhydrous soda-lime silicate glass [182]. This effect was related to the local stress increase during crack propagation and can result in an increased sodium concentration at

the fractured surface, thus triggering local glass corrosion [183]. Another explanation would favour friction of an adhesive water film that is formed by allocated water at the surfaces near to the crack-tip [145], which would drop the precondition of water evaporation from the hydrous glass surface into the vapor phase. However, more research is needed to provide new evidence in support of these explanatory attempts.

Table 6.3: Crack growth exponent n of the equation $v_{av} = A(K_I/\chi_B)^n$ and $\nu = AK_I^n$ of Vickers induced and DCB cracks in soda-lime silicate glasses, respectively. To assure comparability with data of previous studies, n was collected from Refs. [36], [147], [181] for crack propagation rates in the range 10^{-8}–10^{-5} m s^{-1} only. Key: [a]Soda-lime silicate (SLS) glass of different compositions.

Ref.		[36]	[147]	[147]	this work	[36]	this work	[36]	[181]	[147]	[181]
p_{H2O} (Pa)		10^{-6}			30	661	942	1132			
T (°C)		23	25	25	25	23	18	23			
RH (%)		$\approx 10^{-8}$	0.017	0.2	1	24	45	40	50	100	liq. H_2O
Glass	$x_{H2O}(mol\%)$										
SLS[a]	≈ 0.1		91 (ν >2×10^7) 27 (v <2×10^7)	25					18.1±1.6	21	16.4±0.8
0W-MSG0	0.13	148				16±1		16±1			
0W-MSG500	0.75				88±2		20±1				
1W-MSG500	3.15				72±2		20±1				
2W-MSG500	5.89				68±2		22±1				
4W-MSG500	11.62				68±2(ν >2×10^7) 16±1(ν <2×10^7)		27±1				
6W-MSG500	17.08	16			23±1	14±3	24±1				

Figure 6.7 shows that the calibration factor χ_B is close to 0.01 as the critical stress intensity K_{IC} is about unity for dry and hydrous soda-lime silicate glasses [36], [147], [181]. However, the true value of χ_B of the individual glasses is still unknown and for its determination a calibration procedure has to be applied [31], [32], [35]. Figure 6.8 shows such an attempt for 6W-MSG500, as for this glass stable crack growth in air and vacuum was studied earlier using double cantilever beam geometry (DCB) [36]. Due to the large scatter in the DCB data, however, reconciliation of both datasets while respecting the order of decreasing K_I with increasing humidity is difficult and it does not result in more precise identifications of χ_B.

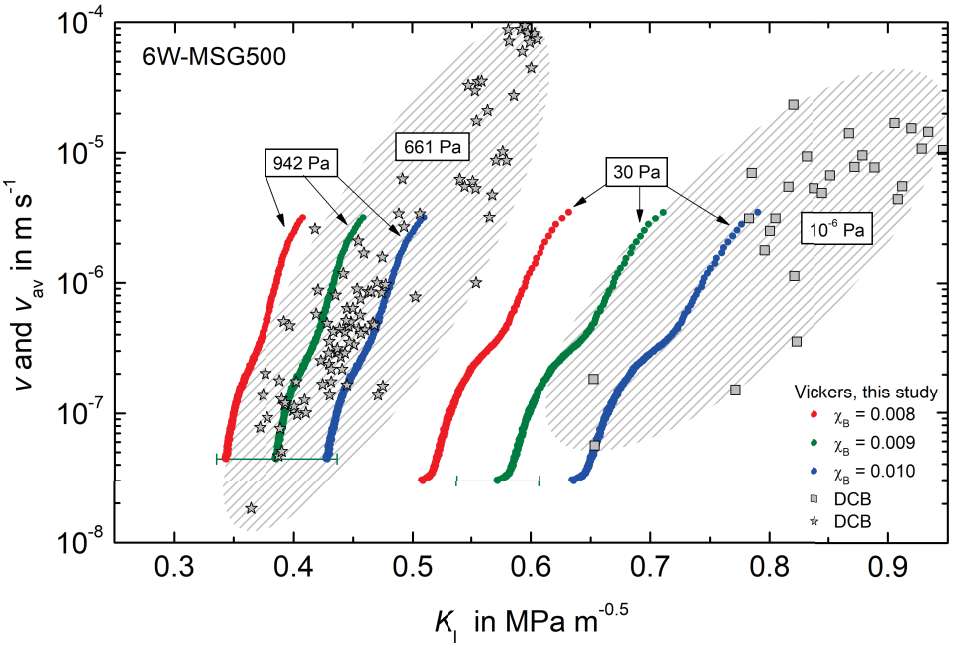

Figure 6.8: Mean crack propagation rate v_{av} (N = 259 and 370) and crack propagation rates ν of single cracks (stress calibrated DCB specimen) of the hydrous glass 6W-MSG500. Stress intensities K_I of the Vickers induced ν_{av} data of this study are shown for χ_B = 0.008 (red dots), 0.009 (green dots) and 0.010 (blue dots). Partial pressure of H_2O as indicated. DCB data from Waurischk et al. [36]. Error bars show standard deviation of the crack length distribution of Table 6.2.

6.5 Conclusions

Automated recording and analysis of a large number of Vickers induced cracks is a promising route to determine the crack growth exponent with higher accuracy. Water is found to promote slow ($<10^{-6}$ m s^{-1}) crack growth independently of its origin. However, water molecules of the environment are more efficient in reducing stress intensity than dissolved water species of the glass structure. When tested in low partial pressure of H_2O, hydrous glasses show a noticeable decrease in the crack growth exponent, which is assumed to be caused by an energy dissipation step.

7

General discussion

The study presented in chapter 3 shows that the incorporation of up to 22 mol% water into soda-borosilicate glass networks decreases the glass transition temperature T_g. The decrease of the reduced glass transition temperature T_g^* (i.e., $T_g^* = T_{g,hydrous}$ / $T_{g,dry}$) can be expressed for each water species by the three component models of Tomozawa and Deubener [40], [51]. Furthermore, it was demonstrated that water has an influence on the mechanical relaxation in soda-borosilicate glasses. Thereby, water is not only decreasing the temperature of the α-relaxation but also that of sub-T_g relaxations, i.e. β-relaxation. It was also shown that for the β-relaxation two different modes can be distinguished, which were then correlated to the water speciation in the glasses. These findings confirmed earlier observations for other glasses made by Day and Reinsch et al. [29], [65]. In comparison to the latter, in the analyzed soda-borosilicate glasses the second β-relaxation mode, i.e. β_{H2O}, was present for water concentrations >3 wt% only. Because this type of relaxation was found to be present at temperatures of approximately 330 K, β-relaxation might also occur even close to room temperature, at least in near surface regions of glasses that are subject to hydration [24] or in the vicinity of the crack tip, where it is known that water can enter the glass network and is transported to [12], [23].

Chapter 4 showed that the Poisson's ratio ν_P is positively correlated with the water content for soda-lime silicate glasses with up to 21.5 mol% water, whereas density and the elastic moduli decrease with increasing water contents in the glass structure, except for the bulk modulus. For the Vickers hardness a decrease of 27% from the dry glass to the most hydrous glass was observed, while the decrease in Young's modulus was found to be >20%. The decreasing influence of water on the latter properties can be described as non-linear for water contents <3 mol%, thereby reflecting the non-linear changes of the species concentrations, along with a change of weak to strong hydrogen bonds [94], [115]. For water contents >3 mol% the properties change linearly with increasing water content. To test the effect of both humidity and structurally bound water on the hardness, Vickers indentations were performed in air, nitrogen gas and toluene. Thereby a time-dependent softening effect was observable for the test of hydrous glasses in dry atmospheres and the test of dry glasses in a humid atmosphere, indicating that the response times of the dissolved water species are equal in both scenarios. The existence of the time-dependent softening effect confirms the observations made by Kranich and Scholze [118], [119] and further indicates that water in the glass structure is capable to relax stressed Si-O-bonds effectively, even at room temperature. Thus, the relaxation of hydrated zones around a propagating crack tip might have a substantial impact on the crack propagation in glasses [45].

Beyond the observations described by chapter 4, the water-induced changes in Poisson's numbers of the MSG glass series may also change the response of the glasses, i.e. densification (small ν_P) vs. conservative shear-flow (high ν_P), when exposed to compressive stresses that occur during hardness measurements with an indenter, as suggested by Rouxel et al. [184]. In further studies, Rouxel et al. [185], [186] report that the driving force for crack growth can be calculated for the various crack patterns of indentation fracture by superimposing a Boussinesq [187] stress field with a Yoffe [188] stress field. By plotting the E/H-ratio (with E = Young's modulus and H = hardness measured with a sharp

indenter, e.g. Vickers, Knoop, Berkovich) over the Poisson's ratio ν_P into such superimposing fields, the driving force for crack growth can be estimated. Figure 7.1 presents the superimposing Boussinesq and Yoffe fields for radial cracks in an indentation cracking map. The data inserted into the indentation cracking map of fig. 7.1 represent the hardness, ν_P and Young's modulus data of the MSG glass series that were measured in chapter 4 of this thesis.

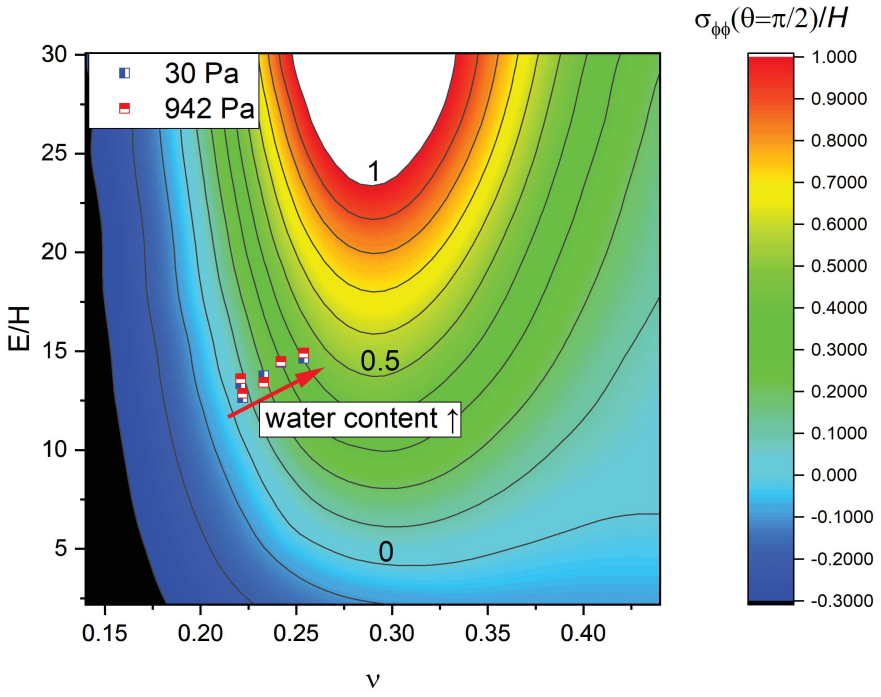

Figure 7.1: Indentation cracking map of the MSG glass series for radial cracks (i.e., $\sigma_{\phi\phi}(\Theta = 2/\pi)/H$, for further details see [186]). The red squares represent the data of the glasses for which the hardness measurements were carried out in the cleanroom ($\approx$ 942 Pa water vapor pressure). The blue squares represent the MSG glasses that were measured in the glovebox ($\approx$ 30 Pa water vapor pressure). The data show that the driving force for radial cracks increases upon hydration of the glasses.

Figure 7.1 shows that the driving force for the radial cracks is increasing with an increasing water content. Thus, the indentation cracking map supports the observation of the increasing crack lengths upon hydration made in chapter 6 of this thesis.

In chapter 5 a statistical analysis of 185 Vickers induced radial cracks in a soda-lime silicate glass, which were initiated in an atmosphere with

1% RH, revealed that the crack propagation rates are controlled by the environmental reaction at the crack tip shortly after crack initiation (i.e. < 1 s). A calibration of the stress intensity factor K_I showed that both, the residual stress χ as well as the exponent n of the expression $K_I = \chi P c^{-n}$(where P = load and c = crack length) exhibit a broad distribution covering ranges from 10^{-16} to 10^4 for χ and from 0.1 to 5 for n. These results indicate that the use of equations relating the crack lengths of Vickers induced radial cracks to K_{IC}-values is not straightforward since the crack propagation rates of such cracks are controlled shortly after the initiation. In context with the existing literature of Quinn & Bradt [31], Gong [170], Vullo & Davis [189], Marshall [32] and the recent publication of Cook [34], the approach developed in the study may contribute for a more concise assessment of indentation fracture toughness methods. However, for a precise calibration of the residual stress factor χ and crack exponent n, it is still necessary to measure K_I using standard methods such as double cantilever beam, double cleavage drilled compression or single edge precracked beam, i.e. the developed approach is not capable for a full replacement of such measuerements.

The statistical approach presented in chapter 5 was used to investigate the crack initiation and growth for hydrous soda-lime silicate glasses as presented by chapter 6. For this purpose, 3279 Vickers induced radial cracks that were initiated in hydrous glasses, were analyzed based on the findings made in chapter 5. Measurements in atmospheres with different humidities revealed that humidity is more efficient than structurally bound water in controlling crack initiation and growth. The data of hydrous glasses measured in dry nitrogen indicate that structural water decreases the crack growth exponent, while the latter remains constant if the glasses are measured in humid air. This observation indicates that water promotes subcritical crack growth in glasses independent of its origin, i.e. from the environment or from the glass structure. However, the observed decrease in the crack growth exponents from 88 to 20 further indicates a change of the reaction stage from stage III to stage I

reactions[1]. While stage I is controlled by the reaction of water molecules of the environment with the glass at the crack tip, crack propagation in stage III is typically independent of water. The observation of this change in reaction mechanism confirms a recent study of Waurischk et al. [36], who also observed a decreasing crack growth exponent with an increasing water content. The authors assume that water molecules escape from the freshly fractured surface and increases the local water vapor pressure in the vicinity of the crack tip, similar to the observation of stress-induced sodium emission of Celarie et al. [36], [183].

[1]In this case the term reaction stage refers to the classification of the different regions in the $\nu - K$ -diagram that were suggested by Wiederhorn [12]. An explanation can be found in chapter 1 of this thesis.

8

General conclusions

In the present thesis the influence of water on the process of subcritical crack growth in silicate glasses was analyzed. Therefore, the processes at the crack tip that take place during crack propagation in a humid environment were mimicked by dissolving water into the glass structure. Based on quantitative and qualitative analyses of the mechanical relaxation, the elastic properties, the hardness and the in-situ observation of the crack propagation in hydrous glasses, the results indicate that structurally bound water contributes to the process of (subcritical) crack growth in silicate glasses. However, the results also show that the influence of structurally bound water on the crack propagation in glasses is a subtle but complex superposition of changes in the mechanical properties, i.e. the mechanism and temperature of mechanical relaxations, changes in the elastic properties and changes in crack growth mechanisms, ultimately affecting the crack propagation. Based on the studies that are presented by this thesis and with respect to the aim of this thesis, the following general conclusions were drawn:

- Water in the glass structure decreases the stress intensity factor K_I of soda-lime silicate glasses and promotes crack propagation. However, the reduction of the stress intensity factor caused by structurally bound water, and most probably water molecules, is less pronounced than the decrease caused by water molecules originating from the

gas phase. This observation indicates that the effect of structurally bound water on the fracture of common glass products, having water contents of approximately 0.04-0.05 wt% [103], [104], is superimposed by the influence of water originating from the gas phase, i.e. humidity.

- The observed decrease in Young's modulus for soda-lime silicate glasses, which is particularly induced by water molecules, can be considered for the description of the mechanical properties in the vicinity of a crack tip. According to Griffith [16], the decrease in Young's modulus contributes to a decrease in critical stress, thus reflecting the decrease in K_I in the presence of water molecules.

- A time dependent softening effect during indentation hardness measurements is present in hydrous soda-lime silicate glasses independent of the origin of water, i.e. structural water or humidity. This emphasizes the findings that mechanical relaxations (i.e. β-relaxation), especially induced by water molecules, in hydrous glasses can take place already close to or at room temperature. Since the propagation of a crack involves the formation of new surface areas, particularly at the flanks and the tip of a propagating crack, the mechanical relaxations related to the hydration of these surfaces may affect the crack propagation rate [23], [25], [28], [41].

- In-situ observation of Vickers induced crack initiation and growth coupled with automated data processing allows for the generation of statistically significant datasets. Considering a statistically significant number of data appears as a more reasonable approach for the estimation of fracture mechanical parameters, i.e. K_I, than the application of standard equations (see, e.g. [33], [171]–[173]) that relate the length of Vickers induced radial cracks to K_{IC}. However, since the propagation rates of Vickers induced cracks are controlled shortly after crack initiation, it also appears reasonable to analyze crack initiation and growth of Vickers induced cracks as separate processes, confirming earlier observations made by Bechgaard et al. [167].

References

[1] L. Wondraczek, J. C. Mauro, J. Eckert, U. Kühn, J. Horbach, J. Deubener, and T. Rouxel, "Towards ultrastrong glasses", *Advanced Materials*, vol. 23, no. 39, pp. 4578–4586, 2011, ISSN: 09359648.

[2] C. Kurkjian, P. Gupta, R. Brow, and N. Lower, "The intrinsic strength and fatigue of oxide glasses", *Journal of Non-Crystalline Solids*, vol. 316, no. 1, pp. 114–124, 2003, ISSN: 0022-3093.

[3] N. P. Lower, R. K. Brow, and C. R. Kurkjian, "Inert failure strain studies of sodium silicate glass fibers", *Journal of Non-Crystalline Solids*, vol. 349, pp. 168–172, 2004, ISSN: 0022-3093.

[4] R. E. Mould and R. D. Southwick, "Strength and static fatigue of abraded glass under controlled ambient conditions: I, general concepts and apparatus", *Journal of the American Ceramic Society*, vol. 42, no. 11, pp. 542–547, 1959, ISSN: 1551-2916.

[5] R. E. Mould and R. D. Southwick, "Strength and static fatigue of abraded glass under controlled ambient conditions: II, effect of various abrasions and the universal fatigue curve", *Journal of the American Ceramic Society*, vol. 42, no. 12, pp. 582–592, 1959, ISSN: 1551-2916.

[6] R. E. Mould, "Strength and static fatigue of abraded glass under controlled ambient conditions: III, aging of fresh abrasions", *Journal of the American Ceramic Society*, vol. 43, no. 3, pp. 160–167, 1960, ISSN: 1551-2916.

[7] R. E. Mould, "Strength and static fatigue of abraded glass under controlled ambient conditions: IV, effect of surrounding medium",

Journal of the American Ceramic Society, vol. 44, no. 10, pp. 481–491, 1961, ISSN: 1551-2916.

[8] L. J. Bonis, J. J. Duga, J. J. Gilman, and R. E. Mould, Eds., *The Strength of Inorganic Glasses: Fracture of Metals, Polymers, and Glasses*, Springer US, 1967, ISBN: 978-1-4684-3153-7.

[9] R. J. Charles, "A review of glass strength", *Progress in ceramic science*, vol. 1, pp. 1–38, 1961.

[10] R. J. Charles, "Static fatigue of glass. I", *Journal of Applied Physics*, vol. 29, no. 11, pp. 1549–1553, 1958, ISSN: 0044-4537.

[11] R. J. Charles, "Dynamic fatigue of glass", *Journal of Applied Physics*, vol. 29, no. 12, pp. 1657–1662, 1958, ISSN: 0044-4537.

[12] S. M. Wiederhorn, "Influence of water vapor on crack propagation in soda–lime glass", *Journal of the American Ceramic Society*, vol. 50, no. 8, pp. 407–414, 1967, ISSN: 1551-2916.

[13] C. Gurney and S. Pearson, "The effect of the surrounding atmosphere on the delayed fracture of glass", *Proceedings of the Physical Society. Section B*, vol. 62, no. 8, pp. 469–476, 1949, ISSN: 0028-0836.

[14] C. E. Inglis, "Stresses in a plate due to the presence of cracks and sharp corners", *Trans Inst Naval Archit*, vol. 55, pp. 219–241, 1913.

[15] P. C. Paris, "A brief history of the crack tip stress intensity factor and its application", *Meccanica*, vol. 49, no. 4, pp. 759–764, 2014, ISSN: 1572-9648.

[16] A. A. Griffith, "The phenomena of rupture and flow in solids", *Philosophical Transactions of the Royal Society A: Mathematical, Physical and Engineering Sciences*, vol. 221, no. 582-593, pp. 163–198, 1921, ISSN: 1364-503X.

[17] F. A. Alshamma and O. A. Jassim, "Dynamic crack propagation in nano-composite thin plates under multi-axial cyclic loading", *Journal of Materials Research and Technology*, vol. 8, no. 5, pp. 4672–4681, 2019, ISSN: 22387854.

[18] L. H. Milligan, "The strength of glass containing cracks", *J. Soc. Glass Technol.*, vol. 13, no. 52, pp. 351–360, 1929.

[19] W. B. Hillig and J. D. Mackenzie, "Modern aspects of the vitreous state", vol. 2, p. 152, 1962.

[20] S. M. Wiederhorn, H. Johnson, A. M. Diness, and A. H. Heuer, "Fracture of glass in vacuum", *Journal of the American Ceramic Society*, vol. 57, no. 8, pp. 336–341, 1974, ISSN: 1551-2916.

[21] S. M. Wiederhorn and L. H. Bolz, "Stress corrosion and static fatigue of glass", *Journal of the American Ceramic Society*, vol. 53, no. 10, pp. 543–548, 1970, ISSN: 1551-2916.

[22] E. Orowan, "The fatigue of glass under stress", *Nature*, vol. 154, no. 3906, pp. 341–343, 1944, ISSN: 1476-4687.

[23] T. A. Michalske and S. W. Freiman, "A molecular interpretation of stress corrosion in silica", *Nature*, vol. 295, no. 5849, pp. 511–512, 1982, ISSN: 1476-4687.

[24] H. Behrens, U. Bauer, S. Reinsch, P. Kiefer, R. Müller, and J. Deubener, "Structural relaxation mechanisms in hydrous sodium borosilicate glasses", *Journal of Non-Crystalline Solids*, vol. 497, pp. 30–39, 2018, ISSN: 0022-3093.

[25] W.-T. Han and M. Tomozawa, "Effect of residual water in silica glass on static fatigue", *Journal of Non-Crystalline Solids*, vol. 127, no. 1, pp. 97–104, 1991, ISSN: 0022-3093.

[26] M. Nogami and M. Tomozawa, "Effect of stress on water diffusion in silica glass", *Journal of the American Ceramic Society*, vol. 67, no. 2, pp. 151–154, 1984, ISSN: 1551-2916.

[27] R. Le Parc, C. Levelut, J. Pelous, V. Martinez, and B. Champagnon, "Influence of fictive temperature and composition of silica glass on anomalous elastic behaviour", *Journal of Physics: Condensed Matter*, vol. 18, no. 32, p. 7507, 2006, ISSN: 0953-8984.

[28] P. J. Lezzi and M. Tomozawa, "An overview of the strengthening of glass fibers by surface stress relaxation", *International Journal of Applied Glass Science*, vol. 6, no. 1, pp. 34–44, 2015, ISSN: 20411286.

[29] S. Reinsch, R. Müller, J. Deubener, and H. Behrens, "Internal friction of hydrated soda-lime-silicate glasses", *The Journal of Chemical Physics*, vol. 139, no. 17, p. 174 506, 2013, ISSN: 0021-9606.

[30] J. H. Seaman, P. J. Lezzi, T. A. Blanchet, and M. Tomozawa, "Modeling slow crack growth behavior of glass strengthened by a subcritical tensile stress using surface stress relaxation", *Journal of the American Ceramic Society*, vol. 98, no. 10, pp. 3075–3086, 2015, ISSN: 1551-2916.

[31] G. D. Quinn and R. C. Bradt, "On the vickers indentation fracture toughness test", *Journal of the American Ceramic Society*, vol. 90, no. 3, pp. 673–680, 2007, ISSN: 1551-2916.

[32] D. B. Marshall, R. F. Cook, N. P. Padture, M. L. Oyen, A. Pajares, J. E. Bradby, I. E. Reimanis, R. Tandon, T. F. Page, G. M. Pharr, and B. R. Lawn, "The compelling case for indentation as a functional exploratory and characterization tool", *Journal of the American Ceramic Society*, vol. 98, no. 9, pp. 2671–2680, 2015, ISSN: 1551-2916.

[33] C. B. Ponton and R. D. Rawlings, "Vickers indentation fracture toughness test part 1 review of literature and formulation of standardised indentation toughness equations", *Materials Science and Technology*, vol. 5, no. 9, pp. 865–872, 1989, ISSN: 0267-0836.

[34] R. F. Cook, "A critical evaluation of indentation crack lengths in air", *Journal of the American Ceramic Society*, vol. 103, no. 4, pp. 2278–2295, 2020.

[35] P. Kiefer, J. Deubener, R. Müller, and H. Behrens, "Statistical analysis of propagation rates of indentation-induced radial cracks in soda-lime-silica glass", *Journal of Non-Crystalline Solids*, vol. 527, p. 119 739, 2020, ISSN: 0022-3093.

[36] T. Waurischk, R. Müller, S. Reinsch, P. Kiefer, J. Deubener, R. Balzer, and H. Behrens, "Crack growth in hydrous soda-lime silicate glass", *Frontiers in Materials*, vol. 7, p. 66, 2020.

[37] P. W. McMillan and A. Chlebik, "The effect of hydroxyl ion content on the mechanical and other properties of soda-lime-silica glass", *Journal of Non-Crystalline Solids*, vol. 38-39, pp. 509–514, 1980, ISSN: 0022-3093.

[38] J. Acocella, M. Tomozawa, and E. B. Watson, "The nature of dissolved water in sodium silicate glasses and its effect on various properties", *Journal of Non-Crystalline Solids*, vol. 65, no. 2, pp. 355–372, 1984, ISSN: 0022-3093.

[39] R. F. Bartholomew, B. L. Butler, H. L. Hoover, and C. K. Wu, "Infrared spectra of a water–containing glass", *Journal of the American Ceramic Society*, vol. 63, no. 9–10, pp. 481–485, 1980, ISSN: 1551-2916.

[40] J. Deubener, R. Müller, H. Behrens, and G. Heide, "Water and the glass transition temperature of silicate melts", *Journal of Non-Crystalline Solids*, vol. 330, no. 1, pp. 268–273, 2003, ISSN: 0022-3093.

[41] M. Tomozawa and E. M. Aaldenberg, "The role of water in surface stress relaxation of glass", *Physics and Chemistry of Glasses: European Journal of Glass Science and Technology Part B*, vol. 58, no. 4, pp. 156–164, 2017, ISSN: 17533562.

[42] D. E. Day and J. M. Stevels, "Effect of dissolved water on the internal friction of glass", *Journal of Non-Crystalline Solids*, vol. 14, no. 1, pp. 165–177, 1974, ISSN: 0022-3093.

[43] W. A. Zdaniewski, G. E. Rindone, and D. E. Day, "The internal friction of glasses", *Journal of Materials Science*, vol. 14, no. 4, pp. 763–775, 1979, ISSN: 1573-4803.

[44] S. V. Nemilov, "Physical ageing of silicate glasses at room temperature: General regularities as a basis for the theory and the possibility of a priori calculation of the ageing rate", *Glass Physics and Chemistry*, vol. 26, no. 6, pp. 511–530, 2000, ISSN: 1608-313X.

[45] M. Tomozawa and R. W. Hepburn, "Surface structural relaxation of silica glass: A possible mechanism of mechanical fatigue", *Journal of Non-Crystalline Solids*, vol. 345-346, pp. 449–460, 2004, ISSN: 0022-3093.

[46] H. R. Shaw, "Obsidian- H_2O viscosities at 1000 and 2000 bars in the temperature range 700°C to 900°C", *Journal of Geophysical Research*, vol. 68, no. 23, pp. 6337–6343, 1963, ISSN: 2156-2202.

[47] D. B. Dingwell, C. Romano, and K.-U. Hess, "The effect of water on the viscosity of a haplogranitic melt under P-T-X conditions relevant to silicic volcanism", *Contributions to Mineralogy and Petrology*, vol. 124, no. 1, pp. 19–28, 1996, ISSN: 1432-0967.

[48] C. Romano, D. B. Dingwell, and K. U. Hess, "The effect of boron on the speciation of water in haplogranitic melts", *Per. Mineral*, vol. 64, pp. 413–431, 1995.

[49] B. C. Schmidt, "Effect of boron on the water speciation in (alumino)silicate melts and glasses", *Geochimica et Cosmochimica Acta*, vol. 68, no. 24, pp. 5013–5025, 2004, ISSN: 0016-7037.

[50] U. Bauer, H. Behrens, M. Fechtelkord, S. Reinsch, and J. Deubener, "Water- and boron speciation in hydrous soda–lime–borate glasses", *Journal of Non-Crystalline Solids*, vol. 423-424, pp. 58–67, 2015, ISSN: 0022-3093.

[51] M. Tomozawa, M. Takata, J. Acocella, E. Bruce Watson, and T. Takamori, "Thermal properties of $Na_2O \cdot 3SiO_2$ glasses with high water content", *Journal of Non-Crystalline Solids*, vol. 56, no. 1, pp. 343–348, 1983, ISSN: 0022-3093.

[52] U. Bauer, H. Behrens, S. Reinsch, E. I. Morin, and J. F. Stebbins, "Structural investigation of hydrous sodium borosilicate glasses", *Journal of Non-Crystalline Solids*, vol. 465, pp. 39–48, 2017, ISSN: 0022-3093.

[53] J. Deubener, H. Behrens, R. Müller, S. Zietka, and S. Reinsch, "Kinetic fragility of hydrous soda-lime-silica glasses", *Journal of Non-Crystalline Solids*, vol. 354, no. 42, pp. 4713–4718, 2008, ISSN: 0022-3093.

[54] H. Scholze, *Glas: Natur, Struktur und Eigenschaften*, Dritte, neubearbeitete Auflage. Berlin, Heidelberg and s.l.: Springer Berlin Heidelberg, 1988, ISBN: 9783662074961.

[55] R. Brückner, "Characteristic physical properties of the chief oxide glass formers and their relation to the structure of glasses: IV", *Glastechnische Berichte*, vol. 37, no. 12, pp. 536–548, 1964.

[56] R. J. Ryder and G. E. Rindone, "Internal friction of simple alkali silicate glasses containing alkaline–earth oxides: I, experimental results", *Journal of the American Ceramic Society*, vol. 43, no. 12, pp. 662–669, 1960, ISSN: 1551-2916.

[57] R. J. Ryder and G. E. Rindone, "Internal friction of simple alkali silicate glasses containing alkaline–earth oxides: II, interpretation and discussion", *Journal of the American Ceramic Society*, vol. 44, no. 11, pp. 532–540, 1961, ISSN: 1551-2916.

[58] D. Day, "The internal friction of glasses containing water", *Wissenschaftliche Zeitschrift der Friedrich Schiller Universität Jena, Math. Nat. Reihe*, vol. 23, no. 2, pp. 293–305, 1974.

[59] M. Coenen, "Mechanische relaxation von Silikatgläsern eutektischer Zusammensetzung", *Zeitschrift für Elektrochemie, Berichte der Bunsengesellschaft für physikalische Chemie*, vol. 65, no. 10, pp. 903–908, 1961, ISSN: 0005-9021.

[60] J. W. Fleming and D. E. Day, "Relation of alkali mobility and mechanical relaxation in mixed–alkali silicate glasses", *Journal of the American Ceramic Society*, vol. 55, no. 4, pp. 186–192, 1972, ISSN: 1551-2916.

[61] K. E. Forry, "Two peaks in the internal friction as a function of temperature in some soda silicate glasses", *Journal of the American Ceramic Society*, vol. 40, no. 3, pp. 90–94, 1957, ISSN: 1551-2916.

[62] B. Roling and M. D. Ingram, "Determination of divalent cation mobilities in glass by dynamic mechanical thermal analysis (DMTA): Evidence for cation coupling effects", *Solid State Ionics*, vol. 105, no. 1-4, pp. 47–53, 1998, ISSN: 0167-2738.

[63] J. E. Shelby and D. E. Day, "Mechanical relaxations in mixed–alkali silicate glasses: I, results", *Journal of the American Ceramic Society*, vol. 52, no. 4, pp. 169–173, 1969, ISSN: 1551-2916.

[64] J. E. Shelby and D. E. Day, "Mechanical relaxations in mixed alkali silicate glasses: II, Discussion", *Journal of the American Ceramic Society*, vol. 53, no. 4, pp. 182–187, 1970, ISSN: 1551-2916.

[65] D. E. Day, "Internal friction of glasses with low water contents", *Journal of the American Ceramic Society*, vol. 57, no. 12, pp. 530–533, 1974.

[66] D. E. Day and J. M. Stevels, "Internal friction of $NaPO_3$ glasses containing water", *Journal of Non-Crystalline Solids*, vol. 11, no. 5, pp. 459–470, 1973, ISSN: 0022-3093.

[67] H. d. Waal, "Influence of proton exchange on internal friction in alkali silicate glasses", *Journal of the American Ceramic Society*, vol. 52, no. 3, pp. 165–166, 1969, ISSN: 1551-2916.

[68] A. Ismail, A. Abdel-Latif, and D. E. Day, "Internal friction of proton–exchanged $Li_2O \cdot Al_2O_3 \cdot 2SiO_2$ Glass", *Journal of the American Ceramic Society*, vol. 55, no. 5, pp. 254–256, 1972, ISSN: 1551-2916.

[69] M. S. Maklad and N. J. Kreidl, *Scientific and Technical Communications of the 9th International Congress on Glass*, no. 1, pp. 75–100, 1971.

[70] S. Indris, P. Heitjans, H. Behrens, R. Zorn, and B. Frick, "Fast dynamics of H_2O in hydrous aluminosilicate glasses studied with quasielastic neutron scattering", *Physical Review B*, vol. 71, no. 6, p. 064 205, 2005.

[71] B. C. Schmidt, H. Behrens, T. Riemer, R. Kappes, and R. Dupree, "Quantitative determination of water speciation in aluminosilicate glasses: A comparative NMR and IR spectroscopic study", *Chemical Geology*, vol. 174, no. 1-3, pp. 195–208, 2001, ISSN: 0009-2541.

[72] S. V. Nemilov, "The review of possible interrelations between ionic conductivity, internal friction and the viscosity of glasses and glass forming melts within the framework of maxwell equations", *Journal of Non-Crystalline Solids*, vol. 357, no. 4, pp. 1243–1263, 2011, ISSN: 0022-3093.

[73] J. V. Fitzgerald, "Anelasticity of glass: III, effect of heat–treatment on the internal friction of tank plate glass", *Journal of the American Ceramic Society*, vol. 34, no. 12, pp. 388–390, 1951, ISSN: 1551-2916.

[74] O. V. Mazurin, "Problems of compatibility of the values of glass transition temperatures published in the world literature", *Glass Physics and Chemistry*, vol. 33, no. 1, pp. 22–36, 2007, ISSN: 1608-313X.

[75] O. V. Mazurin and Y. V. Gankin, "Glass transition temperature: Problems of measurement procedures", *Glass Technology - European Journal of Glass Science and Technology Part A*, vol. 49, no. 5, pp. 229–233, 2008.

[76] R. W. Douglas, W. L. Armstrong, J. P. Edward, and D. Hall, "A penetration viscometer", *Glass Technology - European Journal of Glass Science and Technology Part A*, vol. 6, pp. 52–55, 1965.

[77] N. Bose, G. Klingenberg, and G. Meerlender, "Viscosity measurements of glass melts - certification of reference material", *Glastechnische Berichte*, vol. 74, no. 5, pp. 115–126, 2001.

[78] L. Wondraczek, S. Sen, H. Behrens, and R. E. Youngman, "Structure-energy map of alkali borosilicate glasses: Effects of pressure and temperature", *Physical Review B*, vol. 76, no. 1, p. 014 202, 2007.

[79] D. Giordano, A. R. L. Nichols, and D. B. Dingwell, "Glass transition temperatures of natural hydrous melts: A relationship with shear viscosity and implications for the welding process", *Journal of Volcanology and Geothermal Research*, vol. 142, no. 1-2, pp. 105–118, 2005, ISSN: 0377-0273.

[80] Y. Zhang, Z. Xu, and Y. Liu, "Viscosity of hydrous rhyolitic melts inferred from kinetic experiments, and a new viscosity model", *American Mineralogist*, vol. 88, no. 11-12, pp. 1741–1752, 2003, ISSN: 0003-004X.

[81] M. A. Bouhifd, A. Whittington, J. Roux, and P. Richet, "Effect of water on the heat capacity of polymerized aluminosilicate glasses and melts", *Geochimica et Cosmochimica Acta*, vol. 70, no. 3, pp. 711–722, 2006, ISSN: 0016-7037.

[82] F. Vetere, H. Behrens, F. Holtz, and D. R. Neuville, "Viscosity of andesitic melts—new experimental data and a revised calculation model", *Chemical Geology*, vol. 228, no. 4, pp. 233–245, 2006, ISSN: 0009-2541.

[83] A. G. Whittington, B. M. Hellwig, H. Behrens, B. Joachim, A. Stechern, and F. Vetere, "The viscosity of hydrous dacitic liquids: Implications for the rheology of evolving silicic magmas", *Bulletin of Volcanology*, vol. 71, no. 2, pp. 185–199, 2009, ISSN: 1432-0819.

[84] S. Kohn, R. Dupree, and M. Smith, "A multinuclear magnetic resonance study of the structure of hydrous albite glasses", *Geochimica et Cosmochimica Acta*, vol. 53, no. 11, pp. 2925–2935, 1989, ISSN: 0016-7037.

[85] B. C. Schmidt, N. Zotov, and R. Dupree, "Structural implications of water and boron dissolution in albite glass", *Journal of Non-Crystalline Solids*, vol. 337, no. 3, pp. 207–219, 2004, ISSN: 0022-3093.

[86] J. F. Stebbins, S. Kroeker, S. Keun Lee, and T. J. Kiczenski, "Quantification of five- and six-coordinated aluminum ions in aluminosilicate and fluoride-containing glasses by high-field, high-resolution 27Al NMR", *Journal of Non-Crystalline Solids*, vol. 275, no. 1, pp. 1–6, 2000, ISSN: 0022-3093.

[87] Q. Zeng, H. Nekvasil, and C. P. Grey, "In support of a depolymerization model for water in sodium aluminosilicate glasses:: Information from nmr spectroscopy", *Geochimica et Cosmochimica Acta*, vol. 64, no. 5, pp. 883–896, 2000, ISSN: 0016-7037.

[88] W. J. Malfait, R. Verel, P. Ardia, and C. Sanchez-Valle, "Aluminum coordination in rhyolite and andesite glasses and melts: Effect of temperature, pressure, composition and water content", *Geochimica et Cosmochimica Acta*, vol. 77, pp. 11–26, 2012, ISSN: 0016-7037.

[89] X. Xue, "Water speciation in hydrous silicate and aluminosilicate glasses: Direct evidence from 29Si-1H and 27Al-1H double-resonance NMR", *American Mineralogist*, vol. 94, no. 2-3, pp. 395–398, 2009, ISSN: 0003-004X.

[90] X. Xue and M. Kanzaki, "Al coordination and water speciation in hydrous aluminosilicate glasses: Direct evidence from high-resolution heteronuclear 1H-27Al correlation NMR", *Solid State Nuclear Magnetic Resonance*, vol. 31, no. 1, pp. 10–27, 2007, ISSN: 0926-2040.

[91] P. Del Gaudio, H. Behrens, and J. Deubener, "Viscosity and glass transition temperature of hydrous float glass", *Journal of Non-Crystalline Solids*, vol. 353, no. 3, pp. 223–236, 2007, ISSN: 0022-3093.

[92] A. Stuke, H. Behrens, B. C. Schmidt, and R. Dupree, "H_2O speciation in float glass and soda lime silica glass", *Chemical Geology*, vol. 229, no. 1-3, pp. 64–77, 2006, ISSN: 0009-2541.

[93] A. C. Withers and H. Behrens, "Temperature-induced changes in the NIR spectra of hydrous albitic and rhyolitic glasses between 300 and 100 K", *Physics and Chemistry of Minerals*, vol. 27, no. 2, pp. 119–132, 1999, ISSN: 1432-2021.

[94] E. Stolper, "The speciation of water in silicate melts", *Geochimica et Cosmochimica Acta*, vol. 46, no. 12, pp. 2609–2620, 1982, ISSN: 0016-7037.

[95] H. Behrens and M. Nowak, "Quantification of H_2O speciation in silicate glasses and melts by IR spectroscopy - in situ versus quench techniques", *Phase Transitions*, vol. 76, no. 1-2, pp. 45–61, 2003, ISSN: 0141-1594.

[96] M. Nowak and H. Behrens, "Water in rhyolitic magmas: Getting a grip on a slippery problem", *Earth and Planetary Science Letters*, vol. 184, no. 2, pp. 515–522, 2001, ISSN: 0012-821X.

[97] S. Ohlhorst, H. Behrens, F. Holtz, and B. C. Schmidt, *Water speciation in aluminosilicate glasses*, Balkema, Rotterdam, 2000.

[98] Y. Liu, H. Behrens, and Y. Zhang, "The speciation of dissolved H_2O in dacitic melt", *American Mineralogist*, vol. 89, no. 2-3, pp. 277–284, 2004, ISSN: 0003-004X.

[99] G. W. Scherer, "Use of the Adam–Gibbs equation in the analysis of structural relaxation", *Journal of the American Ceramic Society*, vol. 67, no. 7, pp. 504–511, 1984, ISSN: 1551-2916.

[100] S. Reinsch, C. Roessler, U. Bauer, R. Müller, J. Deubener, and H. Behrens, "Water, the other network modifier in borate glasses", *Journal of Non-Crystalline Solids*, vol. 432, pp. 208–217, 2016, ISSN: 0022-3093.

[101] H. von Rötger, "Elastische Nachwirkung durch Wärmediffusion (Thermische Reibung) und Materiediffusion (Eigentliche innere Reibung) bei periodischen und aperiodischem Vorgang.", *Glastechnische Berichte*, vol. 19, pp. 192–200, 1941.

[102] H. Scholze and N. J. Kreidl, "Chapter 4 - technological aspects of viscosity", in *Glass Science and Technology : Viscosity and Relaxation*, D. Uhlmann and N. Kreidl, Eds., vol. 3, Elsevier, 1986, pp. 233–273, ISBN: 0927-4472.

[103] F. Geotti-Bianchini and L. de Riu, "Infrared spectroscopic analysis of water incorporated in the structure of industrial soda-lime-silica glasses", *Glass Science and Technology*, vol. 68, no. 7, pp. 228–240, 1995.

[104] R. G. C. Beerkens and J. van der Schaaf, "Gas release and foam formation during melting and fining of glass", *Journal of the American Ceramic Society*, vol. 89, no. 1, pp. 24–35, 2006, ISSN: 1551-2916.

[105] L. Merker and H. Scholze, "Der Einfluß des Wassergehaltes von Silikatgläsern auf ihr Transformations-und Erweichungsverhalten", *Glastechnische Berichte*, vol. 35, no. 1, pp. 37–43, 1962.

[106] H. Behrens and A. Stuke, "Quantification of H_2O contents in silicate glasses using IR spectroscopy - a calibration based on hydrous glasses analyzed by Karl-Fischer titration", *Glass Science and Technology*, vol. 76, pp. 176–189, 2003.

[107] M. Nowak and H. Behrens, "The speciation of water in haplogranitic glasses and melts determined by in situ near-infrared spectroscopy", *Geochimica et Cosmochimica Acta*, vol. 59, no. 16, pp. 3445–3450, 1995, ISSN: 0016-7037.

[108] J. Luo, J. Banerjee, C. G. Pantano, and S. H. Kim, "Vibrational sum frequency generation spectroscopy study of hydrous species in soda lime silica float glass", *Langmuir : the ACS journal of surfaces and colloids*, vol. 32, no. 24, pp. 6035–6045, 2016.

[109] M. Takata, M. Tomozawa, and E. B. Watson, "Effect of water content on mechanical properties of Na_2O-SiO_2 glasses", *Journal of the American Ceramic Society*, vol. 65, no. 9, pp. 156–157, 1982, ISSN: 1551-2916.

[110] S. Ito and M. Tomazawa, "Dynamic fatigue of sodium-silicate glasses with high water content", *Le Journal de Physique Colloques*, vol. 43, no. C9, pp. C9-611-C9–614, 1982, ISSN: 0449-1947.

[111] R. J. Hemley, A. P. Jephcoat, H. K. Mao, C. S. Zha, L. W. Finger, and D. E. Cox, "Static compression of H_2O-ice to 128 GPa (1.28 Mbar)", *Nature*, vol. 330, no. 6150, pp. 737–740, 1987, ISSN: 1476-4687.

[112] Richet and Polian, "Water as a dense icelike component in silicate glasses", *Science (New York, N.Y.)*, vol. 281, no. 5375, pp. 396–398, 1998.

[113] P. Richet, A. Whittington, F. Holtz, H. Behrens, S. Ohlhorst, and M. Wilke, "Water and the density of silicate glasses", *Contributions to Mineralogy and Petrology*, vol. 138, no. 4, pp. 337–347, 2000, ISSN: 1432-0967.

[114] H. Scholze, H. Franz, and L. Merker, "Der Einbau des Wassers in gläsern, VI. der Einfluß des Wassers auf einige Glaseigenschaften, insbesondere Dichte und Lichtbrechung", *Glastechnische Berichte*, vol. 32, pp. 421–426, 1959.

[115] R. Limbach, B. P. Rodrigues, and L. Wondraczek, "Strain-rate sensitivity of glasses", *Journal of Non-Crystalline Solids*, vol. 404, pp. 124–134, 2014, ISSN: 0022-3093.

[116] R. E. Hanneman and J. H. Westbrook, "Effects of adsorption on the indentation deformation of non-metallic solids", *The Philosophical Magazine: A Journal of Theoretical Experimental and Applied Physics*, vol. 18, no. 151, pp. 73–88, 1968, ISSN: 0031-8086.

[117] A. P. Gunasekera and D. G. Holloway, "Effect of loading time and environment on the indentation hardness of glass", *Physics and Chemistry of Glasses*, vol. 14, no. 2, pp. 45–52, 1973.

[118] J. Kranich, *Untersuchungen zur Knoop-Mikrohärte von Gläsern: Dissertation*. 1974.

[119] J. Kranich and H. Scholze, "Einfluß verschiedener Messbedingungen auf die Knoop-Mikrohärte von Gläsern", *Glastechnische Berichte*, vol. 49, pp. 135–143, 1976.

[120] C. J. Fairbanks, R. S. Polvani, S. M. Wiederhorn, B. J. Hockey, and B. R. Lawn, "Rate effects in hardness", *Journal of Materials Science Letters*, vol. 1, no. 9, pp. 391–393, 1982.

[121] K. Hirao and M. Tomozawa, "Microhardness of SiO_2 glass in various environments", *Journal of the American Ceramic Society*, vol. 70, no. 7, pp. 497–502, 1987, ISSN: 1551-2916.

[122] G. H. Frischat, "Load-independent microhardness of glasses", *Strength of inorganic glass*, pp. 135–145, 1983.

[123] M. Tomozawa and K. Hirao, "Diffusion of water into oxides during microhardness indentation", *Journal of materials science letters*, vol. 6, no. 7, pp. 867–868, 1987.

[124] J. Berndt, C. Liebske, F. Holtz, M. Freise, M. Nowak, D. Ziegenbein, W. Hurkuck, and J. Koepke, "A combined rapid-quench and H_2 -membrane setup for internally heated pressure vessels: Description and application for water solubility in basaltic melts", *American Mineralogist*, vol. 87, no. 11-12, pp. 1717–1726, 2002, ISSN: 0003-004X.

[125] H. Behrens, C. Romano, M. Nowak, and F. Holtz, "Near-infrared spectroscopic determination of water species in glasses of the system $MAlSi_3O_8$ (M = Li, Na, K): An interlaboratory study", *Chemical Geology*, vol. 128, no. 1-4, pp. 41–63, 1996, ISSN: 0009-2541.

[126] H. J. McSkimin, "Pulse superposition method for measuring ultrasonic wave velocities in solids", *The Journal of the Acoustical Society of America*, vol. 33, no. 1, pp. 12–16, 1961, ISSN: 0001-4966.

[127] J. Deubener, H. Bornhöft, S. Reinsch, R. Müller, J. Lumeau, L. N. Glebova, and L. B. Glebov, "Viscosity, relaxation and elastic properties of photo-thermo-refractive glass", *Journal of Non-Crystalline Solids*, vol. 355, no. 2, pp. 126–131, 2009, ISSN: 0022-3093.

[128] G. V. Blessing, *Dynamic elastic modulus measurements in materials, ASTM STP 1045*, 1990.

[129] B. R. Lawn and D. B. Marshall, "Hardness, toughness, and brittleness: An indentation analysis", *Journal of the American Ceramic Society*, vol. 62, no. 7-8, pp. 347–350, 1979, ISSN: 1551-2916.

[130] J. Sehgal, Y. Nakao, H. Takahashi, and S. Ito, "Brittleness of glasses by indentation", *Journal of Materials Science Letters*, vol. 14, no. 3, pp. 167–169, 1995.

[131] S. Zietka, J. Deubener, H. Behrens, and R. Müller, "Glass transition and viscosity of hydrated silica glasses", *Physics and Chemistry of Glasses: European Journal of Glass Science and Technology Part B*, vol. 48, pp. 380–387, 2007, ISSN: 17533562.

[132] H. Bornhöft and R. Brückner, "Elastic and inelastic properties of soda lime silicate glass melts", *Glass Science and Technology*, vol. 72, pp. 315–328, 1999.

[133] R. Kohlrausch, "Theorie des elektrischen Rückstandes in der Leidener Flasche", *Annalen der Physik und Chemie*, vol. 167, no. 2, pp. 179–214, 1854, ISSN: 00033804.

[134] H. Behrens, "Ar, CO_2 and H_2O diffusion in silica glasses at 2 kbar pressure", *Chemical Geology*, vol. 272, no. 1-4, pp. 40–48, 2010, ISSN: 0009-2541.

[135] M. Ciccotti, "Stress-corrosion mechanisms in silicate glasses", *Journal of Physics D: Applied Physics*, vol. 42, no. 21, p. 214 006, 2009, ISSN: 0022-3727.

[136] S. M. Wiederhorn, T. Fett, J.-P. Guin, and M. Ciccotti, "Griffith cracks at the nanoscale", *International Journal of Applied Glass Science*, vol. 4, no. 2, pp. 76–86, 2013, ISSN: 20411286.

[137] S. M. Wiederhorn, T. Fett, G. Rizzi, M. J. Hoffmann, and J.-P. Guin, "Water penetration—its effect on the strength and toughness of silica glass", *Metallurgical and Materials Transactions A*, vol. 44, no. 3, pp. 1164–1174, 2013, ISSN: 1543-1940.

[138] A. Koike, M. Tomozawa, and S. Ito, "Sub-critical crack growth rate of soda-lime-silicate glass and less brittle glass as a function of fictive temperature", *Journal of Non-Crystalline Solids*, vol. 353, no. 27, pp. 2675–2680, 2007, ISSN: 0022-3093.

[139] B. C. Bunker, "Molecular mechanisms for corrosion of silica and silicate glasses", *Journal of Non-Crystalline Solids*, vol. 179, pp. 300–308, 1994, ISSN: 0022-3093.

[140] S. Ito and M. Tomozawa, "Stress corrosion of silica glass", *Journal of the American Ceramic Society*, vol. 64, no. 11, pp. C-160-C–160, 1981, ISSN: 1551-2916.

[141] D. M. Marsh, "Plastic flow in glass", *Proceedings of the Royal Society of London. Series A. Mathematical and Physical Sciences*, vol. 279, no. 1378, pp. 420–435, 1964, ISSN: 2053-9169.

[142] S. C. Langford, L. C. Jensen, J. T. Dickinson, and L. R. Pederson, "Alkali emission accompanying fracture of sodium silicate glasses", *Journal of Materials Research*, vol. 6, no. 6, pp. 1358–1368, 1991, ISSN: 0884-2914.

[143] T. Fett, J. P. Guin, and S. M. Wiederhorn, "Stresses in ion-exchange layers of soda-lime-silicate glass", *Fatigue Fracture of Engineering Materials and Structures*, vol. 28, no. 6, pp. 507–514, 2005, ISSN: 8756-758X.

[144] T. A. Michalske and V. D. Frechette, "Dynamic effects of liquids on crack growth leading to catastrophic failure in glass", *Journal of the American Ceramic Society*, vol. 63, no. 11-12, pp. 603–609, 1980, ISSN: 1551-2916.

[145] L. Wondraczek, A. Dittmar, C. Oelgardt, F. Celarie, M. Ciccotti, and C. Marliere, "Real-time observation of a non-equilibrium liquid condensate confined at tensile crack tips in oxide glasses", *Journal of the American Ceramic Society*, vol. 89, no. 2, pp. 746–749, 2006, ISSN: 1551-2916.

[146] S. Striepe and J. Deubener, "Effect of lithium-to-magnesium ratio in metaphosphate glasses on crack-tip condensation and sub-critical crack growth", *Journal of Non-Crystalline Solids*, vol. 375, pp. 47–54, 2013, ISSN: 0022-3093.

[147] S. M. Wiederhorn, "Subcritical crack growth in ceramics", in *Fracture Mechanics of Ceramics*, R. C. Bradt, D. P. H. Hasselman, and F. F. Lange, Eds., Boston, MA: Springer US, 1974, pp. 613–646, ISBN: 978-1-4615-7014-1.

[148] E. Gehrke, C. Ullner, and M. Hähnert, "Fatigue limit and crack arrest in alkali-containing silicate glasses", *Journal of Materials Science*, vol. 26, no. 20, pp. 5445–5455, 1991, ISSN: 1573-4803.

[149] A. G. Evans and S. M. Wiederhorn, "Proof testing of ceramic materials—an analytical basis for failure prediction", *International Journal of Fracture*, vol. 10, no. 3, pp. 379–392, 1974, ISSN: 1573-2673.

[150] A. G. Evans and H. Johnson, "The fracture stress and its dependence on slow crack growth", *Journal of Materials Science*, vol. 10, no. 2, pp. 214–222, 1975, ISSN: 1573-4803.

[151] P. C. Paris and M. P. Gomez, "A rational analytic theory of fatigue", *The Trend in Engineering*, vol. 13, no. 1, p. 9, 1961.

[152] N. Pugno, M. Ciavarella, P. Cornetti, and A. Carpinteri, "A generalized Paris' law for fatigue crack growth", *Journal of the Mechanics and Physics of Solids*, vol. 54, no. 7, pp. 1333–1349, 2006, ISSN: 0022-5096.

[153] C. Hühn, A. Erlebach, D. Mey, L. Wondraczek, and M. Sierka, "Ab initio energetics of Si-O bond cleavage", *Journal of computational chemistry*, vol. 38, no. 27, pp. 2349–2353, 2017.

[154] B. P. Rodrigues, C. Hühn, A. Erlebach, D. Mey, M. Sierka, and L. Wondraczek, "Parametrization in models of subcritical glass fracture: Activation offset and concerted activation", *Frontiers in Materials*, vol. 4, p. 1011, 2017.

[155] B. R. Lawn and E. R. Fuller, "Equilibrium penny-like cracks in indentation fracture", *Journal of Materials Science*, vol. 10, no. 12, pp. 2016–2024, 1975, ISSN: 1573-4803.

[156] D. B. Marshall and B. R. Lawn, "An indentation technique for measuring stresses in tempered glass surfaces", *Journal of the American Ceramic Society*, vol. 60, no. 1-2, pp. 86–87, 1977, ISSN: 1551-2916.

[157] Z. Li, A. Ghosh, A. S. Kobayashi, and R. C. Bradt, "Indentation fracture toughness of sintered silicon carbide in the Palmqvist crack regime", *Journal of the American Ceramic Society*, vol. 72, no. 6, pp. 904–911, 1989, ISSN: 1551-2916.

[158] A. Ghosh, A. S. Kobayashi, Z. Li, C. H. Henager JR., and R. C. Bradt, "Vickers microindentation toughness of a sintered SiC in the median-crack regime", *Pacific Northwest Lab., Richland, WA (United States)*, 1991.

[159] T. A. Michalske, W. L. Smith, and E. P. Chen, "Stress intensity calibration for the double cleavage drilled compression specimen", *Engineering Fracture Mechanics*, vol. 45, no. 5, pp. 637–642, 1993, ISSN: 0013-7944.

[160] A. G. Evans and E. A. Charles, "Fracture toughness determinations by indentation", *Journal of the American Ceramic Society*, vol. 59, no. 7-8, pp. 371–372, 1976, ISSN: 1551-2916.

[161] M. Wada, H. Furukawa, and K. Fujita, "Crack resistance of glass on vickers indentation", *Proc. Int. Congr. Glass 10th*, vol. 11, pp. 39–46, 1974.

[162] S. Dériano, A. Jarry, T. Rouxel, J.-C. Sangleboeuf, and S. Hampshire, "The indentation fracture toughness (K_C) and its parameters: The case of silica-rich glasses", *Journal of Non-Crystalline Solids*, vol. 344, no. 1, pp. 44–50, 2004, ISSN: 0022-3093.

[163] S. Striepe, J. Deubener, M. M. Smedskjaer, and M. Potuzak, "Environmental effects on fatigue of alkaline earth aluminosilicate glass with varying fictive temperature", *Journal of Non-Crystalline Solids*, vol. 379, pp. 161–168, 2013, ISSN: 0022-3093.

[164] A. Pönitzsch, M. Nofz, L. Wondraczek, and J. Deubener, "Bulk elastic properties, hardness and fatigue of calcium aluminosilicate glasses in the intermediate-silica range", *Journal of Non-Crystalline Solids*, vol. 434, pp. 1–12, 2016, ISSN: 0022-3093.

[165] T. E. Wilantewicz and J. R. Varner, "A recording microindentation instrument for in situ study of crack initiation in glass", *Journal of Materials Science*, vol. 42, no. 20, pp. 8529–8536, 2007, ISSN: 1573-4803.

[166] B. R. Lawn, T. P. Dabbs, and C. J. Fairbanks, "Kinetics of shear-activated indentation crack initiation in soda-lime glass", *Journal of Materials Science*, vol. 18, no. 9, pp. 2785–2797, 1983, ISSN: 1573-4803.

[167] T. K. Bechgaard, J. C. Mauro, and M. M. Smedskjaer, "Time and humidity dependence of indentation cracking in aluminosilicate glasses", *Journal of Non-Crystalline Solids*, vol. 491, pp. 64–70, 2018, ISSN: 0022-3093.

[168] T. Lacondemine, J. Réthoré, É. Maire, F. Célarié, P. Houizot, C. Roux-Langlois, C. M. Schlepütz, and T. Rouxel, "Direct observation of the displacement field and microcracking in a glass by means of X-ray tomography during in situ vickers indentation experiment", *Acta Materialia*, vol. 179, pp. 424–433, 2019, ISSN: 1359-6454.

[169] Y. Sung, S. Yoshida, Y. Kato, and C. Kurkjian, "Three–dimensional densification measurement of Vickers–indented glass using digital holographic tomography", *Journal of the American Ceramic Society*, vol. 102, no. 10, pp. 5866–5872, 2019, ISSN: 1551-2916.

[170] J. Gong, Y. Chen, and C. Li, "Statistical analysis of fracture toughness of soda-lime glass determined by indentation", *Journal of Non-Crystalline Solids*, vol. 279, no. 2-3, pp. 219–223, 2001, ISSN: 0022-3093.

[171] G. R. Anstis, P. Chantikul, B. R. Lawn, and D. B. Marshall, "A critical evaluation of indentation techniques for measuring fracture toughness: I, direct crack measurements", *Journal of the American Ceramic Society*, vol. 64, no. 9, pp. 533–538, 1981, ISSN: 1551-2916.

[172] T. Miyoshi, N. Sagawa, and T. Sassa, "A study on evaluation of K_{Ic} for structural ceramics", *Transactions of the Japanese Society of Mechanical Engineering, Series A*, vol. 51, pp. 2489–2497, 1985.

[173] K. Niihara, R. Morena, and D. P. H. Hasselman, "Evaluation of K_Ic of brittle solids by the indentation method with low crack-to-indent ratios", *Journal of Materials Science Letters*, vol. 1, no. 1, pp. 13–16, 1982.

[174] K. Hirao and M. Tomozawa, "Diffusion of water into oxides during microhardness indentation", *Journal of Materials Science Letters*, vol. 6, no. 7, pp. 867–868, 1987.

[175] P. Kiefer, R. Balzer, J. Deubener, H. Behrens, T. Waurischk, S. Reinsch, and R. Müller, "Density, elastic constants and indentation hardness of hydrous soda-lime-silica glasses", *Journal of Non-Crystalline Solids*, vol. 521, p. 119 480, 2019, ISSN: 0022-3093.

[176] S. Benbahouche, A. Brient, T. Rouxel, and J.-C. Sangleboeuf, "Effect of water corrosion on cracks and vickers imprints in glass", *International Journal of Fracture*, vol. 175, no. 2, pp. 199–206, 2012, ISSN: 1573-2673.

[177] R. Balzer, H. Behrens, S. Schuth, T. Waurischk, S. Reinsch, R. Müller, M. Fechtelkord, and J. Deubener, "The influence of H_2O and SiO_2 on the structure of silicoborate glasses", *Journal of Non-Crystalline Solids*, vol. 519, p. 119 454, 2019, ISSN: 0022-3093.

[178] R. Balzer, H. Behrens, S. Reinsch, and M. Fechtelkord, "Structural investigation of hydrous phosphate glasses", *Physics and Chemistry of Glasses: European Journal of Glass Science and Technology Part B*, vol. 60, no. 2, pp. 49–61, 2019, ISSN: 17533562.

[179] R. Balzer, H. Behrens, T. Waurischk, S. Reinsch, R. Müller, P. Kiefer, J. Deubener, and M. Fechtelkord, "Water in alkali aluminosilicate glasses", *Frontiers in Materials*, vol. 7, p. 85, 2020.

[180] A. Bernard and E. Bos-Levenbach, "The plotting of observations on probability-paper", *Stichting Mathematisch Centrum. Statistische Afdeling*, no. SP 30a/55, 1955.

[181] E. Gehrke, C. Ullner, and M. Hähnert, "Correlation between multistage crack-growth and time-dependent strength in commercial silicate-glasses: 1. influence of ambient media and types of initial cracks", *Glastechnische Berichte*, vol. 60, pp. 268–278, 1987.

[182] W. A. Lanford, K. Davis, P. Lamarche, T. Laursen, R. Groleau, and R. H. Doremus, "Hydration of soda-lime glass", *Journal of Non-Crystalline Solids*, vol. 33, no. 2, pp. 249–266, 1979, ISSN: 0022-3093.

[183] F. Célarié, M. Ciccotti, and C. Marlière, "Stress-enhanced ion diffusion at the vicinity of a crack tip as evidenced by atomic force microscopy in silicate glasses", *Journal of Non-Crystalline Solids*, vol. 353, no. 1, pp. 51–68, 2007, ISSN: 0022-3093.

[184] T. Rouxel, H. Ji, J. Guin, F. Augereau, and B. Rufflé, "Indentation deformation mechanism in glass: Densification versus shear flow", *Journal of applied physics*, vol. 107, no. 9, p. 094 903, 2010.

[185] T. Rouxel, "Driving force for indentation cracking in glass: Composition, pressure and temperature dependence", *Philosophical Transactions of the Royal Society A: Mathematical, Physical and Engineering Sciences*, vol. 373, no. 2038, p. 20 140 140, 2015.

[186] T. Rouxel, P. Sellappan, F. Célarié, P. Houizot, and J.-C. Sanglebœuf, "Toward glasses with better indentation cracking resistance", *Comptes Rendus Mécanique*, vol. 342, no. 1, pp. 46–51, 2014.

[187] J. Boussinesq, *Application des potentiels à l'étude de l'équilibre et du mouvement des solides élastiques: principalement au calcul des déformations et des pressions que produisent, dans ces solides, des efforts quelconques exercés sur une petite partie de leur surface ou de leur intérieur: mémoire suivi de notes étendues sur divers points de physique, mathematique et d'analyse*. Gauthier-Villars, 1885, vol. 4.

[188] E. Yoffe, "Elastic stress fields caused by indenting brittle materials", *Philosophical Magazine A*, vol. 46, no. 4, pp. 617–628, 1982.

[189] P. Vullo and M. J. Davis, "Comparative study of micro-indentation and chevron notch fracture toughness measurements of silicate and phosphate glasses", *Journal of non-crystalline solids*, vol. 349, pp. 180–184, 2004.

A

List of publications

Peer-reviewed publications

2020

Kiefer, P., Maiwald, M., Deubener, J., Balzer, R., Behrens, H., Waurischk, T., Reinsch, S., Müller, R.:
Automated analysis of slow crack growth in hydrous soda-lime silicate glasses, Frontiers in Materials (accepted manuscript)

Kiefer, P., Deubener, J., Müller, R., Behrens, H.:
Statistical analysis of propagation rates of indentation-induced radial cracks in soda-lime-silica glass, Journal of Non-Crystalline Solids, Vol. 527, 119739

Balzer, R., Behrens, H., Waurischk, T., Reinsch, S., Müller, R., **Kiefer, P.**, Deubener, J., Fechtelkord, M.:
Water in alkali aluminosilicate glasses, Frontiers in Materials, Frontiers in Materials, Vol. 7:85

Waurischk, T., Müller, R., Reinsch, S., **Kiefer, P.**, Deubener, J., Balzer, R., Behrens, H.:
Crack growth in hydrous soda-lime silicate glass, Frontiers in Materials, Vol. 7:66

2019

Kiefer, P., Balzer, R., Deubener J., Behrens, H., Waurischk, T., Reinsch, S., Müller, R. :
Density, elastic constants and indentation hardness of hydrous soda-lime-silica glasses, Journal of Non-Crystalline Solids, Vol. 521, 119480

2018

Behrens, H., Bauer, U., Reinsch, S., **Kiefer, P.**, Müller, R., Deubener, J.:
Structural relaxation mechanisms in hydrous sodium borosilicate glasses, Journal of Non-Crystalline Solids, Vol. 497, pp. 30-39

Conference Abstracts (excerpt)

2019

Kiefer, P., Deubener, J, T., Balzer, R., Behrens, H.:
Water induced changes of density, hardness and elastic moduli in soda-lime silicate-glasses, 25th International Congress on Glass, Boston (MA), USA

Kiefer, P., Deubener, J., Waurischk, T., Balzer, R., Reinsch, S., Müller, R., Behrens, H.:
Subcritical crack growth in water bearing soda-aluminosilicate glasses, 93. Glastechnische Tagung, Nürnberg, Germany

2018

Kiefer, P., Balzer, R., Waurischk, T., Reinsch, S., Müller, R., Behrens, H., Deubener, J.:
Statistical analysis of subcritical crack growth in water bearing soda-lime silicate glasses, 15th International Conference on the Physics of Non-Crystalline Solids 14th European Society of Glass Conference, St. Malo, France

Kiefer, P., Balzer, R., Waurischk, T., Reinsch, S., Müller, R., Behrens, H., Deubener, J.:
Subcritical crack growth in water bearing soda-lime silicate glasses, 92. Glastechnische Tagung, Bayreuth, Germany

Kiefer, P., Waurischk, T., Balzer, R., Reinsch, S., Müller, R., Behrens, H., Deubener, J.:
Statistical analysis of Vickers induced subcritical crack growth in soda-lime silicate glasses, 92. Glastechnische Tagung, Bayreuth, Germany

2017

Kiefer, P., Bornhöft, H., Deubener, J.:
Entstehung und Wachstum von Rissen in Gläsern, Regionales Emaillierertreffen, Lauter-Bernsbach, Germany

Kiefer, P., Balzer, R., Behrens, H., Waurischk, T., Reinsch, S., Müller, R., Deubener, J.:
In-situ Beobachtung und statistische Analyse des unterkritischen Risswachstums in Gläsern, Meeting of the FA I of the Deutsche Glastechnische Gesellschaft, Erlangen, Germany

Kiefer, P., Balzer, R., Behrens, H., Müller, R., Reinsch, S., Deubener, J.:
In-situ observation of sub-critical crack growth in water bearing borate glasses: 7th International Workshop on Flow and Fracture of Advanced Glasses, Aalborg, Denmark

Kiefer, P., Balzer, R., Bauer, U., Behrens, H., Waurischk, T., Müller, R., Reinsch, S., Deubener, J.:
Viscosity of water bearing glasses in the glass transition range – phosphates vs. silicates and borates. 91. Glastechnische Tagung der DGG, Weimar, Germany